HYBRID SIMULATION OF AC-DC POWER SYSTEMS

GLENN W. J. ANDERSON

A thesis presented for the degree of Doctor of Philosophy
in Electrical and Electronic Engineering at the
University of Canterbury, Christchurch, New Zealand.

April 1995

ABSTRACT

Transient stability studies are primarily concerned with the generator response of *ac* power systems and use only steady state type equations to model HV*dc* converter terminals. These equations are adequate for small disturbances at the converter terminals but cannot accurately represent a converters behaviour during, and through its recovery of, a significant transient disturbance. A detailed three phase electromagnetic analysis is necessary to describe the converters correct behaviour.

This thesis describes an accurate and effective hybrid method combining these two types of studies, for analyzing dynamically fast devices such as HV*dc* converters within *ac* power systems.

Firstly, conventional techniques are reviewed for both a transient stability analysis of power systems and for an electromagnetic transient analysis of HV*dc* converters. This review deals in particular with the two programs that constitute the hybrid developed in this thesis.

Various techniques are then examined to efficiently and accurately pass the dynamic effects of an HV*dc* link to an *ac* system stability study, and the dynamic effects of an *ac* system to a detailed HV*dc* link study. An optimal solution is derived to maximise the inherent advantages of a hybrid.

Finally, the hybrid is applied to a test system and its effectiveness in performing its task is shown.

ACKNOWLEDGEMENTS

I would like to express my warmest thanks and gratitude to my supervisors Dr Neville Watson, Dr Chris Arnold, and Professor Jos Arrillaga for their gentle nudging, patience, kindness, and support throughout the course of this research. Acknowledgements must also be made to TransPower NZ Ltd, and to the Templin Travelling Scholarship via NZI Guardian Trust, for their generous financial assistance.

Thanks are especially extended to Dennis Woodford and the staff at the Manitoba HV*dc* Research Centre who provided so much support and encouragement during my time in Canada that it became a very difficult task to leave!

A special thanks and acknowledgement must go to my postgraduate colleague and friend Dr Alan Wood. Without Alan's encouragement, advice, and friendship, I'm not sure if I would ever have made it. Thank you Alan, for always having the time to listen and to laugh.

Thanks also to all my other postgraduate colleagues and friends throughout the years who made life so enjoyable at university, Dr Jose Camacho, Wade Enright, Maria-Luiza Lisboa, Stuart McDonald, Dr Aurelio Medina, Dr S. Sankar, Dr Miguel Villablanca, Dr Mohammed Zavahir, and in particular, my Brazilian friend Julio DeSouza.

Finally, I am indebted to the love and support of my Mother and Father and especially of my wife Romy, who through sometimes difficult times and through much sacrifice, never stopped her encouragement.

CONTENTS

LIST OF FIGURES

LIST OF TABLES

GLOSSARY

Abbreviations

ac	alternating current
AIEE	American Institute of Electrical Engineers
ANSI	American National Standards Institute
AVR	automatic voltage regulator
CIGRE	Conference Internationale de Grands Reseaux Electriques
CSMF	continuous system modelling function
dc	direct current
EMTDC	electromagnetic transient dc program
EMTP	electromagnetic transient program
ESCR	effective short circuit ratio
FACTS	flexible *ac* transmission system
FFT	fast Fourier transform
HV*dc*	high voltage direct current
IEC	International Electro-technical Commission
IEE	Institute of Electrical Engineers
IEEE	Institute of Electrical and Electronic Engineers
NETOMAC	network torsion machine control simulation program
PLL	phase lock loop
PSCAD	power system computer aided design
pu	per unit
QSS	quasi-steady state
rms	root mean square
RTDS	real time digital simulator
SCR	short circuit ratio
SVC	static VAr compensator
TACS	transient analysis of control systems
TC	time constant

TCS	transient converter simulation program
TNA	transient network analyzer
TS	transient stability program
TSE	TS-EMTDC hybrid program
UMIST	University of Manchester Institute of Science and Technology

Symbols

a	off-nominal tap position of converter transformer
$\tilde{a}$	120 degree forward rotation vector
B_c	initial susceptance value of converter entered in TS data file
E_{1_i}	imaginary part of voltage source E_1
E_{1_r}	real part of voltage source E_1
E_d	direct axis component of the internal voltage of a machine
E_f	machine field winding voltage
E_q	quadrature axis component of the internal voltage of a machine
G_c	initial conductance value of converter entered in TS data file
G_r	three phase MVA rating of a machine
H	kinetic energy per rated speed per rated power of a machine
$\tilde{I}$	current represented as a vector quantity
I_a, I_b, I_c	phase currents of phases a, b, and c respectively
I_{ci}	imaginary component of equivalent current source I_c
I_{cr}	real component of equivalent current source I_c
I_d	direct axis component of the armature current of a machine
i_{dc}	instantaneous *dc* component of current
I_{dc}	converter *dc* side current
I_{ds}	*dc* current setting of a converter terminal
I_F	fault current
I_{fac}	fundamental component of *ac* current
I_{mi}	moment of inertia
I_n	initial current through the TSE interface bus
I_q	quadrature axis component of the armature current of a machine
I_{rn}	negative sequence rotor current of a machine
I_s	effective very low frequency value of the armature current of a machine
I_{sn}	negative sequence stator (or armature) current of a machine
j	imaginary number operator (ie.$\sqrt{-1}$)

k_c	current setting controller amplifier gain of a converter terminal
M	angular momentum
N_p	number of pole pairs in a machine
P_a	accelerating power of a machine
P_b	braking power of a machine
P_{dc}	real power into or out of a converter terminal
P_{ds}	*dc* power setting of a converter terminal
P_e	electrical power of a machine
P_f	fundamental component of real power
$P_{f_{ns}}$	fundamental component of negative sequence real power
$P_{f_{ps}}$	fundamental component of positive sequence real power
$P_{f_{zs}}$	fundamental component of zero sequence real power
P_h	total harmonic component of real power
P_m	mechanical power of a machine
P_{rms}	*rms* real power
Q_{dc}	reactive power into or out of a converter terminal
R_a	machine *ac* armature resistance
r_n	negative sequence resistance of a machine
r_p	positive sequence resistance of a machine
R_r	machine rotor resistance
R_s	machine armature resistance
t	time
T	time period
T_a	accelerating torque of a machine
T_{do}	direct axis open circuit time constant of a machine
T_e	electrical torque of a machine
T_m	mechanical torque of a machine
T_{qo}	quadrature axis open circuit time constant of a machine
$\tilde{V}$	vector quantity of voltage
$\|V\|_{pu}$	per unit voltage magnitude
V_a, V_b, V_c	phase voltages of phases a, b, and c respectively
V_{ac}	*ac* commutating voltage
V_{ac_i}	imaginary component of the *ac* voltage
V_{ac_r}	real component of the *ac* voltage
V_d	direct axis armature terminal voltage of a machine
V_{dc}	converter *dc* side voltage
V_{ns}	negative sequence voltage
V_{ps}	positive sequence voltage
V_q	quadrature axis armature terminal voltage of a machine

V_{zs}	zero sequence voltage
X_c	commutation reactance of a converter terminal
X_d	direct axis component of the synchronous reactance of a machine
X_q	quadrature axis component of the synchronous reactance of a machine

α	acceleration (for machines)
α	firing angle of valve(s) at a converter terminal
γ	extinction angle of valve(s) at a converter terminal
δ	displacement of a machine rotor angle with respect to a reference frame
$\dot{\delta}$	machine rotor speed
$\ddot{\delta}$	machine rotor acceleration
δ_e	electrical power angle of a machine
θ_x	phase angle of variable x
θ	rotor angle of a machine with respect to a reference frame
$\dot{\theta}$	machine rotor speed
$\ddot{\theta}$	machine rotor acceleration
μ	commutation angle of valve(s) at a converter terminal
τ	travel time of a travelling wave
ϕ	power factor angle
ψ	phase angle
ω	angular frequency
ω	shaft angular velocity (for machines)
ω_o	machine synchronous speed

In addition, machine variables with the superscript ' denote transient values, and with the superscript " denote sub-transient values.

Chapter 1

INTRODUCTION

1.1 *Ac* Power Systems

The advent in the late 1800's of the *ac* transformer, together with the development of the *ac* motor and polyphase circuitry, signalled the beginning of *ac* power systems as they are known today. The ability to generate large amounts of power at distant locations and transmit this energy via an intricate network to load centres has provided unparalleled support for the advancement of technology and living standards.

An *ac* power network is a complex system containing generators, generator control systems, transmission lines, transformers, induction motors, and other various types of loads. The *ac* transmission network provides a path for predominantly rotating machine generated power to provide light, heat, mechanical forces *etc*. As technology has improved, transmission lines have transported this power at higher and higher voltage levels to minimise power losses in the lines.

The operation of the power system network is dependent on the balance of mechanical and electromagnetic forces maintaining synchronism of the generators. A disturbance on the network may or may not result in the system falling out of synchronism and electrically collapsing. Disturbances can be created by such events as natural component failure, adverse weather, and human error. It is very important to adequately study the response of a system to various disturbances with an accurate simulation model. The simulated system can then be used to determine the adequacy of protection arrangements, the ability of the system to recover from a fault, the effect of any controls, and harmonic resonances that may be excited.

A power system network can be analyzed by many types of studies. One of the simplest is that of a power-flow or load-flow which determines the fundamental frequency, steady state operating conditions of the system. The information derived from this type of study can be used to initialise a stability analysis of the network. This is again at fundamental frequency but performed over time to determine the electro-mechanical stability of the generators in the network after the system has been subjected to a disturbance.

Advanced programs are also available which can model network devices in great detail, down to their individual resistive, inductive, and capacitive elements in each phase. These types of programs can simulate much quicker electromagnetic transients, and by their time domain nature, encompass all frequencies.

1.2 HV*dc* Systems

Certain difficulties are inherent in purely *ac* systems. It is sometimes not practical to interconnect independent *ac* systems for technical, economic, or political reasons. Transmission by *ac* via cables over long distances is not practical, and long haul, bulk power transfer by *ac* suffers considerable power loss due to technical restrictions in the highest transmission voltage level possible with *ac*.

Ironically, *dc* transmission, which had been discarded by power utilities in the early days of power system development, solves or reduces some of these *ac* problems. Direct current conversion has now a very useful place within *ac* power systems. The advent of *dc* within an *ac* power system was made possible with the development of the mercury arc valve in the 1920's. The progress made with the conversion of *ac* to *dc* and back to *ac* again, culminated in the first HV*dc* system linking the Swedish mainland to the Baltic island of Gotland in 1954.

HV*dc* conversion schemes have rapidly increased since this first link was commissioned and there are now some 50 HV*dc* links around the world representing a capacity of approximately 36000 MW [Elahi *et al.*, 1993]. This increase is likely to continue with advancing solid state technology, increasing HV*dc* expertise, and lower costs for conversion equipment.

Dc systems have a number of advantages over their *ac* counterparts [Arrillaga, 1983]. The costs and losses of transmission are less than for *ac* although *dc* conversion terminal costs and losses may offset this gain for all but long transmission distances. Solid state technology in the form of the thyristor is helping to reduce these drawbacks.

Whereas *ac* transmission over long cable lengths is not possible due to the alternating charging current in the cable, *dc* transmission over lengthy submarine or buried cables does not suffer this disadvantage.

A back to back converter station where *ac* is converted to *dc* and this *dc* subsequently converted back to *ac* at the same location, is particularly useful in connecting two separate or asynchronous *ac* systems. These *dc* interconnections do not cause a dramatic increase in the fault levels of the systems and can provide power flow between systems of different frequencies or control philosophies. Since *dc* can be controlled very quickly relative to *ac* by converter valve firing control techniques, it can be also be used for improving *ac* system stability.

Ac system power flows are generally mechanically controlled, which implies a relatively slow response speed. The ability to control at electronic speeds has resulted in new concepts for solid state technology in power systems. Flexible *ac* transmission systems (FACTS) have been proposed and implemented based on rapid thyristor control of series and shunt reactive compensation. Through varying the apparent impedance of transmission lines with this compensation, power can be controlled to flow along a specific path. The loading of existing transmission systems can also be increased to optimal thermal capacity through this technology.

1.3 HV*dc* Modelling

HV*dc* systems can be modelled in various ways depending on the type of study and on the effect they are likely to have on the part of the system being investigated. This is primarily related to the proximity of the HV*dc* converters to the area of concern in the system and to the *ac* system strength. For example, in certain instances when the HV*dc* is distant from the area where a disturbance has being applied, all that may be required is a fixed representation of active and reactive power injections.

Accurate *dc* modelling is particularly important when either end of an HV*dc* system is attached to a weak *ac* system. The dynamic performance of the *dc* may have a significant influence on the stability of the *ac* system.

There are three general ways to model HV*dc* systems within power system programs. These are through use of steady state converter equations, quasi-steady state converter equations, or through detailed, three phase, elemental modelling.

1.3.1 Static Converter Equation Models

In a power flow program, steady state converter equations are used to solve for the *dc* system. Two variables are generally specified to establish the operating point and constraints can be applied to certain variables such as angle or transformer tap if necessary.

In an electro-mechanical stability program, the converter can be represented by either steady state or quasi-steady state equations. A steady state equation model assumes that the *dc* current follows some reference with an appropriate time lag and that the *dc* line is represented by resistance only. Firing angles are calculated from the converter equations and checked to see if they are within limits. A mode shift is assumed if they are not, and the new angles are then calculated. The steady state model offers relatively poor accuracy to its alternatives.

In the quasi-steady state model, the dynamics of the *dc* controllers are also represented along with the possibility of more advanced modelling of the *dc* line through inclusion of reactive components. The HV*dc* model generally includes some user defined controls which must be initialised to minimise any initial transient. The *effects* of the controls are modelled as opposed to the controls themselves. These control effects can include mode shift logic, restart logic, power ramping, voltage dependent current limit, constant variable control modes *etc.*

The steady state and quasi-steady state models are useful for balanced operation and for approximate analysis of unbalanced faults when analyzing the stability of networks with HV*dc* systems. For accurate analysis of unsymmetrical faults, particularly those close to converter terminals and attached to weak *ac* systems, a detailed three phase analysis is essential.

1.3.2 Detailed Three Phase Models

A detailed three phase analysis represents each phase of a device in terms of its individual resistive, inductive, and capacitive elements. There are two commonly used methods

for this type of comprehensive analysis. One is the electromagnetic transient approach based on Dommel's algorithm [Dommel, 1969] and used in programs such as EMTP and EMTDC [Woodford *et al.*, 1983]. In this method, each network inductive and capacitive component is represented by a resistance in parallel with a varying current source. The value of the current source is determined by the component parameters, the time step, and the historical values of node voltages and branch currents. The entire system then, can be broken down into only resistances and current sources.

The second detailed method is that of state space formulation. This solves the entire system as a set of non-linear differential equations where the resistive, inductive, and capacitive elements are explicitly represented.

The electromagnetic transient and the state space forms of analysis are very accurate methods of simulation but are computationally intensive. Time-steps in the order of micro-seconds are required and because of the detailed elemental nature, the program requires the use of large matrices.

1.4 An *Ac-Dc* Stability Hybrid Approach

Conventional stability analysis of *ac* systems incorporating HV*dc* links use either steady state or quasi-steady state representations of the HV*dc* converters. Components are represented by fundamental frequency parameters and are commonly positive sequence or single phase only. While these programs are entirely adequate for representing the dynamic behaviour of generators, they are compromised by their limited representation of such non-linear components as HV*dc* links and FACTS devices.

From the *ac* point of view, it is important that the *dc* system behaves in such a way so that stability and performance of the overall system is maintained. At the inverter end of an HV*dc* system, valve commutation failures can occur if the inverter *ac* voltage suddenly drops. The *dc* voltage is zero during a certain period following a commutation failure and during this period, no active power can be transmitted. This may create a substantial disturbance on the *ac* system and may result in further commutation failures, particularly if the *ac* system is weak. For this reason, it is imperative that commutation failures be accurately modelled particularly when a disturbance is close to a converter terminal.

Voltage unbalance, high frequency transients, magnetising current inrush effects, and transformer saturation due to overvoltages can all contribute to possible commutation failures and cannot be adequately represented by conventional electro-mechanical stability analysis. Recent advances in stability programs offer detailed control solutions and advanced logic for determining HV*dc* control modes, but still cannot provide accurate dynamic analysis of the overall operation and recovery behaviour of a converter [Ong and Hamzeinejad, 1985] [Chapman *et al.*, 1988b] [Chapman *et al.*, 1988a].

Dynamic electromagnetic solutions such as EMTP and EMTDC can provide detailed elemental analysis of converters but are computationally expensive due to large storage requirements and the small time-steps necessary (typically 50μs for *dc* converters). In these types of simulations, the *ac* system representation must be restricted and consequently the *ac* system dynamic response is limited. In both electro-mechanical stability and elec-

tromagnetic transient programs modelling combined *ac* and *dc* systems, one system is always compromised by the limited representation of the other.

A hybrid simulation package takes advantage of the computationally inexpensive dynamic representation of the *ac* system in a stability program, with the accurate dynamic modelling of non-linearities. The slow dynamics of the *ac* system are sufficiently represented by the stability program, while at the same time, the fast dynamic response of the HV*dc* system is accurately modelled by electromagnetic means. A hybrid is also very useful in studying the impact of *ac* system dynamics, particularly weak *ac* systems, on *dc* system transient performance. Disturbance response studies, control assessment, and temporary overvoltage consequences are all typical examples for which a hybrid package is suited. Even for *ac* systems without *dc* converters, a hybrid package is useful for accurate modelling of such components as FACTS devices [Reeve *et al.*, 1991], synchronous or static compensators, and for the study of frequency dependent effects in transmission lines.

1.4.1 A Hybrid Historical Review

Heffernan *et al.* first proposed the detailed modelling of an HV*dc* system within a stability based *ac* system framework [Heffernan *et al.*, 1981]. The *dc* system was modelled using state variable techniques while the *ac* system was represented by a conventional stability program. Information interchange between the two programs required two independent fundamental frequency variables and these were chosen as real power and voltage. The voltage variable was derived by a standard Fast Fourier Transform (FFT) technique while real power was derived from an *rms* approximation.

Reeve and Adapa modified this hybrid idea by moving the interface location away from the converter terminals where distortion and phase imbalance were less prevalent [Reeve and Adapa, 1988] . An EMTP solution was used for the detailed analysis while the rest of the *ac* network was again modelled conventionally with a stability program. Although no mention was made of variable selection for interfacing, a curve fitting approach to fundamental data extraction replaced the *rms* and FFT methods of Heffernan *et al.* This allowed more flexibility for the stability step length to change, since Fourier analysis requires truncation of discrete data at exact multiples of the fundamental period.

A type of hybrid approach is used in the digital program NETOMAC [Kulicke, 1981] for analyzing electro-mechanical and electromagnetic transient phenomena. This program uses two separate modes for modelling to reduce the computational requirements. An instantaneous mode models components in three phase detail with small time steps in a similar way to the EMTP/EMTDC programs. The second mode is a stability mode and models the system in *rms* quantities at fundamental frequency only, with increased time step lengths. The program can switch between the two modes as required while running. The HV*dc* converter is either modelled elementally by resistive, inductive, and capacitive components, or by quasi-steady state equations, depending on the simulation mode. In either mode however, the entire system must be modelled in the same way. When it is necessary to run in the instantaneous mode, a system model of any substantial size would still be very computationally intensive.

1.5 Thesis Aim and Outline

In this thesis, an improved hybrid package has been developed based on the advantages found in the previous methods. A conventional electro-mechanical stability program is used, but in this case was interfaced to the commercially available and validated EMTDC electromagnetic transient program. EMTDC has the advantage of having an advanced graphical package allowing complex models to be easily built up from internal component libraries.

A curve fitting approach to variable measurement similar to Reeve and Adapa is adopted but with an interfacing protocol specifically designed for efficient extraction of the fundamental frequency from distorted and unbalanced waveforms. This allows the more efficient approach of Heffernan *et al.* in using the converter bus as the interface location between the two linked programs. The new hybrid also allows the flexibility of multiple interfaces at locations other than the converter bus. Multiple and independent detailed "islands" are in fact possible within the hybrid for modelling other components such as static VAr compensators and FACTS devices.

The interfacing variable options were examined and suitable variables identified. An efficient implementation of these variables is devised to allow both programs constituting the hybrid to maintain independent phase frames of reference. This prevents any possible drifting problems between the two programs during long simulation runs.

The concept of the NETOMAC hybrid is also implemented allowing the quasi-steady state model of the converter to interchange with the detailed dynamic model when appropriate.

Overall, an advanced and flexible hybrid program is created combining the optimum features of its predecessors. This hybrid is then applied to a realistic test system and various disturbances and effects analyzed.

Chapter 2 outlines the conventional stability analysis of power systems. The stability program used in the hybrid approach of this thesis is described along with the quasi-steady state modelling of HV*dc* converters.

In Chapter 3, an electromagnetic approach to the modelling of HV*dc* systems is summarised. This is based on Dommel's algorithm [Dommel, 1969] and is that used by such programs as EMTP and EMTDC.

Chapter 4 describes the fundamental frequency extraction method used in the hybrid program and compares this to other available frequency extraction methods. A variety of waveform disturbances are used to compare these methods and to derive an optimum window size and shape.

The advanced hybrid stability program is presented in Chapter 5. This is an integration of a positive sequence transient stability program and the electromagnetic transient program EMTDC.

Two important interfacing techniques are investigated in Chapter 6, that of interface variable selection and the interface location. The approach of using *rms* real power as an interface variable in a previous hybrid program is analyzed and alternative variables discussed. The two previous choices of interface location, that of the converter terminal and at some distance from the converter terminal, are examined with results presented.

In Chapter 7, the hybrid program developed is applied to a simplified version of the New Zealand South Island power system connected to an HV*dc* converter terminal. Various studies are performed using both the hybrid algorithm and just the stability program using a quasi-steady state representation of the *dc* converter. Results are presented and analyzed.

The conclusions are summarised in Chapter 8 and possible directions for future work discussed.

Chapter 2

ELECTRO-MECHANICAL TRANSIENT STABILITY

In a typical power system containing components such as generators, transmission lines, and loads, there is a need to ensure that the system is stable. The system stability can be defined as its ability to remain in synchronism when moving from one steady state operating point to another following a system disturbance. A disturbance can be something substantial, such as the loss of a generator or transmission line, or something less dramatic such as a change in load.

There is a natural tendency for parallel synchronous machines to operate in synchronism. If a machine slows down or speeds up then synchronising forces tend to bring it back to synchronous speed. An unbalance, however, between the generation and the load on a network produces a transient which causes the rotors of the synchronous machines to either accelerate or decelerate and swing. The acceleration causing these swings is produced by the accelerating torques exerted on the rotors as discussed in Section 2.2.1. If the rotor swing is large enough, then synchronism of the system may be lost.

Large power system networks can only be studied by digital computer methods due to the size of the matrices involved. Electro-mechanical transient stability analysis requires the solving of two types of equations, algebraic and differential. The network equations are algebraic while the machine equations consist of both algebraic and non-linear differential equations. The algebraic and differential equations can be solved on an iterative basis until a solution is reached for a particular time-step.

In a typical stability program, the initial steady state operating conditions are found from a load-flow analysis of the power system. A balanced three phase system is normally assumed for which only the positive sequence network is necessary to be modelled. The deviations from steady state frequency are small and so fundamental frequency only is considered. Any *dc* offset currents and harmonics in a stability program are also ignored.

2.1 The TS Program

The stability program used throughout this thesis is called TS and was originally developed in its basic form at the University of Manchester Institute of Science and Technology (UMIST) [Arnold, 1976]. It is a conventional multi-machine stability program with a fundamental frequency positive sequence network representation. Advanced component models such as multi-terminal HV*dc* links and static VAr compensators are available if required. The TS program also has the option of modelling both the negative and zero

sequence networks for analysis of unbalanced faults. This chapter presents the basics of transient stability modelling and relates in particular to the TS program.

2.2 Synchronous Machines

The electro-mechanical stability of synchronous machines is usually the most significant factor in transient stability analysis. Synchronous machine models are based on both algebraic and differential equations, the differential equations consisting of the electro-mechanical response aspect and the dynamic behaviour of the electrical characteristics.

2.2.1 Equations of Motion

A synchronous machine is a rotating body and therefore its mechanical equations can be derived from the laws of rotation.

The accelerating torque of a machine is defined by the product of the moment of inertia of the machine (I_{mi}) and the acceleration (α).

$$T_a = I_{mi}\alpha \tag{2.1}$$

In a generating machine, the driving torque is mechanical and the load torque is electrical. The overall accelerating torque is then :-

$$T_a = T_m - T_e \tag{2.2}$$

From equation 2.2 it is obvious that an increase in mechanical torque will provide an acceleration of the machine as will a decrease in the electrical torque.

If θ is defined as the rotor angle of the machine with respect to a reference frame rotating at synchronous speed ω_o then :-

$$\theta = \omega_o t + \delta \tag{2.3}$$

$$\dot{\theta} = \omega_o + \dot{\delta} \tag{2.4}$$

$$\ddot{\theta} = \ddot{\delta} \tag{2.5}$$

where δ = the initial position of the rotor with respect to the synchronously rotating reference frame

If $\ddot{\theta}$ is the acceleration of the rotor, then from equation 2.1 :-

$$\begin{aligned} T_a &= I_{mi}\ddot{\delta} \\ &= I_{mi}\dot{\omega} \end{aligned} \tag{2.6}$$

where ω = the shaft angular velocity

Since power is the product of torque and speed, then from equation 2.6 :-

$$P_a = I_{mi}\ddot{\delta}\omega \tag{2.7}$$

Angular momentum, M, is the product of the moment of inertia and the speed ($I\omega$). If the machine rotor speed is assumed constant at synchronous speed, which is a normal and accepted assumption for stability studies, then M is constant.

The accelerating power is then :-

$$P_a = M\ddot{\delta} \tag{2.8}$$

If the rotational power losses of the machine due to such effects as windage and friction are ignored, then the accelerating power equals the difference between the mechanical power and the electrical power. From equation 2.2, for a generator :-

$$P_a = P_m - P_e \tag{2.9}$$

$$M\ddot{\delta} = P_m - P_e \tag{2.10}$$

Equation 2.10 is known as the swing equation.

Another constant commonly referred to is H, the kinetic energy at rated speed per the rated power of the machine. H can be denoted as the inertia constant of the machine and is usually given in units of $(\frac{MWs}{MVA})$.

The angular momentum M can be defined in terms of H as follows:-

$$M = \frac{2G_r H}{\omega_o} \tag{2.11}$$

where G_r is the three phase MVA rating of the machine and ω_o is the synchronous speed. Inserting equation 2.11 into equation 2.10 gives :-

$$\frac{2G_r H}{\omega_o}\ddot{\delta} = P_m - P_e \tag{2.12}$$

or

$$\ddot{\delta} = \frac{\omega_o}{2G_r H}[P_m - P_e] \tag{2.13}$$

The *electrical* power angle δ_e is related to the angle δ by :-

$$\delta_e = N_p\delta \tag{2.14}$$

where N_p =number of pole pairs of the machine. Equation 2.13 then becomes :-

$$\ddot{\delta}_e = \frac{p\omega_o}{2G_r H}[P_m - P_e] \tag{2.15}$$

The mechanical motion of the synchronous machine can now be described by rewriting the second order differential equation (equation 2.15) into two first order differential equations.

$$\dot{\omega} = \frac{p\omega_o}{2G_r H}[P_m - P_e] \tag{2.16}$$

$$\dot{\delta_e} = \omega - \omega_o \tag{2.17}$$

where ω = actual machine speed

These equations describe the rotational swing of a synchronous machine. The swing curves of a network of machines will determine whether or not the system is able to remain in synchronism following a disturbance.

2.2.2 Electrical Equations

The electrical characteristic equations describing a three phase synchronous machine are commonly defined by a two dimensional reference frame. This is well documented in power system literature [Kimbark, 1956] [Clarke, 1950] and consists of using Park's transformations to transform currents and flux linkages (and therefore voltages) into two fictitious windings located on axes 90 degrees apart [Park, 1929] [Park, 1933]. These axes are fixed with respect to the rotor position. One axis coincides with the centre of the magnetic poles of the rotor (the d axis) while the other lies along the magnetic neutral axis (the q axis). Electrical quantities can then be expressed in terms of d and q axis parameters.

Since the synchronous machine has an inertia, preventing the flux linkages from changing instantaneously, machine models can be defined for steady state, transient, and sub-transient conditions depending on the speed of the external changes to the machine. The *d-q* phasor diagram for the *transient* machine model is shown in Figure 2.1.

Each phasor quantity can be represented in terms of its d and q axis components *ie.*:-

$$I = I_d + jI_q \tag{2.18}$$

$$V = V_d + jV_q \tag{2.19}$$

$$E = E_d + jE_q \tag{2.20}$$

The algebraic equations for the synchronous machine transient model in Figure 2.1 can be written as follows :-

$$E'_d - V_d = R_a I_d - X'_q I_q \tag{2.21}$$

$$E'_q - V_q = X'_d I_d + R_a I_q \tag{2.22}$$

where

E' = transient internal voltage
V = armature terminal voltage
R_a = *ac* armature resistance

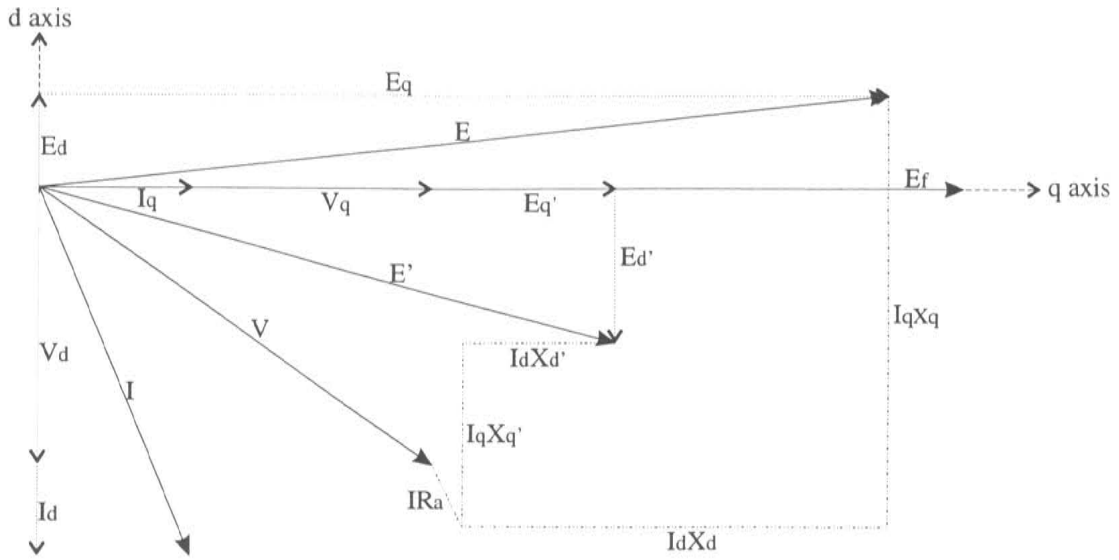

Figure 2.1 Phasor representation of a synchronous machine in the transient state

X' = transient reactance
I = armature current
and subscripts $_d$ and $_q$ denote the d axis and q axis components of the parameter respectively

These equations lead to the formulation of the transient differential equations :-

$$\frac{dE'_q}{dt} = \frac{\left[E_f - (X_d - X'_d)I_d - E'_q\right]}{T'_{do}} \tag{2.23}$$

$$\frac{dE'_d}{dt} = \frac{\left[(X_q - X'_q)I_q - E'_d\right]}{T'_{qo}} \tag{2.24}$$

where

E_f = field winding voltage
X = synchronous reactance
T'_o = transient open circuit time constant

The development of sub-transient equations is very similar to that for transient equations and yields the differential equations :-

$$\frac{dE''_q}{dt} = \frac{\left[E'_q - (X'_d - X''_d)I_d - E''_q\right]}{T''_{do}} \tag{2.25}$$

$$\frac{dE''_d}{dt} = \frac{\left[E'_d + (X'_q - X''_q)I_q - E''_d\right]}{T''_{qo}} \tag{2.26}$$

where

E'' = sub-transient internal voltage
X'' = sub-transient reactance
T_o'' = sub-transient open circuit time constant

Although the synchronous machine model is commonly represented as a voltage source behind a fixed impedance (either the transient or sub-transient reactance and the armature resistance), it is actually modelled in transient stability programs as a current source in parallel with a fixed admittance.

Advanced models can, to some extent, take into account saturation of the machine. This is possible in the TS program and is achieved by modification of the current injection used in representing the machine. The single phase, fundamental frequency nature of stability programs will, however, always limit the usefulness of this modelling.

2.2.3 Synchronous Machine Controllers

When stability analysis involves simulation times longer than about one second, any effects due to machine controllers such as speed governors and automatic voltage regulators must be incorporated.

It is no longer a reasonable assumption to consider the mechanical power (P_m) constant after the first transient stability swing. The variation in P_m must then be taken into account as it can have a significant effect on the system. The automatic voltage regulator can also have an appreciable effect on transient stability in its varying of the field voltage in attempting to maintain the terminal voltage constant. Speed and voltage controller models are thus necessary in a stability program.

Composite controller models can be constructed in the TS program to simulate the standard IEEE controller models [IEEE, 1968] [IEEE, 1973].

2.3 Static Network Components

With the positive sequence, fundamental frequency nature of stability programs, it is common to represent static equipment such as transmission lines and transformers by lumped equivalent π circuit parameters in the same way as with power-flow programs. The impedances of these network components are converted to admittances and included in an overall network admittance matrix. Fundamental frequency representation is deemed adequate since the frequency variation in stability analysis is usually small.

Loads in the network can be represented in a number of ways. The simplest method is to consider a load as a constant impedance. A better method is to use a general load characteristic [Dandeno and Kundur, 1973] where :-

$$P = k_p(V)^{pv}(f)^{pf} \tag{2.27}$$

$$Q = k_q(V)^{qv}(f)^{qf} \tag{2.28}$$

k_p and k_q are constants and dependent on initial values of P and Q. The values of pv, qv, pf, and qf are related to the type of load. Static loads are to a practical extent, unaffected by frequency (*ie.* $pf = qf = 0$) and with constant impedance loads, the factors qv and pv square the voltage value.

Typical values for load characteristic parameters are given in Table 2.3 [Berg, 1973].

Load Type	*pv*	*qv*	*pf*	*qf*
Fluorescent lamp	1.2	3.0	-1.0	2.8
Filament lamp	1.6	0	0	0
Heater	2.0	0	0	0
Induction motor (half load)	0.2	1.6	1.5	-0.3
Induction motor (full load)	0.1	0.6	2.8	1.8
Reduction furnace	1.9	2.1	-0.5	0

Table 2.1 Typical characteristic load equation parameters

HV*dc* converters can also be represented in this manner however each converter has its own control characteristics and due to its size, is a critical component and needs to be modelled accurately. HV*dc* links can sink or source significant amounts of power and their operations are crucial to system stability. The next section deals with the modelling of these devices in more detail.

2.4 HV*dc* Converter Modelling

HV*dc* converters are becoming increasingly more common in power systems and require special attention in power system analysis software. HV*dc* links, aluminium smelters, chlorine producing equipment *etc.* all rely on the conversion from *ac* to *dc*, and in the case of HV*dc* links, back to *ac* again. HV*dc* modelling can be quite complex since dynamically, the HV*dc* converter operates rapidly and usually under constraint from multiple control mechanisms. When perturbations are small, however, the HV*dc* response is predictable and very fast, and a modified steady state model is acceptable to use. Many electro-mechanical transient stability programs, including TS, utilise this approach.

2.4.1 The Six Pulse Converter Bridge

A basic building block of HV*dc* links is the three phase six pulse or Graetz converter bridge as shown in Figure 2.2. These bridges can be used on their own or more commonly, phase shifted through the converter transformer and connected in series on the *dc* side to produce a higher pulse number output.

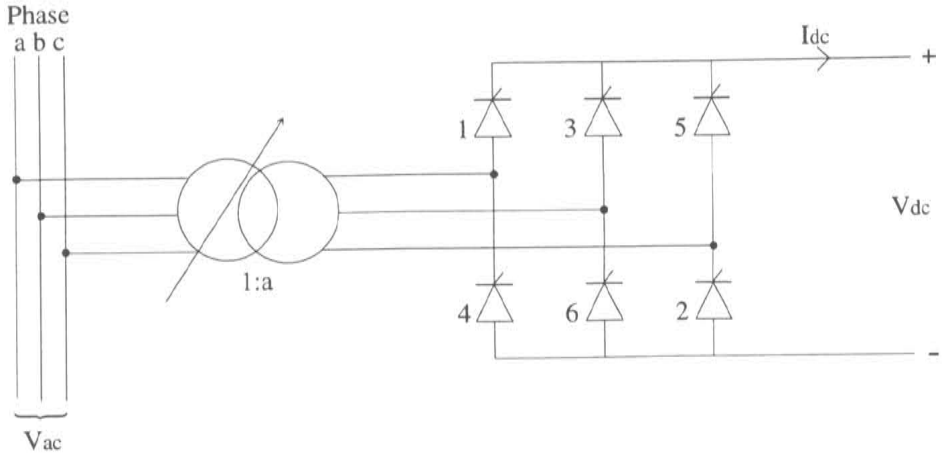

Figure 2.2 3 phase Graetz bridge

The analysis of the *ac-dc* conversion process is widely available in power system literature [Adamson and Hingorani, 1960] [Kimbark, 1971] [Arrillaga, 1983] and can produce the basic *dc* voltage equation for rectification :-

$$V_{dc} = \frac{3\sqrt{2}}{\pi} a V_{ac} \cos\alpha - \frac{3}{\pi} X_c I_{dc} \tag{2.29}$$

where

$V_{dc} = dc$ voltage
$a =$ off-nominal tap position of converter transformer
$V_{ac} = ac$ commutating voltage
$\alpha =$ firing angle of thyristor valve
$X_c =$ commutation reactance
$I_{dc} = dc$ current

The rectified *dc* voltage waveform is shown in Figure 2.3 with the "a" phase current shown underneath. When valve 1 or 4 in Figure 2.2 is conducting, then phase "a" current will flow as shown in Figure 2.3. The other phase currents will similarly flow when their respective valves are conducting. Any commutation reactance present in a converter prevents the phase current from changing instantly, and a period known as the commutation period, represented by the commutation angle (μ), exists as shown. With controlled valves such as thyristors, it is also possible to delay the normal conduction starting point of the valve by the firing angle (α).

The *ac* phase current is a quite distorted sinusoid and consequently has a high harmonic content. It is usual to install filters at the converter terminals to assist in eliminating these inherent conversion harmonics. Where filtering exists, it is usual to treat this as the point of sinusoidal *ac* waveforms and the reactance between this point and the converter valves, which is normally just the converter transformer, the commutation reactance.

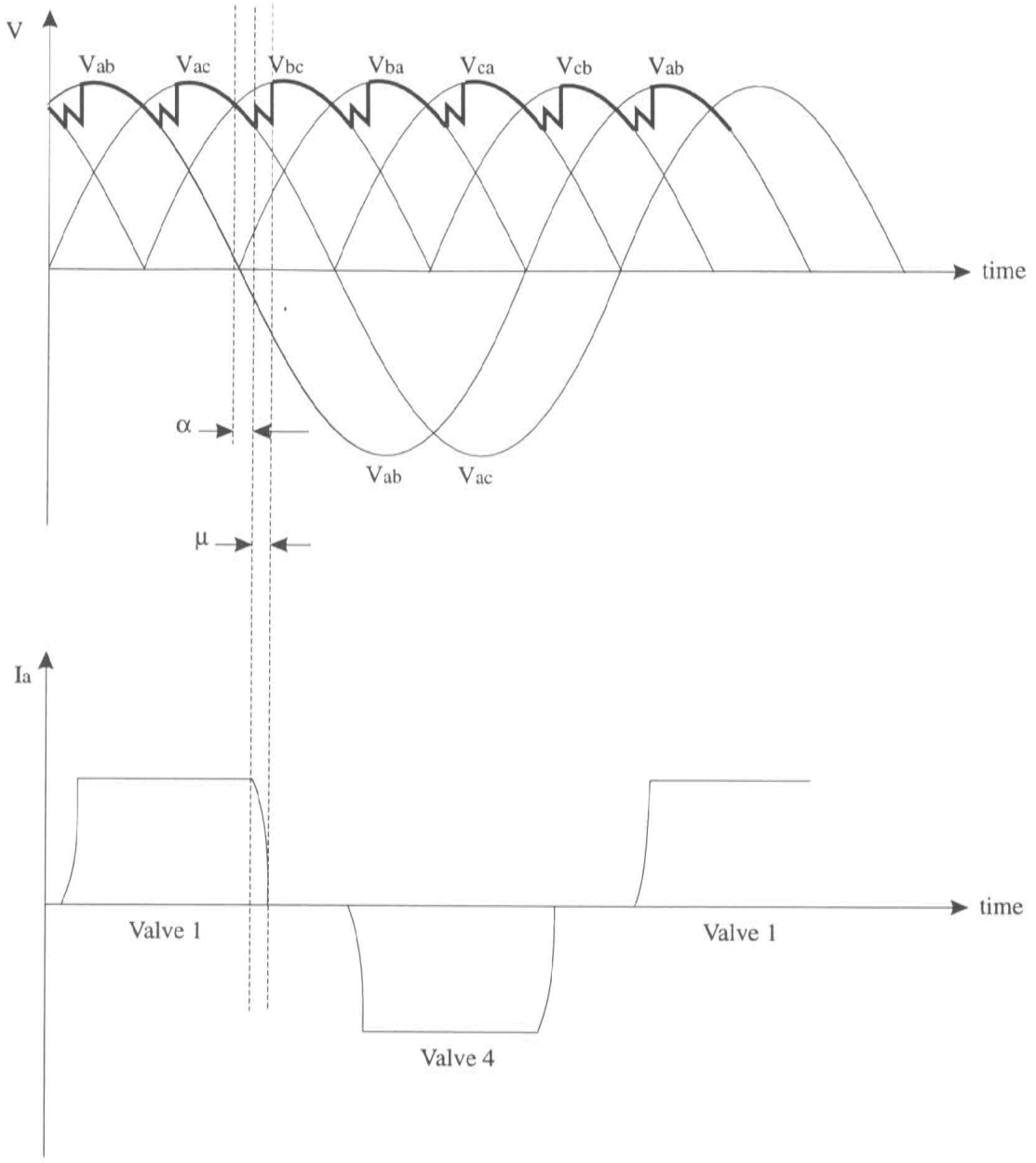

Figure 2.3 Voltage and phase current for rectification

Further analysis of the conversion process results in equations linking the commutation angle μ and the firing angle α [Arrillaga, 1983]:-

$$\mu = \cos^{-1}\left[\cos\alpha - \frac{\sqrt{2}X_c I_{dc}}{aV_{ac}}\right] - \alpha \tag{2.30}$$

and the *rms* fundamental component of *ac* current and the *dc* current :-

$$I_{f_{ac}} = k\frac{\sqrt{6}}{\pi}aI_{dc} \tag{2.31}$$

where

$$k = \frac{\sqrt{[\cos 2\alpha - \cos 2(\alpha+\mu)]^2 + [2\mu + \sin 2\alpha - \sin 2(\alpha+\mu)]^2}}{4\,[\cos\alpha - \cos(\alpha+\mu)]} \tag{2.32}$$

for $\mu \leq 60°$

Power equations can also be specified :-

$$P_{dc} = \sqrt{3} V_{ac} I_{f_{ac}} \cos\phi = V_{dc} I_{dc} \tag{2.33}$$

$$Q_{dc} = \sqrt{3} V_{ac} I_{f_{ac}} \sin\phi \tag{2.34}$$

and

$$\cos\phi = \frac{\cos\alpha + \cos(\alpha+\mu)}{2} \tag{2.35}$$

where

P_{dc} = the real power into the rectifier terminal
Q_{dc} = the reactive power into the rectifier terminal
ϕ = the power factor angle

Inversion from *dc* to *ac* is a similar process to rectification where the firing or delay angle is controlled and extended beyond 90 degrees. An active *ac* system is also required on the inverter side to provide a commutating *ac* voltage. Similar equations to rectification can be written but with the firing angle being replaced with the extinction angle γ. The relationship between various angles is given in Figure 2.4.

The *dc* equations given are only valid when the commutation angle μ is less than 60 degrees. If the commutation angle is beyond this, more than one valve will be conducting current and the equations will no longer apply. In the TS program, a shutdown procedure can occur for the *dc* terminal affected. Abnormal operation at an inverter terminal can cause the inverter bridge(s) to be bypassed, while abnormal operation at a rectifier terminal can cause the rectifier bridge(s) to be blocked [Giesner and Arrillaga, 1970].

2.4.2 Solution of the *dc* Equations

Electro-mechanical transient stability programs are conventionally initialised from load-flow solutions. The parameters for any *dc* link are also taken from the load-flow solution. Any current or power setting of a converter terminal can be calculated, if necessary, from these parameters. For a two terminal link, the power setting can be equated to the initial power flow and the current setting then calculated. For multi-terminal links, the current setting can be determined from the active and reactive power transfer and the voltage at

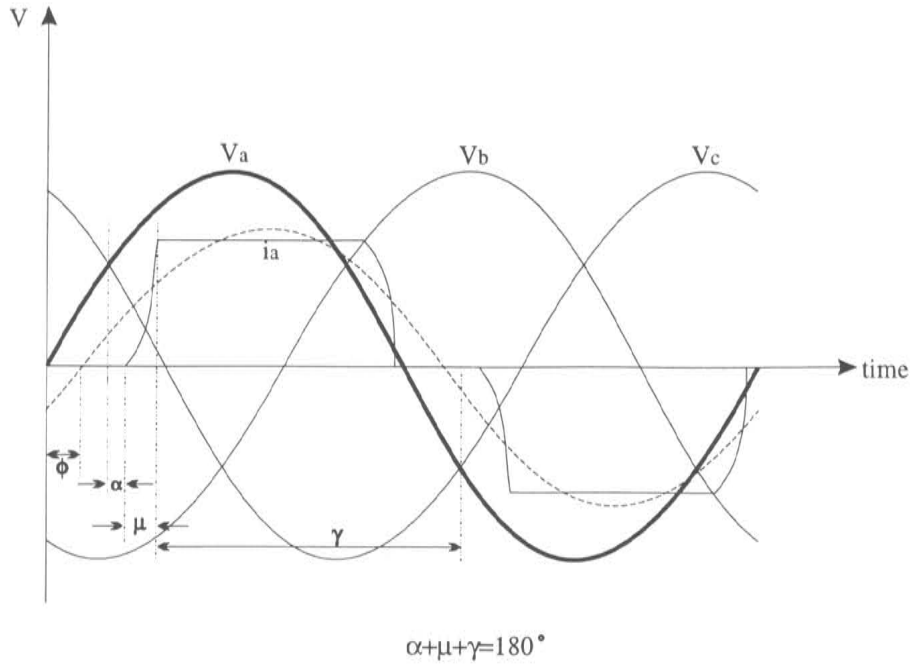

Figure 2.4 Angle relationships

the converter terminal *ie.* :-

$$I_{dc} = \frac{\sqrt{P_{dc}^2 + Q_{dc}^2}}{\frac{3\sqrt{2}}{\pi} a V_{ac} k} \tag{2.36}$$

$$V_{dc} = \frac{P_{dc}}{I_{dc}} \tag{2.37}$$

The current setting can then be calculated from the *dc* voltage and current :-

$$I_{ds} = I_{dc} + \frac{V_{dc}}{k_c} \tag{2.38}$$

where

I_{ds} = current setting
k_c = current setting controller amplifier gain

The power setting is simply the product of *dc* voltage and the current setting :-

$$P_{ds} = I_{ds} V_{dc} \tag{2.39}$$

Normally, one of the HV*dc* link terminals is specified to be in a constant voltage mode, while any other terminals are likely to be in a constant current mode. A rectifier terminal in

a constant voltage mode is at minimum firing angle (α_{min}) while an inverter terminal in a constant voltage mode is at minimum extinction angle (γ_{min}). In a constant current mode, a terminals firing or extinction angle is simply controlled to maintain a set *dc* current.

In the TS program, the mode of any *dc* terminal is tested at each time-step to ensure that the control mode is correct. For the rectifier terminal, equating equations 2.29 and 2.38 to eliminate I_{dc} and solving for V_{dc} gives :-

$$V_{dc_{(test)}} = \frac{\frac{\sqrt{2}aV_{ac}\cos\alpha_{min}}{X_c} - I_{ds}}{\frac{\pi}{3X_c} - \frac{1}{k_c}} \tag{2.40}$$

If $V_{dc} < V_{dc_{(test)}}$ and the terminal is in constant voltage mode, or $V_{dc} > V_{dc_{(test)}}$ and the terminal is in constant current mode, then the mode is incorrect. A new mode is then assumed and the mode determination re-examined. This is similarly done for the inverter terminal.

Once the mode is established, the other variables at the terminals can be evaluated. The firing, commutation, and power angles can be calculated from equations 2.29, 2.30, and 2.35 respectively, while the power can be determined from equations 2.33 and 2.34.

Each terminal of a converter can be represented by an admittance and a current source in the overall *ac* network equation as shown in Figure 2.5. An admittance value for the converter terminal, to include in the overall network admittance matrix, is derived from initial load-flow results :-

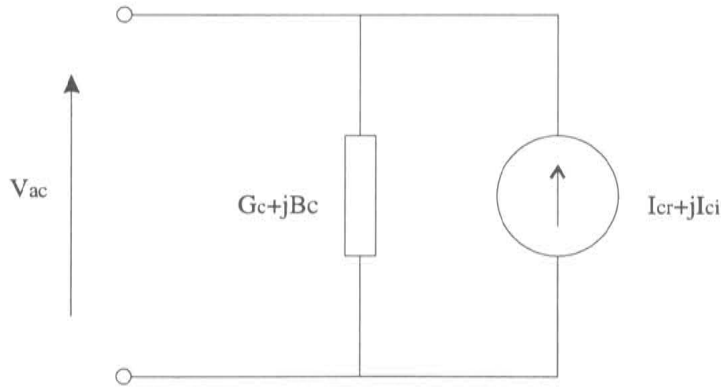

Figure 2.5 Converter representation

$$G_c = \frac{P_{dc}}{V_{ac}^2} \tag{2.41}$$

$$B_c = \frac{-Q_{dc}}{V_{ac}^2} \tag{2.42}$$

The current injections at each time-step can be calculated by working out the admittance difference between the actual and initial values of the converter at each step *ie.* :-

$$G = \frac{P_{dc}}{V_{ac}^2} - G_c \tag{2.43}$$

$$B = \frac{-Q_{dc}}{V_{ac}^2} - B_c \tag{2.44}$$

.... and adjusting the current source appropriately to compensate :-

$$I_{cr} = -V_{ac_r} G + V_{ac_i} B \tag{2.45}$$

$$I_{ci} = -V_{ac_i} G - V_{ac_r} B \tag{2.46}$$

where

I_{cr} = the real component of the converter equivalent current source
I_{ci} = the imaginary component of the converter equivalent current source
V_{ac_r} = the real component of V_{ac}
V_{ac_i} = the imaginary component of V_{ac}

The *ac* and *dc* systems are solved sequentially until convergence is obtained.

2.4.3 HV*dc* Controls

It is also necessary to model HV*dc* controls in electro-mechanical transient stability programs [Arrillaga and Arnold, 1990]. A terminal controller measures input variables at a terminal and modifies the firing/extinction angle or the current setting as required.

A central controller is also necessary, having control over the overall link. This control must measure variables at all terminals and should be capable of changing the current order or setting, the firing/extinction angle, or any other terminal variables as required.

Controls are generally built up from generic building block functions such as integrators, limiters, mathematical functions *etc.*

2.5 Network Solution

The overall system network is represented by a complex and square admittance matrix and a vector of injected currents. The form of the network equation is the same as for load-flow and fault programs *ie.*

$$[I_{inj}] = [Y][V] \tag{2.47}$$

where

$[I_{inj}]$ = vector of injected currents
$[Y]$ = admittance matrix
$[V]$ = node voltage vector

The solving of equation 2.47 for the node voltages can be done in several ways. The most obvious is to obtain the inverse admittance matrix and solve $[V]$ directly. The admittance matrix is sparse, however, whereas the inverse admittance matrix is full. These matrices can also be very large since their size is proportional to the square of the number of buses. A method exploiting the sparsity of the admittance matrix is a preferred solution.

The TS program uses a very economical method for solving equation 2.47 in conjunction with sparsity techniques to take advantage of the sparsity of $[Y]$. Bifactorisation techniques are used where the admittance matrix is reduced to an upper triangular form and the node voltage vector solved by backward substitution [Zollenkopf, 1972]. The admittance matrix need only be re-triangularised whenever the network topology undergoes a change. A fault application or removal at an existing bus does not affect the network topology but the bifactored matrix elements must be re-evaluated.

The integration method used by TS for the solving of the differential equations is the implicit trapezoidal method [Dommel and Sato, 1972]. This is numerically stable and works well for stiff systems.

Chapter 3

ELECTROMAGNETIC TRANSIENT ANALYSIS

In electro-mechanical stability studies, the concern is predominantly with the oscillatory response of generators after a disturbance. Electromagnetic analysis on the other hand, investigates the relatively fast electromagnetic interactions between circuit elements, and the effects of travelling wave propagation along transmission lines.

As the speed of response of some power system components increases, non-linear interactions between components and controls can cause waveform distortion degrading system performance. Analysis by conventional fundamental frequency means, such as with load-flow and electro-mechanical stability programs, are inadequate for these problems. Electromagnetic transient analysis however, is one effective method of modelling these effects.

The phrase "electromagnetic transient analysis" can actually encompass many different methods of simulation including z-transform analysis [Humpage *et al.*, 1980], state space analysis [Kuh and Rohrer, 1965], travelling wave methods [Dommel and Meyer, 1974], the use of Transient Network Analyzers (TNAs) *etc.* Electromagnetic transient analysis in this thesis, however, refers only to the simulation technique proposed by Dommel and described in this chapter [Dommel, 1969]. This type of approach is now widely used for accurate power system simulation, particularly for *ac* systems incorporating dynamically fast devices that are subject to multiple switchings over short periods such as HV*dc* converters, FACT systems, and static VAr compensators.

3.1 Electromagnetic Transient Programs

The algorithm proposed by Dommel in 1969 led to the development of a program called EMTP (the ElectroMagnetic Transient Program) in the early 1970's by the Bonneville Power Administration. This was an excellent platform for *ac* system studies but some difficulties were encountered, because of frequent switchings, when users tried to model HV*dc* systems within EMTP. This encouraged the development of a new program, based on the same EMTP algorithm, called EMTDC (the ElectroMagnetic Transient DC program). EMTDC was created at Manitoba Hydro in Canada, and initially concentrated on appropriate models for HV*dc* converters and controls. Enhancement of the program continued at the Manitoba HV*dc* Research Centre and EMTDC now has accurate and advanced models for both *ac* and *dc* system components. In recent development, emphasis has been placed on the quick assembly of complex power systems through graphical

component libraries.

EMTP also went through considerable development with the introduction of models for rapidly switched components. A system to model control functions, TACS (Transient Analysis of Control Systems), was also introduced in the late 1970's. TACS is particularly suitable for modelling HV*dc* controls but can also be used for other purposes such as machine controllers. Transmission line models in EMTP have been well validated and the modelling of transmission cables is also possible.

Another widely used program that is based on the EMTP algorithm is called NETOMAC [Kulicke, 1981]. NETOMAC is actually a combination of an electromagnetic and an electro-mechanical transient analysis. The electromagnetic transient mode dynamically simulates the power system as with the EMTP approach, while the electro-mechanical mode models components as fundamental frequency positive sequence as in the stability program method presented in Chapter 2. The program automatically changes mode when conditions require it during a simulation run.

3.1.1 Network Formulation

Electromagnetic transient programs, basing their modelling on Dommel's algorithm, represent lumped inductors and capacitors as resistive elements in parallel with a current source as shown in Figure 3.1. Through this method, complex networks of devices represented by elemental components can be reduced to a network of only conductances and current sources. This approach is based on the application of the trapezoidal rule in the integration of the first order linear differential equations describing either an inductor or a capacitor.

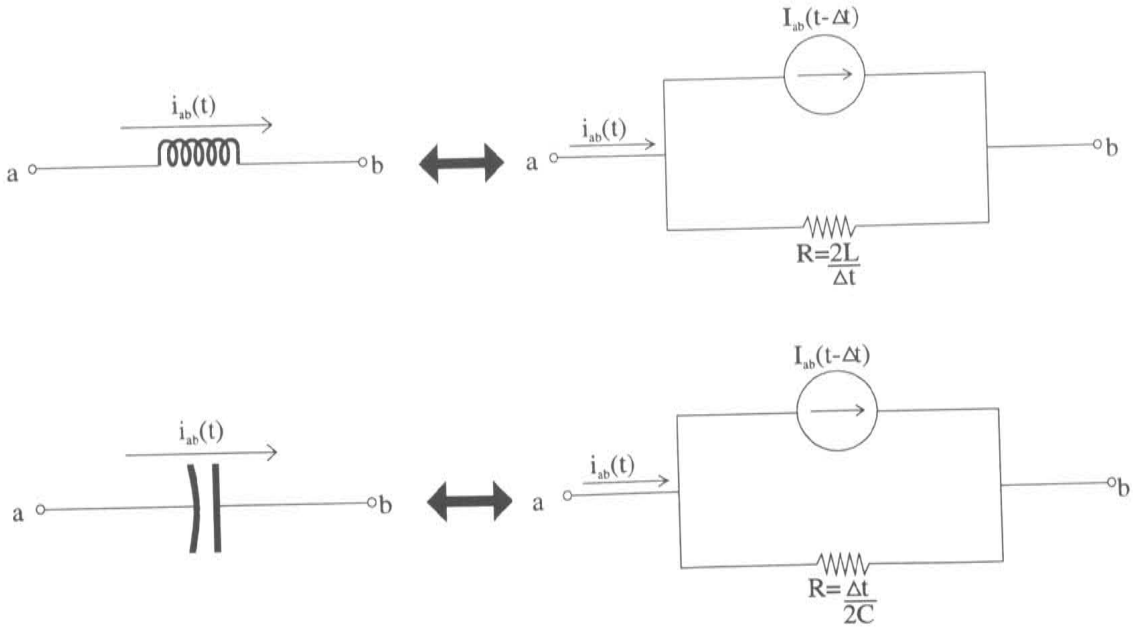

Figure 3.1 Modelling of reactive components

For the inductor, the current source value is :-

$$I_{ab}(t-\Delta t) = i_{ab}(t-\Delta t) + \frac{\Delta t}{2L}\left[V_a(t-\Delta t) - V_b(t-\Delta t)\right] \tag{3.1}$$

and for the capacitor :-

$$I_{ab}(t-\Delta t) = -i_{ab}(t-\Delta t) + \frac{2C}{\Delta t}\left[V_a(t-\Delta t) - V_b(t-\Delta t)\right] \tag{3.2}$$

where

Δt = the interval between successive time-steps in the calculation
$V_a(t-\Delta t)$ = Node "a" voltage at the previous time-step
$V_b(t-\Delta t)$ = Node "b" voltage at the previous time-step
$i_{ab}(t-\Delta t)$ = current flowing from node "a" to node "b" at the previous time-step

The current sources depend on both time and historical values and it is necessary to update these sources at each time-step. The resistance (or conductance) values only change when switching in the network takes place.

From Figure 3.1, at a given time-step, the current through a reactive element is :-

$$i_{ab}(t) = \frac{V_a(t) - V_b(t)}{R} + I_{ab}(t-\Delta t) \tag{3.3}$$

where

$R = \frac{2L}{\Delta t}$ for an inductor or
$R = \frac{\Delta t}{2C}$ for a capacitor

An admittance nodal solution is then used to solve the set of linear equations which can be written from the computer model of conductances and current sources.

In matrix form :-

$$[i(t)] - [I(t-\Delta t)] = [G]\,[V] \tag{3.4}$$

where

$[V]$ = vector of node voltages
$[G]$ = the nodal admittance matrix
$[i(t)]$ = vector of nodal current injections
$[I(t-\Delta t)]$ = vector of current source history terms

The total number of nodes in the network can be divided into two groups and equation 3.4 partitioned as follows :-

$$\begin{bmatrix} i_A(t) \\ \cdots \\ i_B(t) \end{bmatrix} - \begin{bmatrix} I_A(t-\Delta t) \\ \cdots \\ I_B(t-\Delta t) \end{bmatrix} = \begin{bmatrix} G_{AA} & \vdots & G_{AB} \\ \cdots & \cdots & \cdots \\ G_{BA} & \vdots & G_{BB} \end{bmatrix} \begin{bmatrix} V_A \\ \cdots \\ V_B \end{bmatrix} \tag{3.5}$$

If vector $[V_A]$ denotes known voltage values, and vector $[V_B]$ denotes unknown voltage values, then the unknown voltages can be determined from :-

$$[G_{AA}]\,[V_A] = [i_A(t)] - [I_A(t - \Delta t)] - [G_{AB}]\,[V_B(t)] \tag{3.6}$$

3.1.2 Travelling Waves

The common method of analysis for travelling waves is based on Bergeron's technique of using linear relationships between voltage and current [Bergeron, 1949]. This method utilises a distributed L-C parameter travelling wave line model with lumped resistance. The model is essentially single frequency and produces a constant surge impedance.

Figure 3.2 Example transmission line

Bergeron analysis of the transmission line in Figure 3.2 gives rise to the model in Figure 3.3 :-

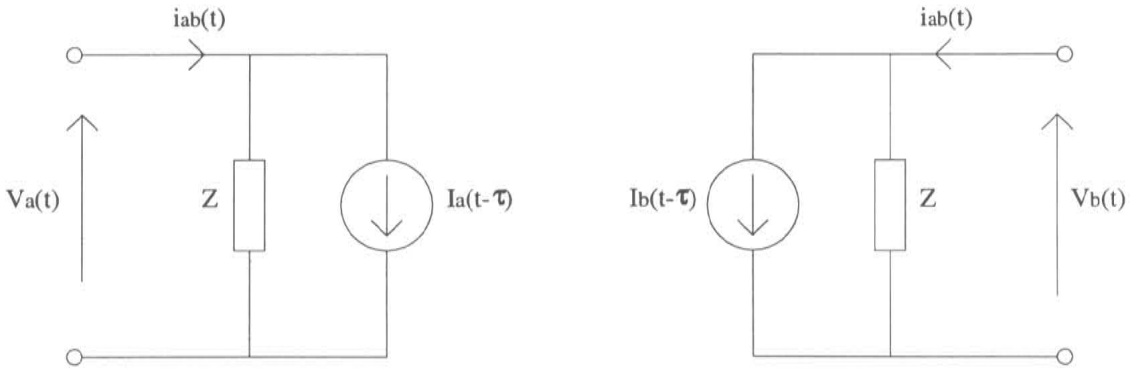

Figure 3.3 Transmission line model

The equations for the model are :-

$$i_{ab}(t) = \frac{V_a(t)}{Z} + I_a(t - \tau) \tag{3.7}$$

$$i_{ba}(t) = \frac{V_b(t)}{Z} + I_b(t - \tau) \tag{3.8}$$

where

τ = travel time of the wave
Z = surge impedance of transmission line

The current sources in Figure 3.3, $I_a(t-\tau)$ and $I_b(t-\tau)$, are historical values and therefore known. They can be defined as :-

$$I_a(t-\tau) = \frac{-V_b(t-\tau)}{Z} - i_{ba}(t-\tau) \tag{3.9}$$

$$I_b(t-\tau) = \frac{-V_a(t-\tau)}{Z} - i_{ab}(t-\tau) \tag{3.10}$$

More advanced analysis of transmission lines is possible by taking into account frequency dependence of the distributed parameters. All parameters, including the resistance, can be distributed and the frequency response calculated at multiple frequencies over a specified range. Approximating functions can then be created consisting of a number of poles and zeros that will match the calculated results at each specified frequency. This can be done for all transmission line modes. The approximating functions are then used in the analysis of the line.

3.2 Program Selection for the Hybrid Application

An *ac-dc* hybrid approach for power system simulation, where a detailed three phase program is combined with an electro-mechanical stability program, was outlined in Section 1.4 of this thesis. The original hybrid approach of Heffernan *et al.* used a state variable program, TCS, for its detailed analysis [Heffernan *et al.*, 1981]. Reeve and Adapa in a later hybrid chose the electromagnetic program EMTP [Reeve and Adapa, 1988]. The reasons for the EMTP approach over TCS given by Reeve and Adapa were that TCS offered only a customised *dc* solution and that the program was non-standard and unvalidated. TCS, however, has now been more comprehensively validated and the *dc* solution can now be easily modified to cover any configuration [Arrillaga *et al.*, 1991].

The electromagnetic programs EMTP and EMTDC are widely used in the power system field and both offer the efficiency and accuracy necessary for the detailed part of hybrid solutions. The state space formulation, although perhaps more accurate for fast switching devices, is inherently a complex and time-consuming process. The more popular EMTP/EMTDC formulation based on Dommel's algorithm was therefore maintained for the hybrid described in this thesis.

EMTDC has been more specifically designed for HV*dc* systems which is precisely the part of the power system requiring detailed modelling in a hybrid. EMTDC is also now encompassed by a graphical user interface, PSCAD (Power System Computer Aided Design), which simplifies the assembly of complex circuits and controls. A graphical representation of the required circuit can be built up visually from established component

libraries and then from this, the data and source code files necessary for simulation can be automatically written.

EMTDC also utilises the concept of subsystems (refer Section 3.3.3) which can improve the speed of the solution if the circuit is complex. The subsystem approach is also valuable in a hybrid package when multiple detailed "islands" in the overall stability representation are necessary. Each island modelled in detail can be represented as one independent subsystem in EMTDC. This provides an alternative solution to modelling multiple islands in one system and then having to employ sparsity techniques to minimize computation time. For these reasons, the EMTDC program was chosen as the detailed analysis for the hybrid package described in Chapter 5.

3.3 The EMTDC Program

3.3.1 Network Solution

In Section 3.1.1, the network solution of electromagnetic transient programs was shown to be of the form :-

$$[I] = [G][V] \tag{3.11}$$

where the node voltages must be calculated from the conductances and the injected currents.

To maximise both speed and efficiency, EMTDC uses a solution based on an algorithm proposed by Tinney and Walker [Tinney and Walker, 1967]. In this method, inversion of the conductance matrix is avoided and replaced by triangularisation. Sparsity is not exploited to maintain compatibility with earlier versions of the EMTDC program. This has an additional advantage of slightly increasing the speed of the solution by eliminating the need for re-indexing the collapsed non-zero conductance elements. Storage memory required is not reduced but through the use of subsystems, this is not a significant problem.

The EMTDC solution also employs some specialised features such as the interpolation of switching instants between the discrete time-step dictated solution points. Switching interpolation takes place after the solving of the linear equations to find the new node voltages. All switching devices are then polled, and the node voltages and branch currents interpolated back to their switching instant. After the history terms are recalculated at the exact point of switching, a final interpolation is applied to restore the solution back to its regular time-step location.

Switching actions can often cause chatter between successive time-steps in programs such as EMTDC which are trapezoidal integration based. A half time-step interpolation process is also implemented to avoid node voltage and branch current chatter that is possible in inductor and capacitor elements respectively.

3.3.2 *Dc* System Analysis

An HV*dc* system can consist of many components, some of which are also common to *ac* systems. The heart of conversion from *ac* to *dc* or vice versa is the converter valve group component. A typical 6 pulse, 3 phase Graetz bridge is shown in Figure 3.4. The basic equations relating to the conversion of *ac* to *dc* have already been outlined in Section 2.3 of Chapter 2.

EMTDC uses a modular approach to the converter valve group component, to simplify the complex firing and phase displacement co-ordination between the individual valves. These valves are generally controllable and either mercury arc vacuum tubes or solid state thyristors.

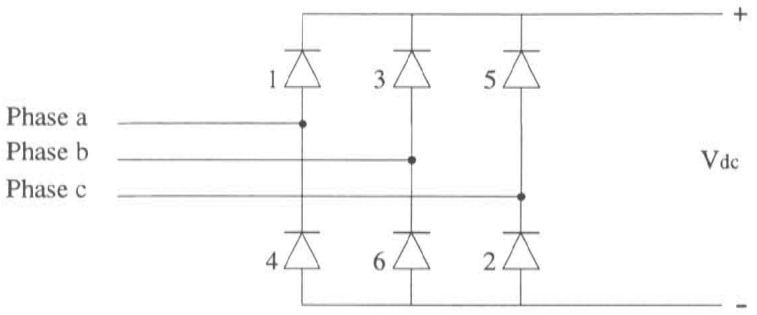

Figure 3.4 3 phase Graetz bridge

The elemental representation of an individual valve is shown in Figure 3.5. The valve can be represented by a switch with the switch position closed for the valve turned on, and open for the valve turned off. The valve switch can then be modelled as a variable impedance with a very low or high resistance value depending on its state. The advantage of this is that the topology of the circuit is constant while only the parameter values change with time. An R-C snubber circuit usually exists across the valve as shown :-

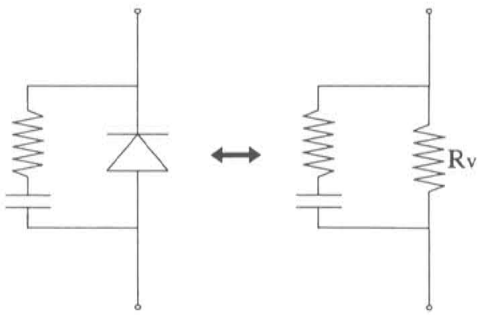

where Rv is a low or high resistance value depending on the valve state

Figure 3.5 Valve equivalent circuit

EMTDC has two firing control systems available. One is based on the phase locked oscillator while the second is a more advanced system based on a transvektor PLL os-

cillator [Gole and Sood, 1990] and incorporates interpolation for the switching of valves between time-steps.

HV*dc* converter controls are also necessary and are vital to the dynamic operation of an HV*dc* system. EMTDC uses a library of Continuous System Modelling Functions (CSMF's) to model such functions as integrators, limits, logic functions, delays *etc*. These building block control components are then interfaced to the electrical circuit of the *ac-dc* system.

3.3.3 Subsystems

EMTDC uses the concept of disconnected sub-networks or subsystems in the solution of power system circuits. Where possible, the overall system is split into discrete subsystems. This can usually be done where a part of the overall electric circuit is connected to other parts by only transmission lines. The transmission line model is represented by travelling waves and so at a given time-step, a perturbation in a part of the circuit separated by a transmission line will not impact on the rest of the circuit in that same time-step. Only at the arrival of the travelling wave will the perturbation be transferred. Electric circuits separated by transmission lines can then be decoupled and entered into EMTDC as separate subsystems.

Since subsystems are decoupled, a separate conductance matrix can be utilised for each individual subsystem. This eliminates the necessity for one large overall conductance matrix and considerably reduces the number of zero elements. Any switching event in a subsystem will now only affect that particular subsystem conductance matrix.

The use of subsystems reduces the necessity for sparsity techniques and is one reason why EMTDC stores the full conductance matrix for each subsystem. Since collapsing and re-indexing the conductance matrix is not necessary, the overall solution can be a faster process.

3.3.4 The Algorithm

A simplified steering flow chart for EMTDC is given in Figure 3.6. After the initialisation of arrays, a simulation can be started from either a data file or a snapshot. A data file is automatically generated by EMTDC's PSCAD front-end once the graphical representation of the network has been entered. A snapshot is a file created during a previous simulation run of EMTDC. During a simulation, and at a desired instant in time, a snapshot can be taken of the circuit, storing the parameter information for all the devices at that moment. This snapshot can then be used as the starting point for another simulation run if required.

Once the input data is read, the main time loop is entered and the time is advanced by one time-step. The current injection history terms are then calculated and any transmission line data processed. The first of two user definable subroutines, the DSDYN (Digital System DYNamic) file is then entered. Any statements representing a time domain model or process are contained in this file. The DSDYN file is again, automatically generated through the PSCAD front-end from the graphical system network that a user has entered.

The node voltages are now found by solving the network equation. If any switching in

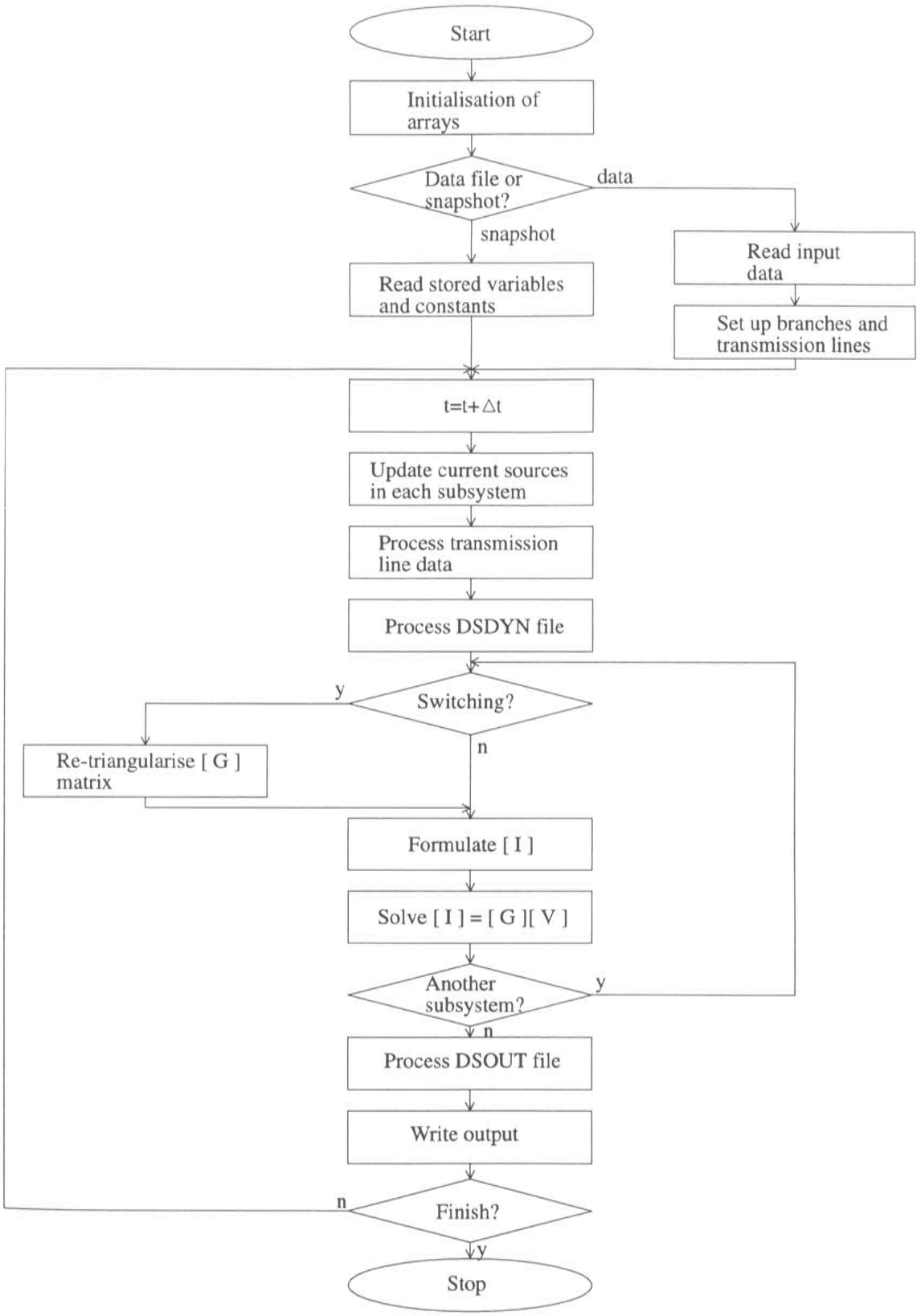

Figure 3.6 EMTDC steering routine

the network occurs in a particular subsystem, the conductance matrix for that subsystem is re-triangularised.

The second of the user defined subroutines, also generated through the PSCAD front-end, is then called. The DSOUT (Digital System OUTput) file defines any output variables to be monitored. These variables are written out to a file and the main time loop continued until the program finish time is reached.

Chapter 4

FUNDAMENTAL FREQUENCY EXTRACTION

Extracting the fundamental frequency from distorted and unbalanced discrete waveforms is often required in power system analysis. Fundamental frequency data can be required for voltage stability purposes, control, or for hybrid program interfacing as described in Chapter 5. Hybrid programs require fundamental frequency data to be extracted from the point oriented waveform analysis of the part of the system modelled in detail. This fundamental frequency three phase data is then converted to positive sequence, and included in an electro-mechanical transient stability program representing the rest of the power system.

Various methods can be utilised to extract fundamental frequency data from time domain waveforms including Fourier transform processing and curve fitting. Waveforms can be quite distorted and unbalanced under fault conditions which can make extraction of data difficult. An efficient curve fitting algorithm for extracting fundamental frequency data is described in this chapter. The technique is used to extract information from a variety of distorted and unbalanced waveforms and the results compared with the fast Fourier transform method. Different windowing techniques are used for both Fourier analysis and the curve fitting algorithm and the results presented.

4.1 Data Extraction Methods

4.1.1 *Rms* Approximation

One of the simplest methods for determining a waveforms fundamental frequency information is to use an *rms* approximation. From discrete data, *rms* values are very quick and easy to evaluate. These values include not only the fundamental frequency component but also all of the harmonic components present in the waveform. If the sum of the harmonic components are small, then the data can be used as an approximation to fundamental frequency. Heffernan *et al.* , when deriving variables for hybrid interfacing, showed that *rms* voltage was not generally a good approximation for true fundamental frequency voltage [Heffernan *et al.*, 1981]. The *rms* real power however, was used as an approximation to fundamental real power on the basis that harmonic real power flow will result only from in-phase components of harmonic voltage and current. The assumption was made that if a system contains only a low resistive component, then the harmonic real power flow is not significant. This is not entirely valid for all system configurations,

particularly at the inverter end of HV*dc* links, and should not be assumed [Bowles, 1970]. Under fault conditions in particular, where the waveform can be severely distorted, use of an *rms* value is not an accurate approximation for a fundamental frequency component. In addition, no phase information is available with *rms* derived quantities. The use of *rms* quantities and particularly *rms* real power as an interfacing variable is discussed further in Chapter 6.

4.1.2 Fourier Transform

The discrete Fourier transform (DFT) is a very common tool for harmonic analysis and widely used when analyzing distorted waveforms. It is especially useful to separate out periodic components from a waveform which may not visually display periodicity. The DFT can be derived from the continuous Fourier transform and is inherently useful for digital computers since both the time and frequency domains can be represented by discrete values. Because of the transforms discrete nature however, data must be periodically truncated for analysis. This must be done at a multiple of the longest periodic component of the waveform analyzed. The effect of truncation at other than a period multiple is to introduce spectral leakage into the analysis [Harris, 1978].

The difficulty with the DFT is that it is computationally expensive. The mathematical equations necessary to solve a full DFT are proportional to n^2 where n is the number of samples per truncated period [Bloomfield, 1976]. In the electromagnetic transient analysis of power systems, particularly if *dc* converters are modelled, time-steps are in the order of $50\mu s$. Over a cycle of a 50 Hz wave, there are 400 samples at this sampling rate. This generates around 160,000 equations to solve per cycle and so makes the DFT computationally prohibitive.

The Fast Fourier Transform (FFT) is an algorithm for computing the DFT of a data series at all of the Fourier frequencies using relatively few arithmetic operations [Bloomfield, 1976] [Brigham, 1988]. It has the advantage of the computational time being proportional to only $n \log_2 n$ compared with n^2 for the DFT [Kay and Marple, 1981]. For this reason it is a desirable method to solve the DFT and commonly used in power system harmonic analysis.

This method was also used by Heffernan *et al.* in the extraction of fundamental frequency information. Various shaped data windows were used to counter spectral leakage due to non-periodic noise effects. Windows were shown to have minimal effect on results. The use of these different window functions also suffers from a trade-off between leakage and resolution since with data windows other than unit rectangular, the FFT is less accurate in resolving frequencies.

4.1.3 Curve Fitting

In Fourier analysis, all the Fourier frequency components of the distorted waveform can be derived. However in the hybrid analysis described in this thesis, only fundamental frequency information is required. Using a simple curve fitted approach, this fundamental component only is measured.

Curve fitting selects the best fit of a curve to a waveform and measures the discrete residual values between the waveform and the fitted curve. In a least squares method, the size of these residuals are measured by the sum of their squared values. This is then minimised to obtain the least squared error, and the amplitude and phase of the best fitted curve calculated. Least squares curve fitting has both computational and theoretical advantages over Fourier processing. Its disadvantage though, is that it can be sensitive to a few "large" errors. Large perturbations in the analyzed waveform can affect the transform of less highly structured data [Bloomfield, 1976]. A least squares curve fitted approach is most useful when periodicity clearly exists in the data. This is the case in the power system field since the fundamental component is most commonly predominant. Also of particular advantage is that in a curve fitted approach, it is not necessary to truncate data exactly every period as with the Fourier transform.

4.2 The Curve Fitting Algorithm

A curve fitting algorithm was developed to extract the fundamental frequency data based on a least squared error technique. It can be described as follows:- Assume a sinewave signal with a frequency of ω radians per second and a phase shift of ψ relative to some arbitrary time T_o.

$$y(t) = Asin(\omega t - \psi) \tag{4.1}$$

where $\psi = \omega T_0$

This can be rewritten as :-

$$y(t) = Asin(\omega t)cos(\omega T_0) - Acos(\omega t)sin(\omega T_0) \tag{4.2}$$

Letting $C_1 = Acos(\omega T_0)$ and $C_2 = Asin(\omega T_0)$ and if $sin(\omega t)$ and $cos(\omega t)$ are represented by functions $F_1(t)$ and $F_2(t)$ respectively, then :-

$$y(t) = C_1F_1(t) + C_2F_2(t) \tag{4.3}$$

$F_1(t)$ and $F_2(t)$ are known if the fundamental frequency ω is known. However, the amplitude and phase of this frequency generally need to be found, so the equation has to be solved for C_1 and C_2. If the signal $y(t)$ is distorted, then its deviation from a sinusoid can be described by an error function E.

$$x(t) = y(t) + E \tag{4.4}$$

For a least squares method of curve fitting, the size of the error function is measured by the sum of the individual residual squared values such that :-

$$E = \sum_{i=1}^{n} \{x_i - y_i\}^2 \tag{4.5}$$

where $x_i = x(t_0 + i\Delta t)$ and $y_i = y(t_0 + i\Delta t)$.

From equation 4.3 :-

$$E = \sum_{i=1}^{n} \{x_i - C_1 F_1(t_i) - C_2 F_2(t_i)\}^2 \tag{4.6}$$

where the residual value r at each discrete step is defined as :-

$$r_i = x_i - C_1 F_1(t_i) - C_2 F_2(t_i) \tag{4.7}$$

In matrix form :-

$$\begin{bmatrix} r_1 \\ r_2 \\ \vdots \\ r_n \end{bmatrix} = \begin{bmatrix} x_1 \\ x_2 \\ \vdots \\ x_n \end{bmatrix} - \begin{bmatrix} F_1(t_1) & F_2(t_1) \\ F_1(t_2) & F_2(t_2) \\ \vdots & \vdots \\ F_1(t_n) & F_2(t_n) \end{bmatrix} \begin{bmatrix} C_1 \\ C_2 \end{bmatrix} \tag{4.8}$$

or

$$[\,r\,] = [\,X\,] - [\,F\,]\,[\,C\,] \tag{4.9}$$

The error component can be described in terms of the residual matrix as follows :-

$$\begin{aligned} E &= [\,r\,]^T\,[\,r\,] \\ &= \begin{bmatrix} r_1 & r_2 & \dots & r_n \end{bmatrix} \begin{bmatrix} r_1 \\ r_2 \\ \vdots \\ r_n \end{bmatrix} \\ &= r_1^2 + r_2^2 + \cdots + r_n^2 \\ &= \Big[[X] - [F][C]\Big]^T \Big[[X] - [F][C]\Big] \\ &= [X]^T[X] - [C]^T[F]^T[X] - [X]^T[F][C] + [C]^T[F]^T[F][C] \end{aligned} \tag{4.10}$$

This error then needs to be minimised.

$$\begin{aligned} \frac{\partial E}{\partial C} &= -2[F]^T[X] + 2[F]^T[F][C] = 0 \\ [\,F\,]^T\,[F][C] &= [F]^T[X] \\ [\,C\,] &= \Big[[F]^T[F]\Big]^{-1}[F]^T[X] \end{aligned} \tag{4.11}$$

If $[A] = [F]^T[F]$ and $[B] = [F]^T[X]$ then :-

$$[C] = [A]^{-1}[B] \tag{4.12}$$

and hence :-

$$
\begin{aligned}
[A] &= \begin{bmatrix} F_1 \\ F_2 \end{bmatrix} [\, F_1 \quad F_2 \,] \\
&= \begin{bmatrix} F_1F_1(t_i) & F_1F_2(t_i) \\ F_2F_1(t_i) & F_2F_2(t_i) \end{bmatrix} \\
&= \begin{bmatrix} a_{11} & a_{12} \\ a_{21} & a_{22} \end{bmatrix}
\end{aligned}
$$

Elements of matrix $[A]$ can then be derived as shown :-

$$
\begin{aligned}
a_{11_n} &= \begin{bmatrix} F_1(t_1) \\ \vdots \\ F_1(t_n) \end{bmatrix}^T \begin{bmatrix} F_1(t_1) \\ \vdots \\ F_1(t_n) \end{bmatrix} \\
&= \sum_{i=1}^{n-1} F_1^2(t_i) + F_1^2(t_n) \\
&= a_{11_{n-1}} + F_1^2(t_n) \qquad (4.13) \\
etc.
\end{aligned}
$$

Similarly :-

$$
\begin{aligned}
[B] &= \begin{bmatrix} F_1(t_i)x(t_i) \\ F_2(t_i)x(t_i) \end{bmatrix} \\
&= \begin{bmatrix} b_1 \\ b_2 \end{bmatrix}
\end{aligned}
$$

and

$$b_{1_n} = b_{1_{n-1}} + F_1(t_n)x(t_n) \qquad (4.14)$$

$$b_{2_n} = b_{2_{n-1}} + F_2(t_n)x(t_n) \qquad (4.15)$$

From these matrix element equations, C_1 and C_2 can be calculated recursively using sequential data.

4.3 Results

The curve fitting algorithm (CFA) was used to analyze typical waveform derived from various disturbances and compared to results obtained with Fourier Analysis using the fast Fourier transform (FFT). The waveforms were generated with $50\mu s$ spaced samples, typical of the step-length necessary to model HV*dc* converters in electromagnetic transient programs. The effect of different sized data windows and window shapes were investigated for the various disturbances.

In many cases, such as with hybrid interfacing, the extracted fundamental frequency values are required only at discrete intervals ranging from less than a cycle to many cycles of the fundamental. Power system disturbances are often transient effects and consequently of short duration. The analysis extracted fundamental frequency data at intervals of a cycle or less to recover this transient information.

The CFA analysis was first applied using two different unit magnitude window sizes. Window sizes of one fundamental period and of half of this period were investigated for their performance. Fourier analysis using the FFT was also performed for a period length in the same way as the CFA for comparison purposes. These three techniques used fixed discrete rectangular shaped windows in a non-staggered manner as shown in Figures 4.1(a) and 4.1(b). A staggered CFA approach was also investigated where a window size of a period length was used in an overlapping manner to produce results twice every period (Figure 4.1(c)). Finally, a squared decay weighted window was also used to produce CFA results every half of a fundamental period (Figure 4.1(d)). This window shape was designed to give emphasis on the more recent trends of the waveform. It is effectively a non-discrete or infinitely sized moving window. The weighted decay drop over a fundamental period was equal to 50 percent.

Discontinuities in an analyzed waveform present problems since it is not accurate to apply analysis over a discontinuity and assume periodicity. Analysis from a point of discontinuity should, if possible, commence again at that point. Analysis that requires a fixed fundamental period length must then wait at least until that period has elapsed before a result is obtainable. When the waveform to be analyzed is derived from an analysis program, as in the case of hybrid program interfacing, a fault application time is known and often entered in the data file before the analysis is run. This prior knowledge of a discontinuity can be used to reset the fundamental frequency extraction process if required.

In many disturbances the fundamental frequency is not constant and can vary over the fault application and recovery times. The CFA can very easily accept a varying tracked frequency to monitor and this is also possible with Fourier analysis [Sachdev and Giray, 1985] [Giray and Sachdev, 1989]. The rectangular window size of a fundamental period length however, dictates a relatively wide bandwidth over this fundamental frequency and hence small variations in this frequency are almost imperceptible in the magnitude output.

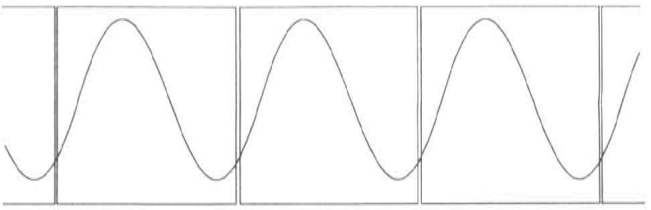

a) Discrete window of fundamental period length

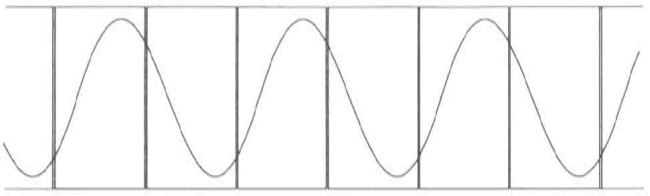

b) Discrete window of half fundamental period length

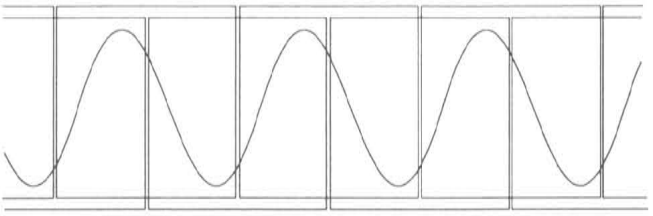

c) Staggered discrete window of fundamental period length

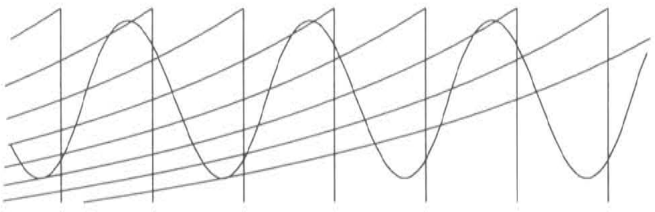

d) Continuous window with decay weighting

Figure 4.1 Analysis techniques

4.3.1 Amplitude Variation

The fundamental component of an analyzed waveform is often subject to considerable variation. In the case of power system voltages, both overvoltage and voltage depression are common.

In *ac* systems incorporating HV*dc* links, a fault at the inverter end of the *dc* link can cause valve blocking at the rectifier end. This can cause a major load rejection and consequently a voltage rise at the rectifier converter, especially if any reactive power compensation is still on line. Overvoltages can be particularly severe for *ac* systems having low short circuit capacities.

Long term amplitude fluctuation over a few cycles is not difficult to extract, however short term transient variation presents more of a problem. This could easily be caused by the high speed response of static VAr compensation systems in attempting to maintain a desired voltage profile [Hauth *et al.*, 1982].

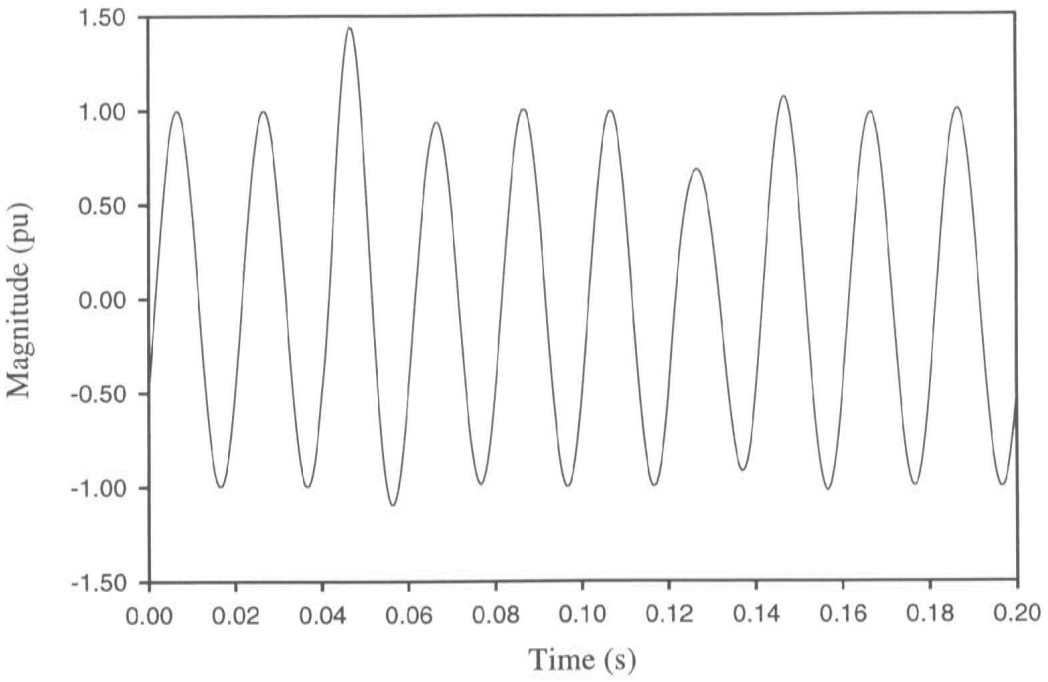

Figure 4.2 Amplitude variation

Figure 4.2 shows an amplitude modulated waveform with a fundamental frequency component of 50 Hz. The waveform represents possible shorter term transient amplitude variation in a power system variable. Each technique has been applied to this waveform. In Figure 4.3, the magnitude results are plotted against the modulating envelope of the amplitude variation shown in Figure 4.2, to enable comparison of the amplitude variation tracking properties. The phase results for each analysis are given in Figure 4.4 and should ideally be maintained constant.

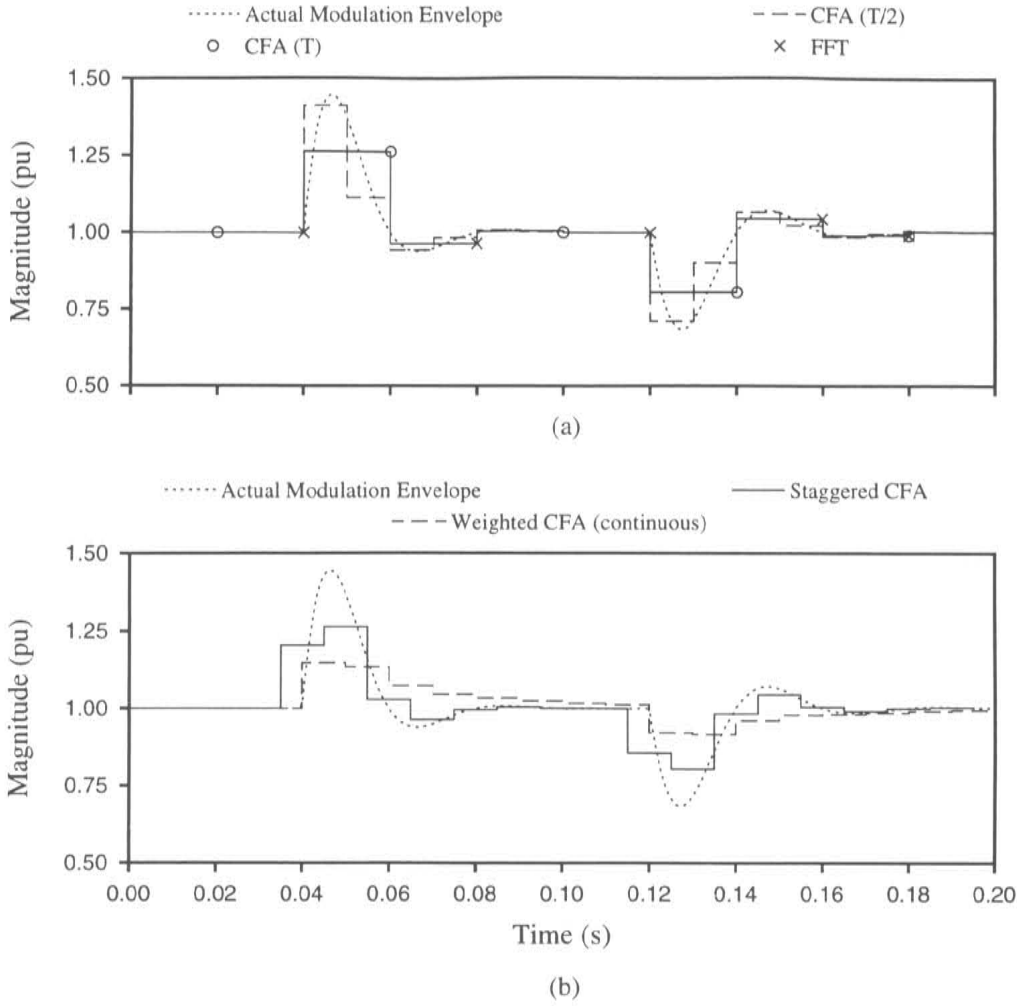

Figure 4.3 Magnitude analysis of amplitude variation

The magnitudes for the three discrete non-staggered approaches are shown in Figure 4.3(a). The CFA and the FFT methods using a window size of the fundamental period (T) give practically identical results. Since the modulation is relatively rapid, changing considerably over a period, the CFA using a shorter window (T/2) tracks the envelope more accurately. For this type of aperiodic waveform amplitude irregularity, the shorter the window size, the better the tracking, particularly for fast amplitude changes. The first overshoot of the envelope reaches 1.45*pu* while the following depression corresponds to 0.95*pu*. FFT and CFA analysis of a period window size track this as a 1.26*pu* overshoot and a 0.98*pu* depression and hold these values over the length of their analysis window. The CFA analysis using half a period window size tracks the envelope to a 1.4*pu* overshoot followed by a 0.96*pu* depression.

The magnitudes for the staggered approaches are displayed in Figure 4.3(b). The staggered CFA method tracks the modulation envelope reasonably well. Since its analysis window is a fundamental period but staggered by half a period, it does suffer a disadvantage when its window crosses a sharp change in the waveform. The presence of the change in

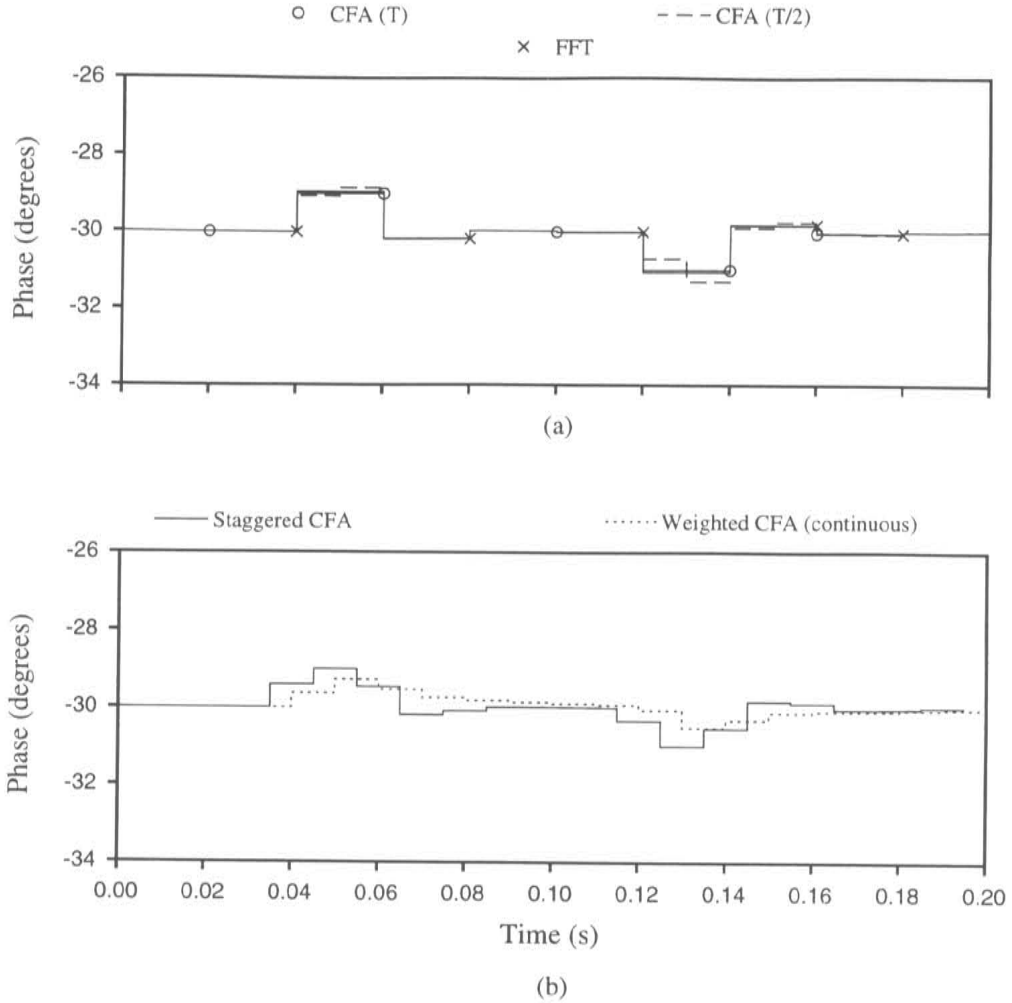

Figure 4.4 Phase analysis of amplitude variation

the analysis result is extended beyond its actual bound. The more that the analysis window is staggered, the more accurate the tracking, however there will always be a boundary extension in the result when a sudden change occurs in the analyzed waveform. When possible, the analysis process should be modified so as not to apply an analysis window over a sudden change or discontinuity boundary.

The decay weighted technique does not perform well and is delayed and damped with the first depression unable to be tracked. For very quick amplitude variations, the staggered techniques are not as useful as those using fixed discrete windows. Slower variations, over a period or longer, do not pose such difficulties and would be tracked better.

The phase results of the five techniques are shown in Figures 4.4(a) and 4.4(b). All approaches give less than a 3 percent error during the amplitude variations. The continuous decay weighted approach again shows a delayed action to the variations in the waveform.

4.3.2 Harmonics

Harmonics can be caused by many power system components. Static power converters, for example, inherently generate harmonics, while rotating machines and transformers do so primarily under transient disturbances. These harmonics may be enhanced by system resonances between capacitive and inductive elements in the network. Transients and switching surges can also caused damped oscillatory waves with a frequency determined by a systems configuration and parameters [Arrillaga *et al.*, 1985].

The first of the harmonic waveforms analyzed represents a constant $1pu$ fundamental frequency severely distorted by six pulse converter harmonics up to the 13^{th} order (Figure 4.5). This is representative of an *ac* waveform at a converter bus without any filtering. The per unit magnitudes of the harmonics are the worst case possible and are given by the reciprocal of their harmonic order.

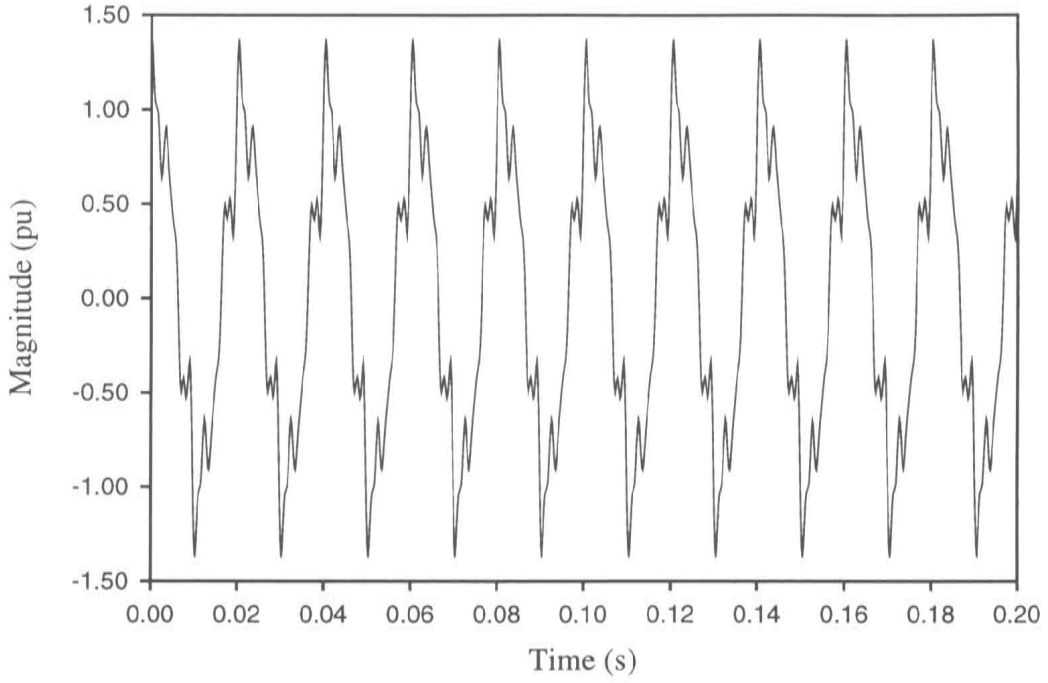

Figure 4.5 Six pulse converter harmonics

Figure 4.6 displays the fundamental frequency magnitude as interpreted by each technique. The Fourier Transform technique displays a magnitude of exactly $1pu$ while the CFA full period technique is slightly higher at $1.002pu$. The CFA half period fixed window technique analysis shows a slightly higher result than the CFA full period at $1.005pu$. The waveform disturbing effect in this case is periodic as opposed to aperiodic in the amplitude modulated case, and so as expected, the staggered CFA approach shows no difference to the non-staggered approach. These two approaches should only significantly differ around any discontinuity, large aperiodic distortion, or fast amplitude variation. The decay weighted analysis shows a low value of about $0.991pu$. The differences with the curve fitted approaches are small, but display a slight drawback of this technique

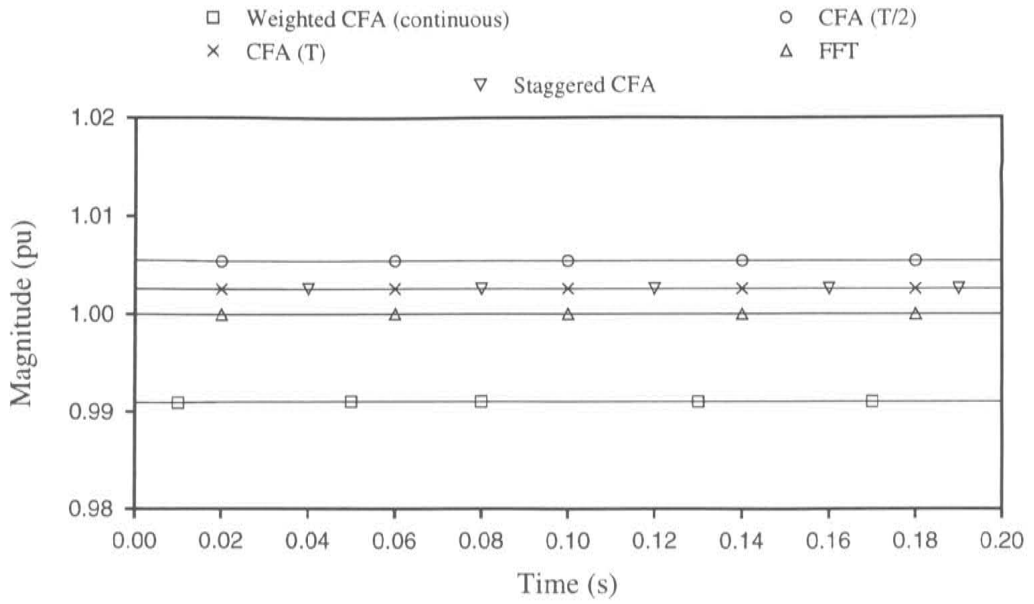

Figure 4.6 Analysis of converter harmonics

when analyzing severely distorted waveforms. It is inherently less capable of accurately resolving the desired frequency when subjected to very large variations or disturbances whether periodic or not. The waveform analyzed is however an extreme case of converter harmonic effects and even so, the magnitude results, especially for a CFA window size of one full period, are only minimally in error.

The phase results for the converter affected waveform were all effectively the same, giving the expected value of 60 degrees to within less than half a percent error.

The second of the harmonically affected waveforms analyzed is represented by a fundamental frequency of $1pu$ magnitude but this time with the effect of a 3^{rd} harmonic of 30 percent of the fundamental magnitude. This shows the effect that a low order harmonic may have on the recovery of fundamental frequency. The waveform is shown in Figure 4.7.

Magnitude results for the various techniques are shown in Figure 4.8(a). All of the fixed window approaches give a result of practically $1pu$. Since this is again a periodic interference, the staggered CFA gives the same results as the non-staggered full period CFA and is consequently not shown.

The result from the continuous window with weighted decay shows a slight drop in its magnitude but is still also effectively $1pu$.

Phase results are similar to the magnitude results and shown in Figure 4.8(b). The decay weighted window technique had a small error in its result of 2 degrees.

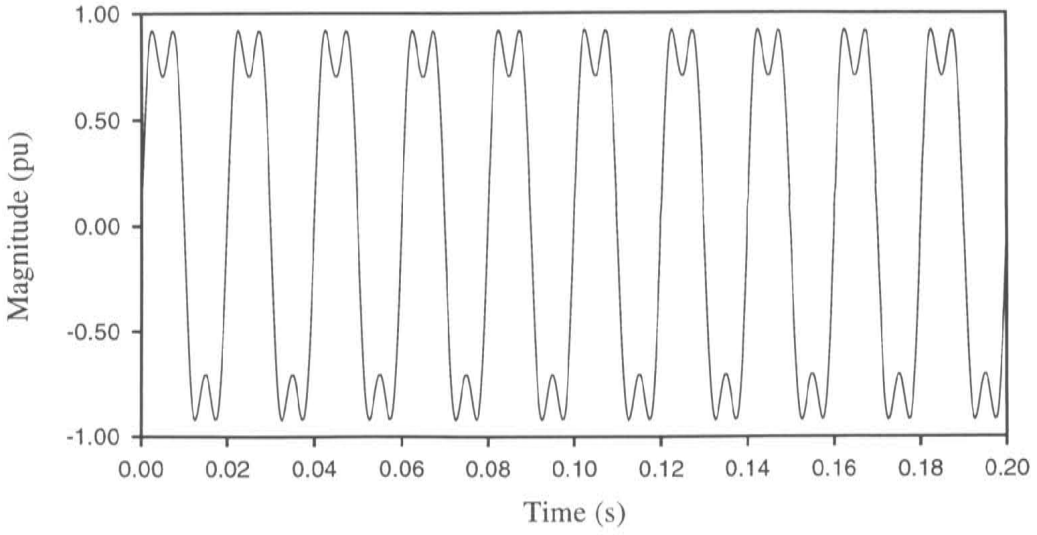

Figure 4.7 Waveform distorted by low order harmonics

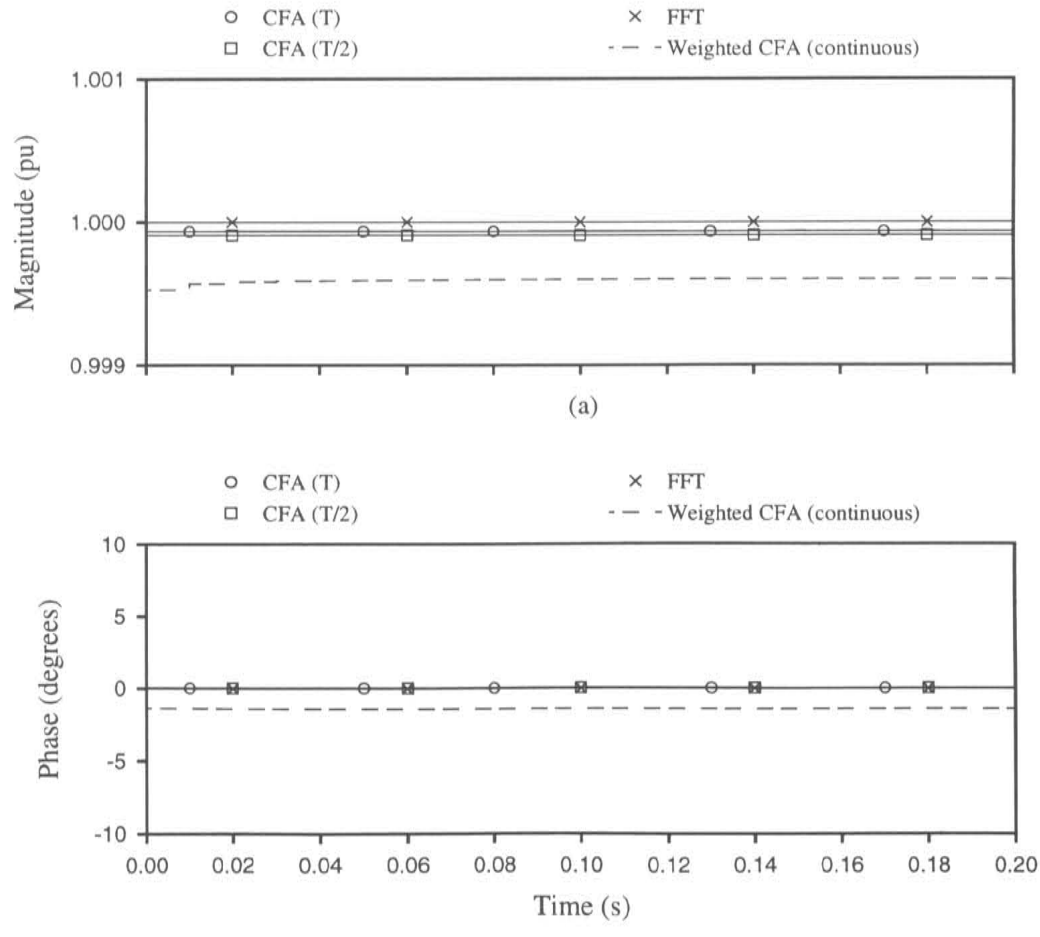

Figure 4.8 Analysis of low order harmonics

The next waveform analyzed involved an aperiodic high frequency (377 Hz) ringing which decayed away from an initial magnitude of $0.6pu$ over approximately a fundamental cycle (Figure 4.9). The fundamental component was again constant at $1pu$ magnitude.

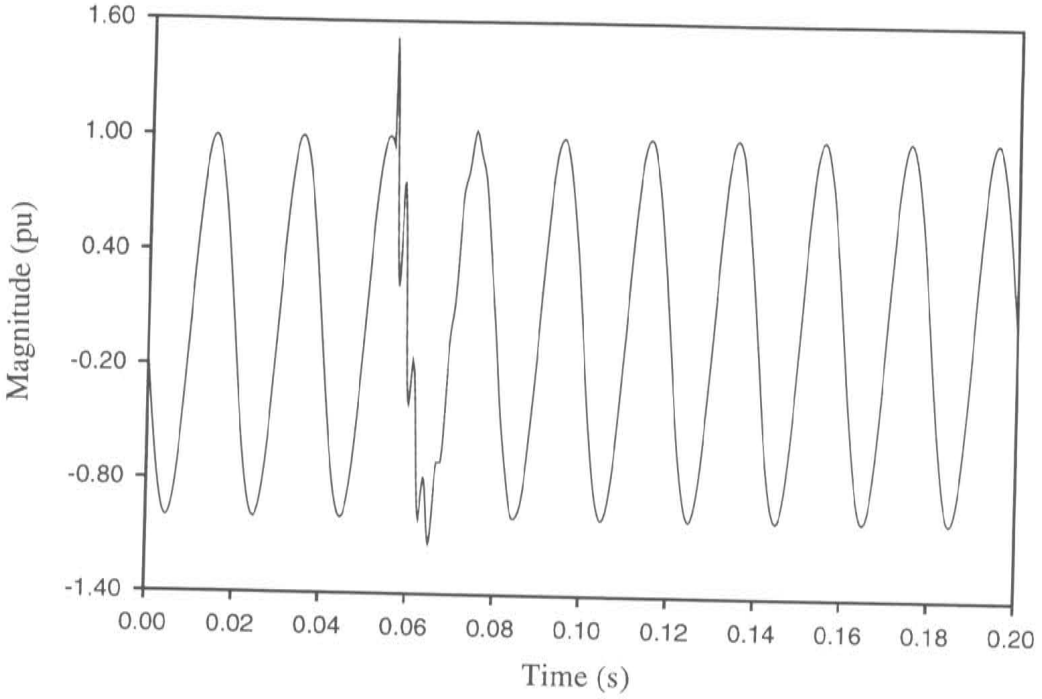

Figure 4.9 High frequency ringing

The fixed non-staggered window technique results can be seen in Figure 4.10(a). Both the FFT and CFA results for a window size of a fundamental period are the same and rise to an error of 1 percent for a window length and then dip nearly 0.2 percent. The CFA result using a half period window size rises to a 2 percent error but only for its own window length. The dip is similarly about twice the error for half the time.

The magnitude results for the staggered approaches are shown in Figure 4.10(b). The continuously weighted CFA approach, similar to its amplitude variation response, delays and to some extent holds the disturbing effect. This approach is obviously slower to recover from the harmonic ringing. The staggered CFA technique had a similar initial rise and depression to the non-staggered full period techniques. A slight improvement over the full period approaches was evident in the half period step following the initial rise and depression.

Phase responses for the waveform were very good for the four discrete window techniques and within 4 degrees of the correct value (Figure 4.10(c)). The weighted continuous window technique did not perform as well and produced a considerable overshoot error. Reducing the weighted decay rate would reduce this overshoot error but prolong the disturbing effect on the results.

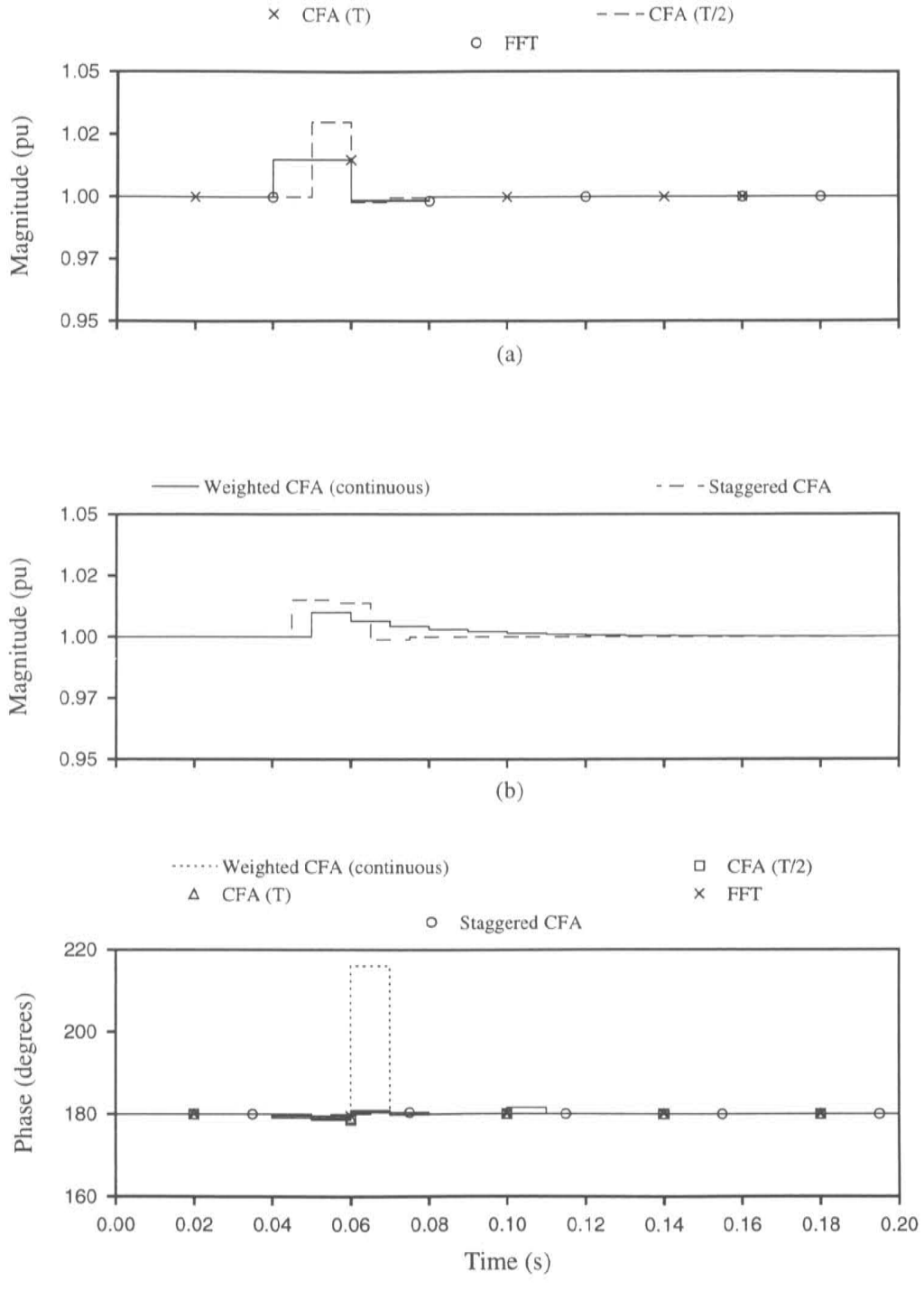

Figure 4.10 Analysis of high frequency ringing

4.3.3 *Dc* Offset

When a transformer with residual flux density in its core is connected to a power system network it can be driven to high saturation levels producing magnetisation currents of many times that normally produced. This magnetisation current decays over time primarily as a function of the primary winding resistance. In practice, this can occur over many seconds especially for larger transformers. The magnetisation current can include a relatively high initial *dc* component [Arrillaga *et al.*, 1985] [Arrillaga, 1983].

Dc can also exist on the *ac* side in a combined *ac-dc* system due to fundamental modulation of the *dc* current. This inherently generates both second harmonic positive sequence and *dc* into the *ac* system [Arrillaga, 1983].

A decaying *dc* offset with an initial magnitude of $0.3pu$ was applied to a $1pu$ fundamental frequency waveform with a discontinuity as shown in Figure 4.11. The magnitude analysis is shown in Figure 4.12(a). The results for the non-staggered FFT and CFA techniques using window sizes of a fundamental period were very similar at approximately $1pu$. The CFA technique with a half period window size was not so effective, displaying a fundamental oscillation superimposed on the true fundamental frequency result. The oscillation magnitude was almost equivalent to the actual *dc* magnitude. A full period analysis window is necessary with the CFA technique to reject any *dc* influence. A window size less than a period length will suffer from fundamental ripple as a result of *dc*.

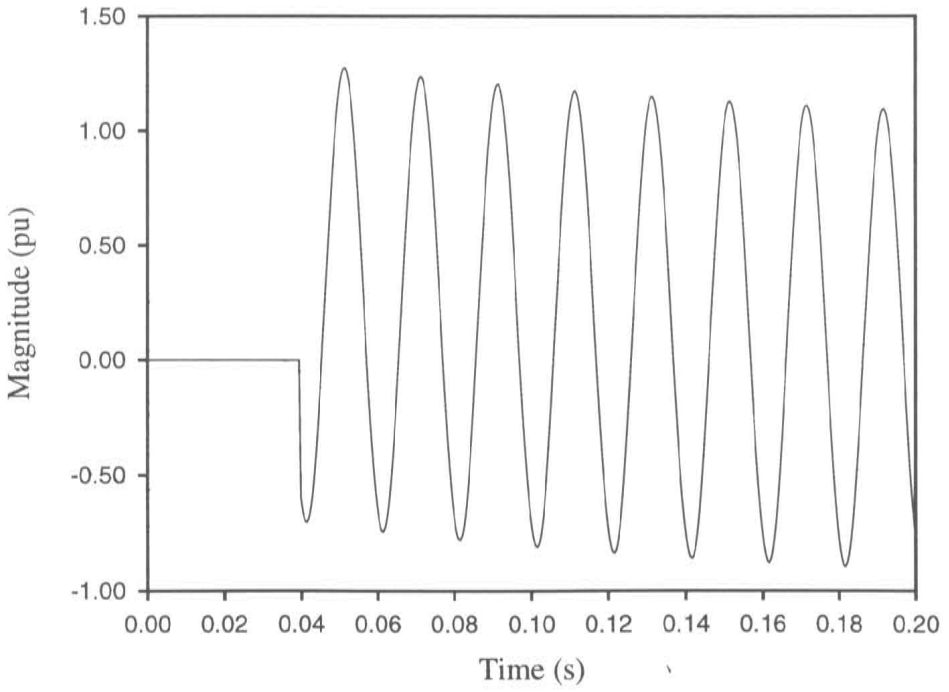

Figure 4.11 *Dc* offset

The result from the CFA fixed but staggered window of fundamental period was also good, displaying a slight fundamental oscillation but of a very low magnitude of $0.006pu$ peak error at its worst point (Figure 4.12(b)). The decay weighted window had

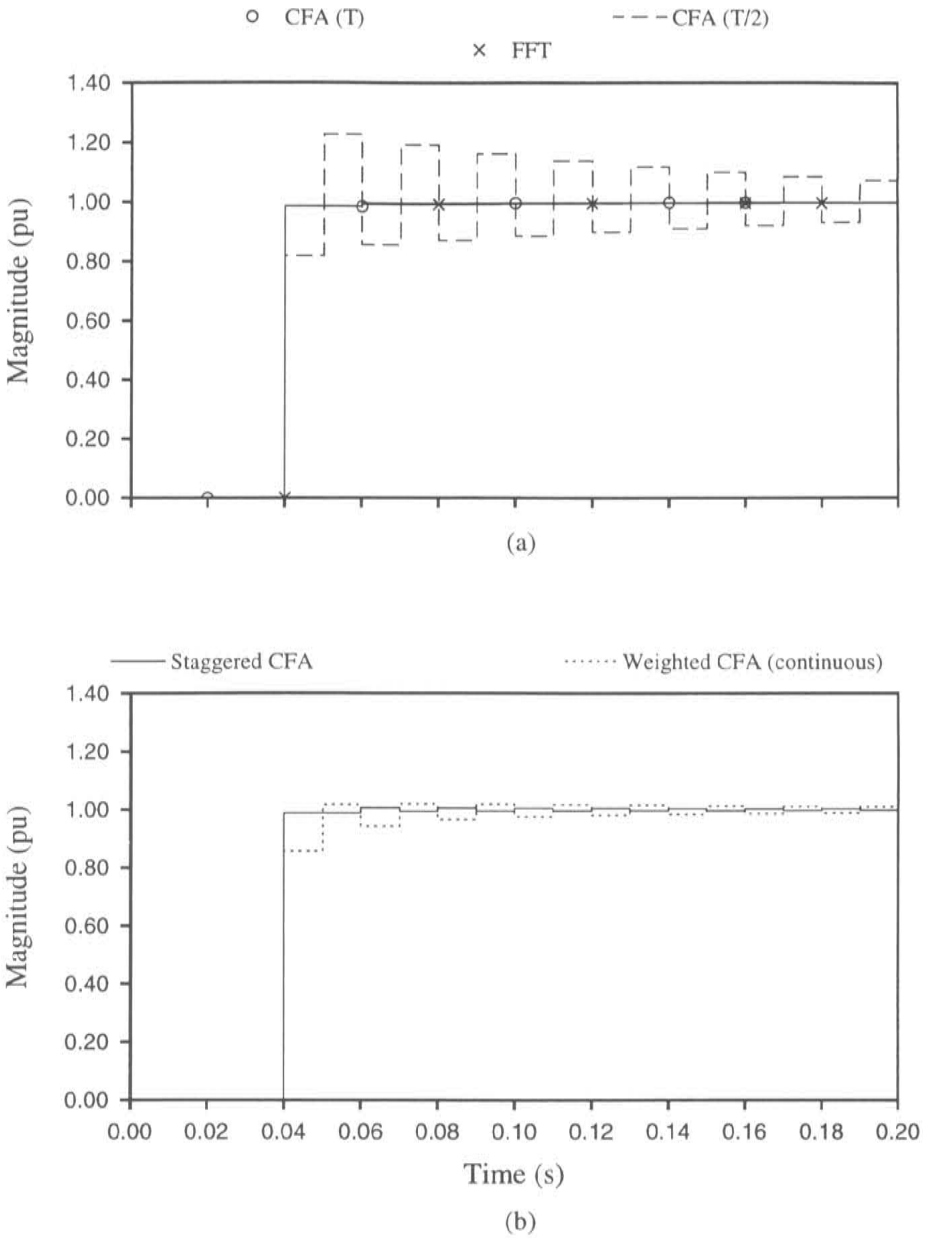

Figure 4.12 Magnitude analysis of *dc* offset

a stronger fundamental oscillation although not nearly as predominant as the fixed half period window technique.

The phase results showed trends similar to the magnitude results. The fixed window lengths of fundamental period and the staggered fixed period window all gave good phase results.

Strong fundamental oscillation existed on the fixed half period analysis while a smaller fundamental oscillation was present on the decay weighted window technique.

4.3.4 Simulated Fault Waveform

The final waveform analyzed was derived from the electromagnetic transient analysis program EMTDC described in the previous chapter. The signal was created using the CIGRE HV*dc* benchmark model [Szechtman *et al.*, 1991] (refer Appendix A.1) coupled to a simple *ac* system on the rectifier side with a short circuit capacity of four. A single phase fault was applied at the rectifier terminal and the voltage at this bus monitored. The generated wave is shown is Figure 4.13. Figures 4.14(a) and 4.14(b) show the magnitude responses of the various techniques on the simulation waveform. The fixed full period window results using both the CFA and the FFT gave visually identical results.

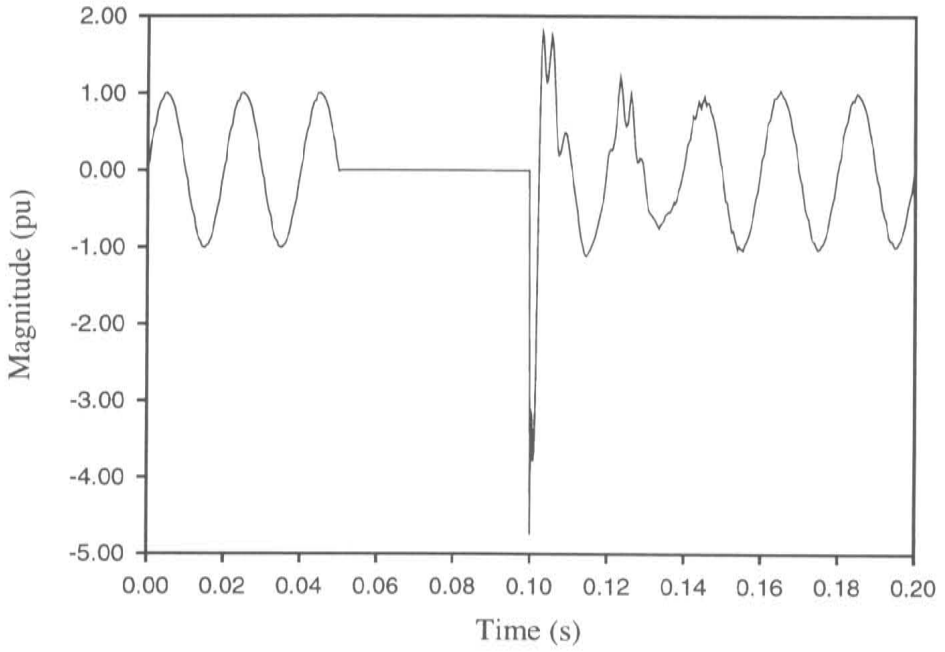

Figure 4.13 Simulated fault waveform

Figure 4.14(a) compares the half period fixed window with the full period and shows the greater amplitude response of the smaller window. A complete Fourier analysis of the first cycle after the fault is removed, however, shows considerable harmonic components including *dc*. As shown previously, the *dc* component can cause the fundamental result from a half period fixed window length to be significantly different than it actually is.

The decay weighted window (Figure 4.14) displayed an obvious delay in its results especially when the waveform was recovering to its normal magnitude after the fault. A high initial peak was also registered which again could have been partially due to the presence of *dc*. The staggered full period analysis displayed very good results for both initial value and amplitude variation tracking. At both the fault application and removal, the staggering process was reset so as not to apply an analysis window over the discontinuity.

Phase results for the waveform are shown in Figure 4.15. The analysis using the full and half period discrete windows are very similar except for an initially larger decrease

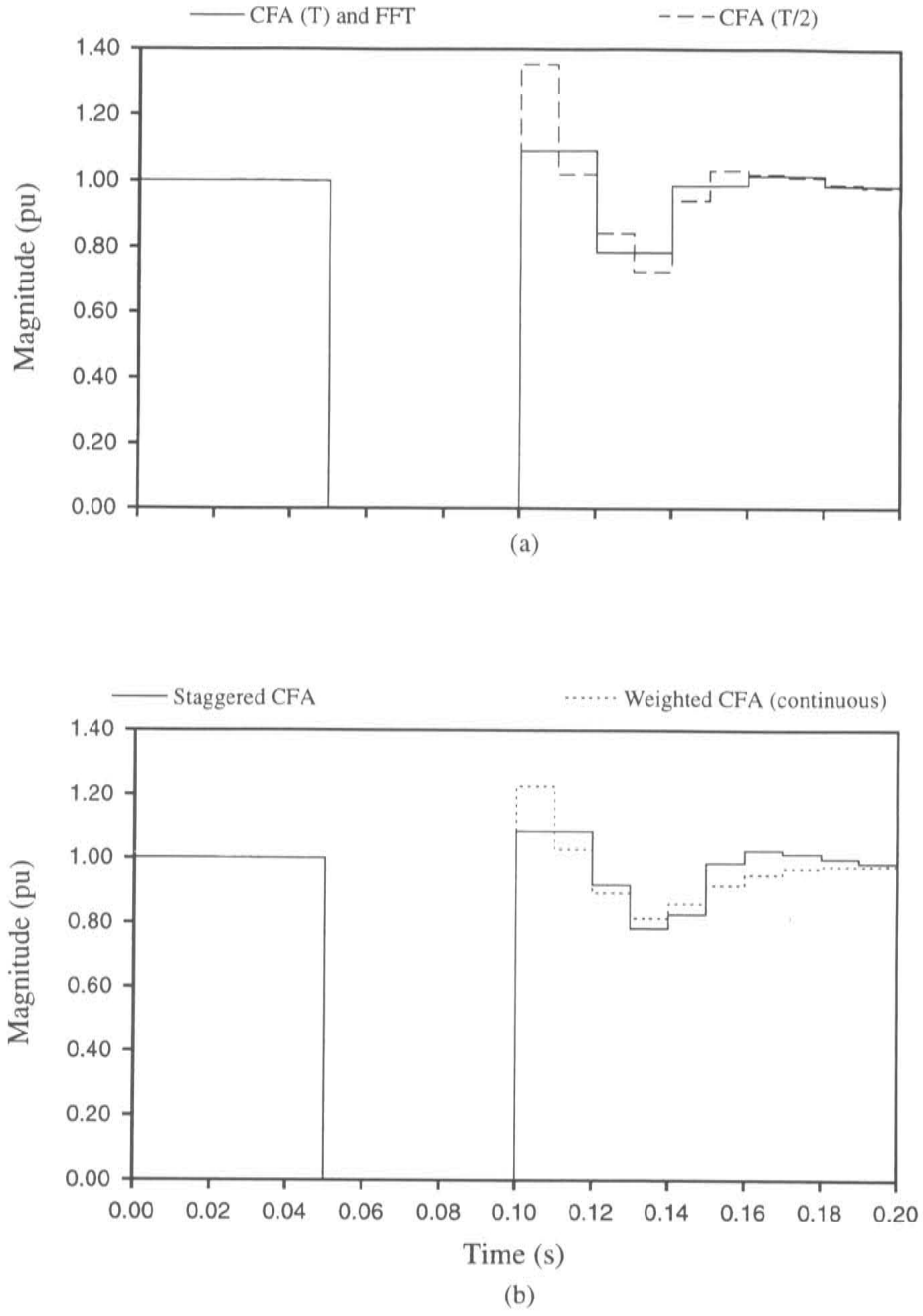

Figure 4.14 Post-fault magnitude analysis

in the half period window results directly after the fault removal. The phase response increased in both cases about 20 degrees above normal after this initial decrease, before settling near to its pre-fault value. Close inspection of the faulted waveform reveals a slight fluctuation in the fundamental frequency after the fault was removed. Since in the results presented, the fundamental frequency was not tracked but maintained at a constant 50 Hz, this varying frequency could cause a definite phase shift effect in the results.

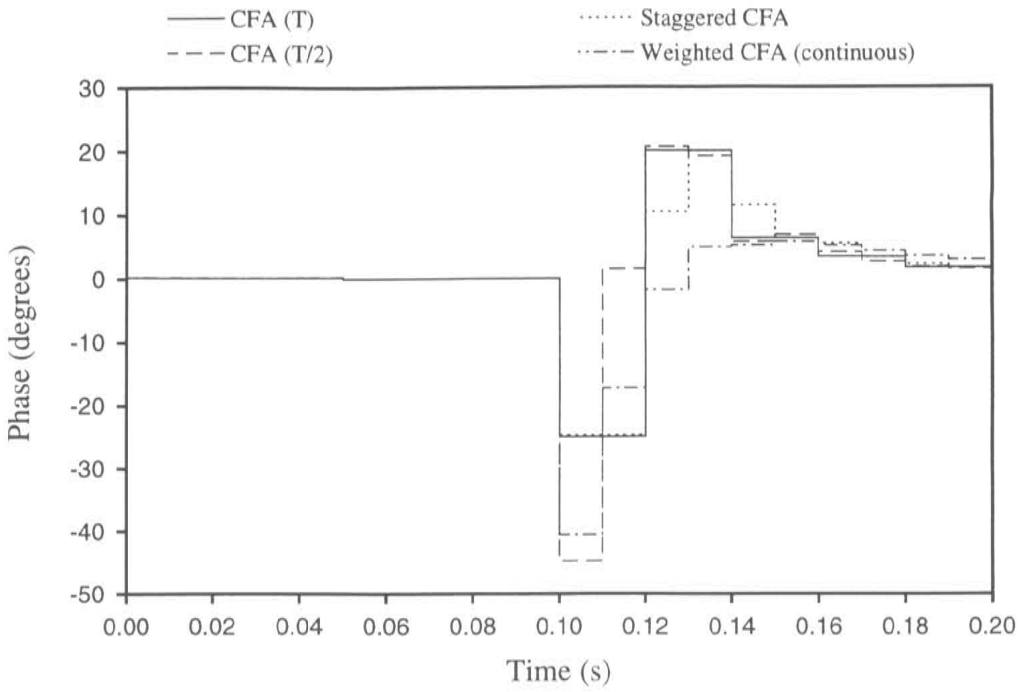

Figure 4.15 Post-fault phase analysis

4.4 Summary

Fourier and curve fitted analysis was applied to a number of typical waveform disturbances to extract transient fundamental frequency data.

The curve fitting algorithm compared extremely well to Fourier analysis when the same fundamental period window was used. Responses to amplitude variations, harmonic interference, and the addition of a *dc* component were all practically identical. Given the computational advantage of the CFA over the FFT then it is considered to be a better choice if only the fundamental frequency is required.

A window size of less than a fundamental period was shown to respond quickly to any amplitude variation but suffered from interference in the presence of *dc*. For this reason, it is not an advisable method for extracting accurate fundamental frequency data.

Staggering a full fundamental period window so that results are obtainable twice every cycle gave very good results. The generation of results every half cycle gave a better general tracking response than using a non-staggered full period approach. The more that a period window is staggered over a fundamental cycle, the better the tracking properties of the analysis. Response to fast amplitude changing or aperiodic disturbances is marginally affected across the boundaries of these disturbances, however any periodic effects will have no additional consequences when compared with non-staggered techniques of the same window size.

Using a decaying window shape tended to give delayed response and accentuated droop or overshoot effects on its results and was consequently not as useful as the other

approaches.

An *ac-dc* hybrid program using an electromagnetic analysis method for detailed analysis, is constrained to time-steps in the order of 50 to 100μs. With these time-steps, and with an analysis window of a period length, there is no problem with any violation of the Nyquist criteria for fundamental frequency.

If fundamental frequency data is required at discrete intervals of a fundamental cycle, then a CFA analysis of a non-staggered fundamental period length is considered the optimum choice. When data is required at discrete intervals of less than a cycle, a CFA analysis with a similar length of a fundamental period used in a staggered manner is considered the optimum choice. The CFA technique allows very good results for all disturbing effects while at the same time providing computational efficiency with its curve fitted approach. A further advantage is that the window analysis length is not restricted to precisely one period of the fundamental frequency but can be extended beyond this if necessary. If any *dc* component is likely to be present then the window size should not be reduced below the width of a fundamental period.

Chapter 5

HYBRID SIMULATION OF AC-DC POWER SYSTEMS

Chapter 1 of this thesis introduced a hybrid approach combining an electro-mechanical transient stability program with a detailed electromagnetic transient analysis program. A hybrid approach is necessary to accurately model the electromagnetic dynamic behaviour of fast controlled devices such as HV*dc* converters or FACTS devices, while maintaining a full electro-mechanical representation of the *ac* system. This type of modelling is particularly important for faults at or near the terminals of any rapidly controlled device, especially when the *ac* system is weak.

This chapter presents a new hybrid algorithm to enhance the modelling accuracy of *ac-dc* systems. The basic concept of the hybrid is shown in Figure 5.1.

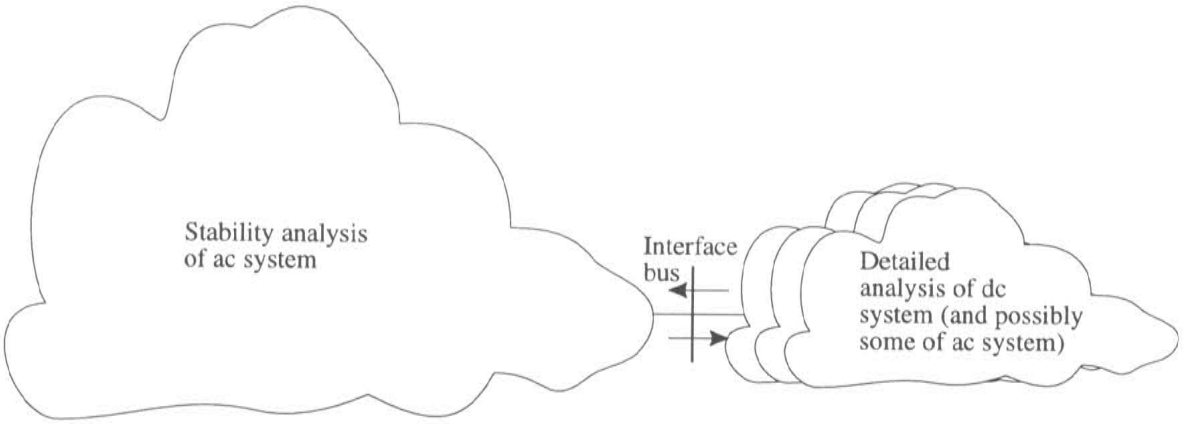

Figure 5.1 The hybrid concept

The hybrid approach is not, however, restricted to *ac-dc* applications only. A particular part of an *ac* system may sometimes require detailed three phase modelling and this same hybrid approach can then be used. Applications include the detailed analysis of synchronous or static compensators, FACTS devices [Reeve *et al.*, 1991], or the frequency dependent effects of transmission lines.

Detailed modelling can also be applied to more than one independent part of the complete system. For example, if an *ac* system contained two HV*dc* links, then both links could be modelled independently in detail and included in one overall *ac* electro-mechanical stability representation.

5.1 The TS-EMTDC Hybrid

The hybrid developed consists of a conventional electro-mechanical stability program, TS [Arnold, 1976], and an established electromagnetic transient program EMTDC [Woodford, 1985]. Chapters 2 and 3 introduce the basic analysis principles of the TS and EMTDC programs respectively.

The hybrid utilises the stability program TS as the steering program while EMTDC is called as a subroutine. The interfacing code is written in separate routines to the existing programs since an aim of the hybrid development is to only minimally modify TS and EMTDC. This allows the developed interface techniques to be easily applied to other stability and detailed dynamic programs if required.

In Chapter 1, previous hybrid approaches were reviewed. In the two approaches using interfacing between detailed dynamic and stability programs, Heffernan *et al.* modelled only the *dc* system in detail while Reeve and Adapa modelled in detail the *dc* system plus a portion of the *ac* system [Heffernan *et al.*, 1981] [Reeve and Adapa, 1988]. The TS-EMTDC (or TSE) hybrid described in this chapter is designed to have multiple interface buses at any location for complete flexibility. An analysis to determine the optimum location of the interface point is presented in Chapter 6.

5.1.1 System Splitting

Initially, the TSE hybrid reads in the data files, and runs the entire network of systems 1 and 2 in the stability program, until electro-mechanical steady state equilibrium is reached. This is shown in the example of Figure 5.2(a). The quasi-steady state representation of the converter is sufficient for this as no fault or disturbance has yet been applied. At a selectable point in time, prior to a network disturbance occurring, the TS network is split up into the two independent and isolated systems, system 1 and system 2.

For the sake of clarity, system 1 is classified as the *ac* part of the system modelled by the stability program TS, while system 2 is the part of the system modelled in detail by EMTDC.

The snapshot data file is now used to initialise the EMTDC replacement of the TS representation of system 2. The two programs are then interfaced and the network disturbance can be applied. The system 2 representation in TS is isolated but kept up to date during the interfacing at each TS time-step to allow tracking between programs. The *ac* network of system 1 modelled in the stability program also supplies interface data to this system 2 network in TS as shown in Figure 5.2(b).

While the disturbance effects abate, the quasi-steady state representation of system 2 in TS and the EMTDC representation of system 2 are tracked. If both of these system 2 models produce the same results within a predefined tolerance and over a set period, the complete system can then be reconnected and used by TS, and the EMTDC representation terminated. This allows better computational efficiency, particularly for long simulation runs.

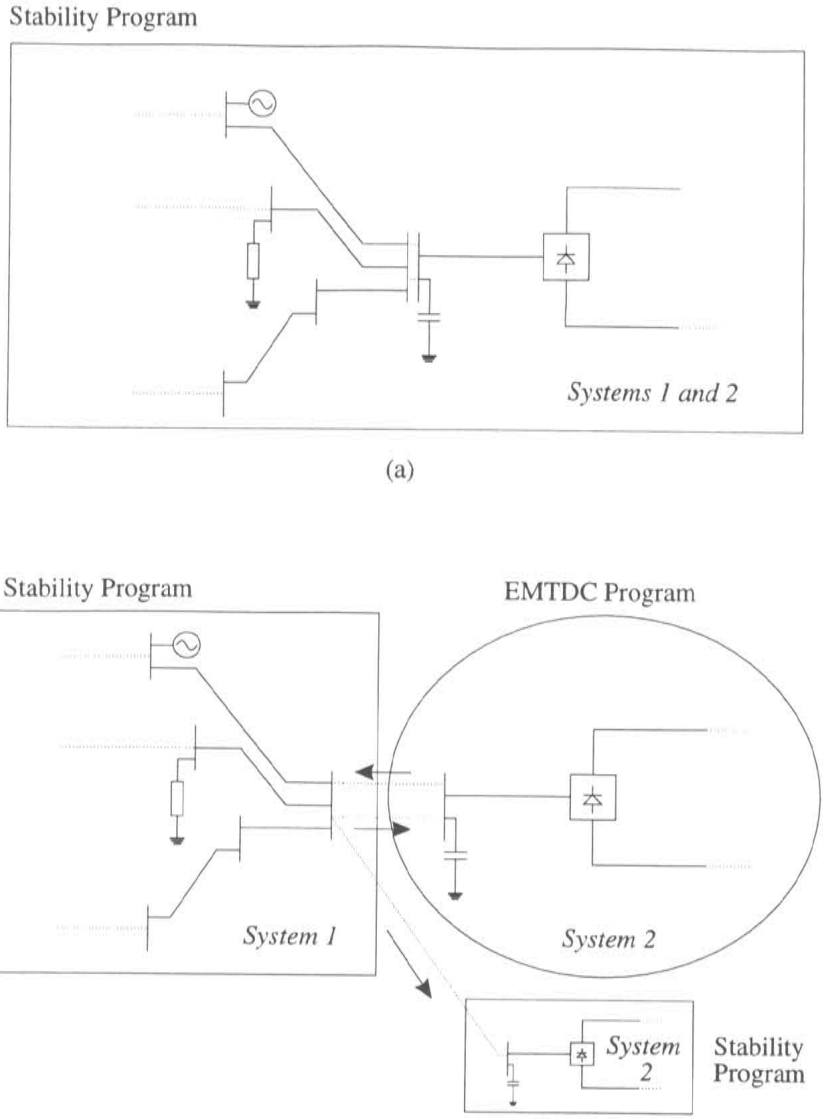

Figure 5.2 Example of interfacing procedure

5.1.2 Program Modifications

To enable EMTDC to be called as a subroutine from TS requires a small number of changes to its structure. The EMTDC algorithm is split into three distinct segments, an initialising segment, the main time loop, and a termination segment. This allows TS to call the main time loop for discrete periods as required when interfacing. The EMTDC options which are normally available when beginning a simulation run are moved to the interface data file and read from there. The equivalent circuit source values, which TS updates periodically, are located in the user accessible DSDYN file of EMTDC (refer Chapter 3).

The TS program requires only minor modifications. The first is the calling of the interfacing routine during the TS main time loop as shown in Figure 5.3. The complete TS network is also split into system 1 and system 2 and isolated at the interface points,

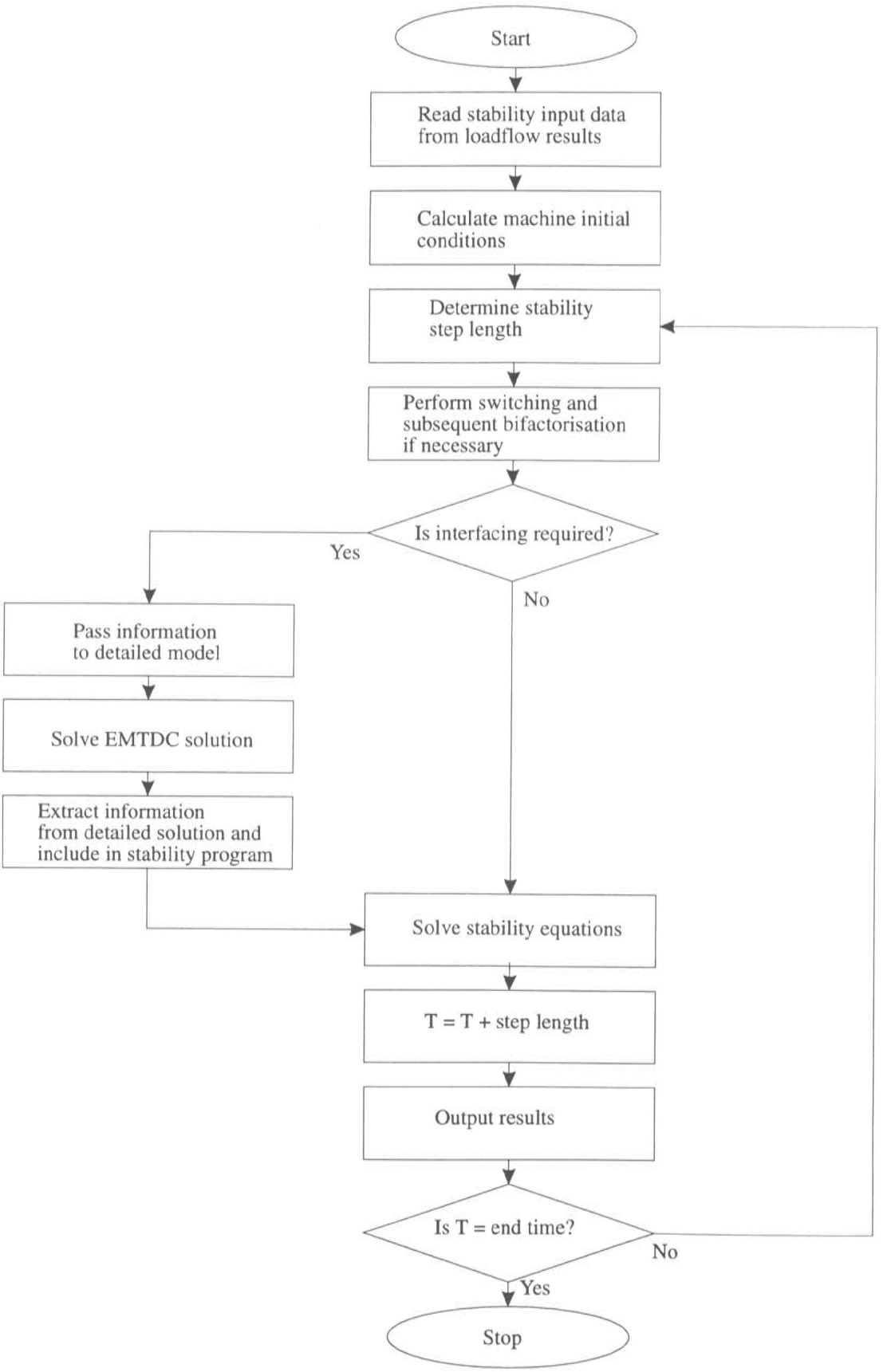

Figure 5.3 Modified TS steering routine

but this is performed in separate code to TS. The only other direct modification inside TS is the inclusion of the interface current injections at each TS network solution.

5.1.3 Data Flow

Data for the detailed EMTDC model is entered in the program database via the PSCAD graphics. Equivalent circuits are used at each interface point to represent the rest of the system not included in the detailed model. This system is then run until steady state is reached and a "snapshot" taken. This snapshot holds all the relevant data for the components at that point in time and can be used as the starting point when interfacing the detailed model with the stability program.

The stability program is initialised conventionally through load-flow results via a data file. An interface data file is also read by the TSE hybrid and contains information such as the number and location of interface buses, analysis options, and timing information. The data flow diagram is shown in Figure 5.4.

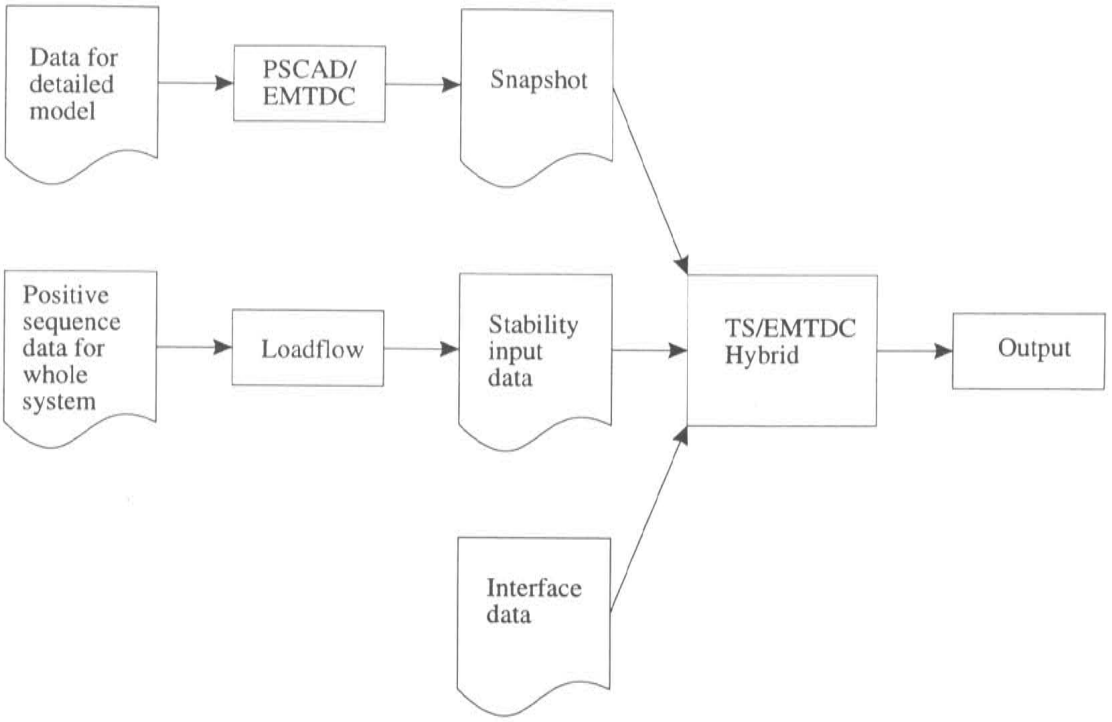

Figure 5.4 Data flow

5.2 Interfacing Parameters

Hybrid simulation requires information interchange to occur between the two separate algorithms. An equivalent circuit representing the network modelled in the stability

program is used in EMTDC, and vice versa. The equivalent circuits can be represented as shown in Figure 5.5, where $\tilde{E}_1$ and $\tilde{Z}_1$ can represent the equivalent circuit of system 1, and $\tilde{I}_c$ and $\tilde{Z}_2$ the equivalent circuit of system 2.

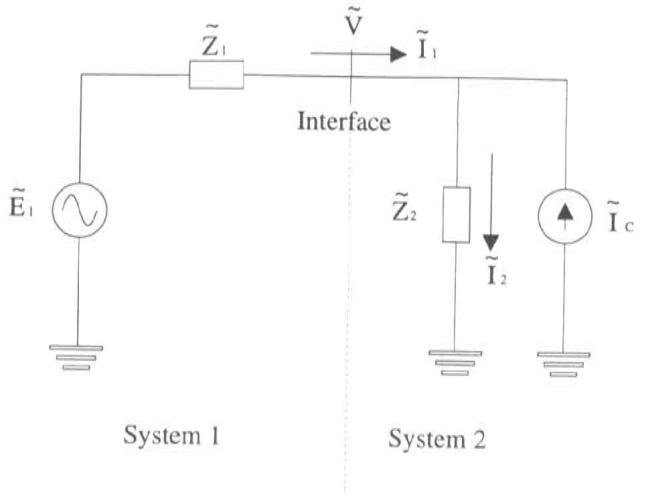

Figure 5.5 Representative circuit

5.2.1 Interface Equivalent Impedances

The complexity of the equivalent impedance representation varies considerably between the two programs.

In the TS program, $\tilde{I}_c$ and $\tilde{Z}_2$ represent the detailed part of the system modelled by EMTDC. TS, being positive sequence and fundamental frequency based, is concerned only with the fundamental real and reactive power in or out-flow through the interface. The equivalent impedance $\tilde{Z}_2$ then is arbitrary, since the current source $\tilde{I}_c$ can be varied to provide the correct power flow.

To avoid any possible numerical instability, an estimated value for $\tilde{Z}_2$ is given, calculated simply from the initial load-flow results. This value is maintained constant throughout the duration of the simulation.

The EMTDC program represents system 1 by an equivalent circuit symbolised by the source $\tilde{E}_1$ and the impedance $\tilde{Z}_1$ shown in Figure 5.5. A simplified $\tilde{Z}_1$ can consist of an $R-L$ series impedance, representing the fundamental frequency equivalent of system 1.

This impedance value can be derived in a conventional manner from the results of a load-flow, and a fault analysis at the interface bus.

From a loadflow, the initial current through the interface bus can be found and the initial interface bus voltage is known. A fault analysis can easily determine the fault current through the interface for a short circuit fault to ground. If the network requiring conversion to an equivalent circuit is represented by a Thevenin source $\tilde{E}_1$ and Thevenin impedance $\tilde{Z}_1$ as shown in Figure 5.6, these values can be found as follows :-

From the loadflow circuit :-

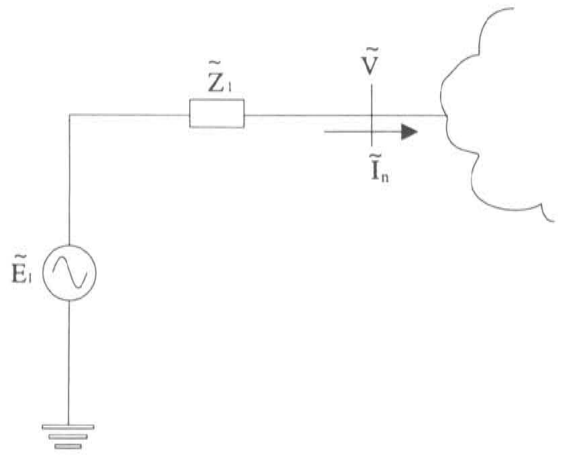

(a) Loadflow circuit

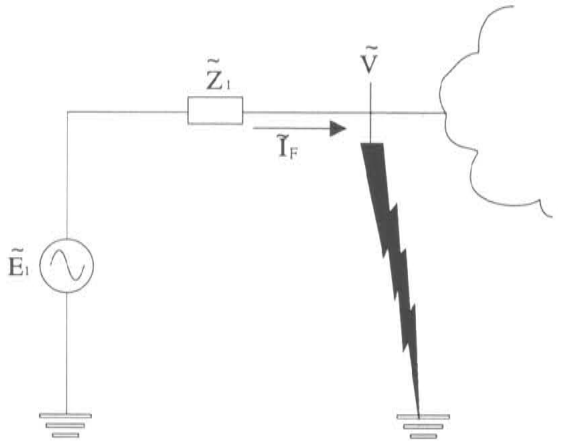

(b) Fault circuit

Figure 5.6 Derivation of Thevenin equivalent circuit

$$\tilde{E}_1 = \tilde{I}_n \tilde{Z}_1 + \tilde{V} \tag{5.1}$$

and from the fault circuit :-

$$\tilde{E}_1 = \tilde{I}_F \tilde{Z}_1 \tag{5.2}$$

Combining these equations gives :-

$$\tilde{Z}_1 = \frac{\tilde{V}}{\tilde{I}_F - \tilde{I}_n} \tag{5.3}$$

$\tilde{E}_1$ can then be found from either equation 5.1 or 5.2.

During a transient, the impedance of the synchronous machines in system 1 can change. The net effect on the fundamental power in or out of the equivalent circuit, however, can be represented by varying the source $\tilde{E}_1$ and keeping $\tilde{Z}_1$ constant.

EMTDC is a "point on wave" type program, and consequently models all frequencies, not just the fundamental. A more advanced equivalent impedance that is accurate for

harmonic frequencies as well is the ideal solution. This is investigated in detail in Chapter 6.

5.2.2 Interface Equivalent Sources

Information from the EMTDC model representing system 2 (refer Figure 5.5) is used to modify the source of the *equivalent circuit* of system 2 in the stability program TS. Similarly, data from TS is used to modify the source of the equivalent circuit of system 1 in EMTDC. These equivalent sources are normally updated at each TS step length (refer Section 5.3). From Figure 5.5, if both $\tilde{Z}_1$ and $\tilde{Z}_2$ are known, additional information is still necessary to determine update values for the sources $\tilde{I}_c$ and $\tilde{E}_1$. This information can be selected from the interface parameters of voltage $\tilde{V}$, current $\tilde{I}_1$, real power P, reactive power Q, and the power angle ϕ.

The interface voltage and current along with the phase angle between them have been chosen to interchange the information between programs. The reasons for the selection of these interface parameters is discussed in Chapter 6.

5.2.3 Measurement and Phase Conversion

An efficient recursive curve fitting algorithm is described in Chapter 4 to extract fundamental frequency information from the discrete point oriented waveforms produced by detailed programs such as EMTDC.

Analysis of the discrete data from EMTDC is performed over a fundamental period interval, but staggered to produce results at intervals less than a fundamental period. This allows the greatest accuracy in deriving fundamental results from distorted waveforms.

The stability program requires only positive sequence data so data from the three *ac* phases at the interface(s) is analyzed and converted to positive sequence by conventional means. The positive sequence voltage, for example, can be derived as follows :-

$$\tilde{V}_{ps} = \frac{1}{3}\left(\tilde{V}_a + \tilde{a}\tilde{V}_b + \tilde{a}^2\tilde{V}_c\right) \tag{5.4}$$

where

$\tilde{V}_{ps}$ = positive sequence voltage
$\tilde{V}_a, \tilde{V}_b, \tilde{V}_c$ = phase voltages
$\tilde{a}$ = 120 degree forward rotation vector (ie. $a = 1\angle 120°$)

Positive sequence data from the stability program is converted to three phase through simple multiplication of the rotation vector. For the voltage :-

$$\tilde{V}_a = \tilde{V}_{ps} \tag{5.5}$$

$$\tilde{V}_b = \tilde{a}^2\tilde{V}_{ps} \tag{5.6}$$

$$\tilde{V}_c = \tilde{a}\tilde{V}_{ps} \tag{5.7}$$

Some transient stability programs, such as TS, have the additional capability of modelling negative and zero sequence networks. If this option is utilised, sequence data from a stability program can then be converted to three phase through the following formulae :-

$$\tilde{V}_a = \tilde{V}_{ps} + \tilde{V}_{ns} + \tilde{V}_{zs} \tag{5.8}$$

$$\tilde{V}_b = \tilde{a}^2\tilde{V}_{ps} + \tilde{a}\tilde{V}_{ns} + \tilde{V}_{zs} \tag{5.9}$$

$$\tilde{V}_c = \tilde{a}\tilde{V}_{ps} + \tilde{a}^2\tilde{V}_{ns} + \tilde{V}_{zs} \tag{5.10}$$

where

$\tilde{V}_{ns}$ = negative sequence voltage
$\tilde{V}_{zs}$ = zero sequence voltage

Similarly, any unbalance in system 2 can be accommodated in the transient stability program.

5.2.4 Implementation

In Figure 5.5, $\tilde{E}_1$ and $\tilde{Z}_1$ represent the equivalent circuit of system 1 modelled in EMTDC, while $\tilde{Z}_2$ and $\tilde{I}_c$ represent the equivalent circuit of system 2 modelled in the stability program. $\tilde{V}$ is the interface voltage and $\tilde{I}_1$ the current through the interface which is assumed in the direction shown. The data from EMTDC can be incorporated into the stability analysis through the following means.

From the detailed EMTDC simulation, the magnitude of the interface voltage and current are measured, along with the phase angle between them. This information is used to modify the equivalent circuit source ($\tilde{I}_c$) of system 2 in TS. The updated $\tilde{I}_c$ value can be derived in the following manner :-

From Figure 5.5 :-

$$\tilde{E}_1 = \tilde{I}_1\tilde{Z}_1 + \tilde{V} \tag{5.11}$$

$$\tilde{V} = \tilde{I}_2\tilde{Z}_2 \tag{5.12}$$

$$\tilde{I}_2 = \tilde{I}_1 + \tilde{I}_c \tag{5.13}$$

From equations 5.12 and 5.13 :-

$$\tilde{V} = \tilde{I}_1\tilde{Z}_2 + \tilde{I}_c\tilde{Z}_2 \tag{5.14}$$

From equation 5.11 :-

$$\begin{aligned}\tilde{E}_1 &= I_1Z_1\angle(\theta_{I_1} + \theta_{Z_1}) + V\angle\theta_V \\ &= I_1Z_1\cos(\theta_{I_1} + \theta_{Z_1}) + jI_1Z_1\sin(\theta_{I_1} + \theta_{Z_1}) + V\cos\theta_V + jV\sin\theta_V\end{aligned} \tag{5.15}$$

The power factor angle ϕ between the voltage and the current is measured and known. θ_{I_1} can then be expressed as :-

$$\theta_{I_1} = \theta_V - \phi \tag{5.16}$$

From equation 5.15 :-

$$\begin{aligned}\tilde{E}_1 &= I_1 Z_1 \cos(\theta_V + \beta) + jI_1 Z_1 \sin(\theta_V + \beta) + V\cos\theta_V + j\sin\theta_V \\ &= I_1 Z_1(\cos\theta_V \cos\beta - \sin\theta_V \sin\beta) + V\cos\theta_V \\ &\quad + j\left[I_1 Z_1(\sin\theta_V \cos\beta + \cos\theta_V \sin\beta) + V\sin\theta_V\right]\end{aligned} \tag{5.17}$$

where $\beta = \theta_{Z_1} - \phi$

If $\tilde{E}_1 = E_{1r} + jE_{1i}$ then equating real terms only :-

$$E_{1r} = (I_1 Z_1 \cos\beta + V)\cos\theta_V + (-I_1 Z_1 \sin\beta)\sin\theta_V \tag{5.18}$$

Now $\tilde{Z}_1$ is known and constant throughout the simulation. From EMTDC, the magnitude values of V, I, and the phase difference ϕ are also known and hence so is β. $\tilde{E}_1$ can be determined in the TS phase reference frame from knowing $\tilde{Z}_1$ and the previous values of interface current and voltage from TS, through use of equation 5.11.

Now since :-

$$A\cos x + B\sin x = \sqrt{A^2 + B^2}\cos(x \pm \psi) \tag{5.19}$$

where $\psi = \tan^{-1}\left[\mp\frac{B}{A}\right]$.

then by letting :-

$$A = I_1 Z_1 \cos\beta + V \tag{5.20}$$

$$B = -I_1 Z_1 \sin\beta \tag{5.21}$$

$$x = \theta_V \tag{5.22}$$

the voltage angle θ_V in the TS phase reference frame can be calculated :-

$$\theta_V = \cos^{-1}\left[\frac{E_{1r}}{\sqrt{A^2 + B^2}}\right] - \psi \tag{5.23}$$

$$\left(\psi = \tan^{-1}\left[\frac{-B}{A}\right]\right) \tag{5.24}$$

From θ_V, it is possible to work out θ_{I_1} from equation 5.16. The equivalent current source $\tilde{I}_c$ can subsequently be calculated by rearranging equation 5.14 :-

$$\tilde{I}_c = \frac{V}{Z_2}\angle(\theta_V - \theta_{Z_2}) - I_1\angle\theta_{I_1} \tag{5.25}$$

In a similar way, data from the transient stability program simulation can be used to calculate a new Thevenin source voltage magnitude for the equivalent circuit of system 1 in the EMTDC program. Knowing the voltage and current magnitude at the TS program interface and the phase difference between them, by a similar analysis the voltage angle in the EMTDC phase reference frame is :-

$$\theta_V = \cos^{-1}\left[\frac{I_{cr}}{\sqrt{C^2 + D^2}}\right] - \psi \tag{5.26}$$

where I_{cr} is the real part of $\tilde{I}_c$, and :-

$$C = \frac{V}{Z_2}\cos\theta_{Z_2} - I_1\cos\phi \tag{5.27}$$

$$D = \frac{V}{Z_2}\sin\theta_{Z_2} - I_1\sin\phi \tag{5.28}$$

$$\phi = \theta_V - \theta_{I_1} \tag{5.29}$$

$$\psi = \tan^{-1}\left[\frac{-D}{C}\right] \tag{5.30}$$

Knowing the EMTDC voltage angle θ_V allows calculation of the EMTDC current angle θ_{I_1} from equation 5.29. The magnitude value of E_1 can then be derived from equation 5.11.

5.3 Interaction Protocol

Curve fitting analysis is applied to measure the variables from EMTDC over staggered discrete fundamental period window lengths, while the transient stability program variables are read directly at the interface. The data from each program must then be interchanged at appropriate points during the hybrid simulation run. The timing of this data interchange between the TS and EMTDC programs is important, particularly around discontinuities caused by fault application and removal.

There are three possible ways to usefully exchange information between the two programs. Figure 5.7 shows these three approaches and assumes, for simplicity, that the TS step length equals the fundamental period length (T).

Figure 5.7(a) demonstrates both programs interchanging information at the TS time-step, every period. This method effectively passes the previous time-step information from one program to the other. Previous time-step $(t - \Delta t)$ data is used to update the equivalent circuit for the present time-step.

Figure 5.7(b) shows the use of the previous time-step data in passing information from TS to EMTDC, but present time-step data when passing information from EMTDC to TS.

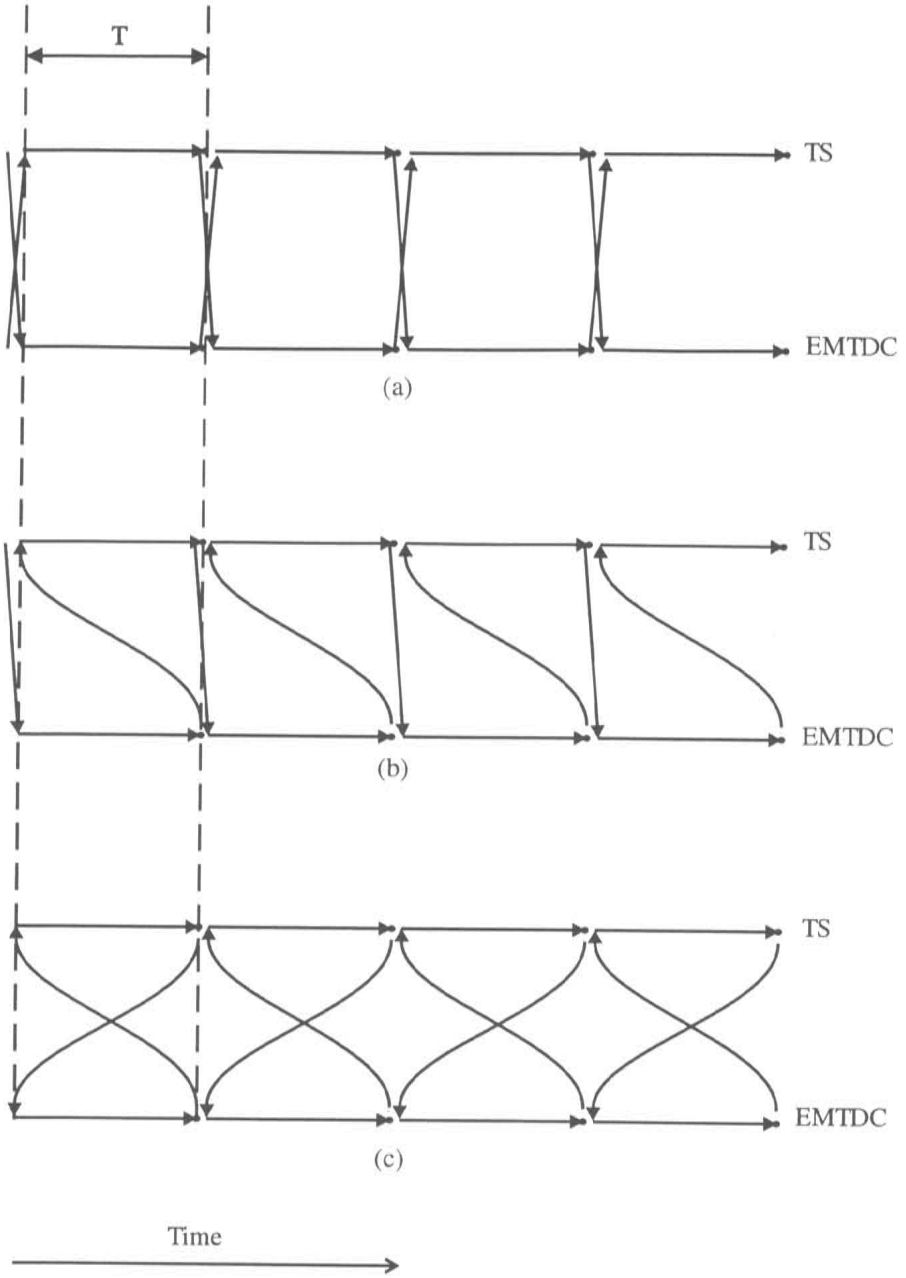

Figure 5.7 Interfacing methods

When the two programs are concurrent in time, TS passes its information to EMTDC. EMTDC then runs to $t + \Delta t$, and the information gathered over this present time-step given back to TS at time t. TS now runs to $t + \Delta t$, using equivalent circuit information current for the time-step being solved for, and catches up to EMTDC.

The final option is shown in Figure 5.7(c) and represents the use of present time-step information for both data paths. For example, TS is run to time $t + \Delta t$ and the information from this run used to update the TS equivalent in EMTDC at time t. EMTDC is then also run to time $t + \Delta t$ and similarly, the equivalent circuit of the EMTDC solution in TS is updated. This process is then repeated over the same time-step until the data passed between successive runs is effectively the same. This is consequently an iterative

procedure and as such, increases the computation time and complexity of the interfacing.

The *ac* system, being generally electro-mechanically responsive due to rotating machines, exhibits a relatively slow dynamic response to any disturbances. The accuracy of previous time-step information passed from TS to EMTDC therefore is an adequate assumption. Any fast controlled device such as an HV*dc* converter, exhibits fast load dynamics. Present time-step information is thus more appropriate to pass from EMTDC to TS in the solving of the TS network equation. The optimum method to use then, is that in Figure 5.7(b). It is non-iterative and therefore computationally economical, yet at the same time accounts adequately for the dynamics of the respective loads.

The interfacing philosophy can be modified to a cross between the methods of Figures 5.7(a) and (b) to cater for TS step lengths that are less than a fundamental period. This is a more typical situation. The information exchange protocol for this is shown in Figure 5.8. A portion of the figure is sequentially numbered to show the order of occurrence of the variable interchange. In the example, the stability step length is exactly one half a fundamental period.

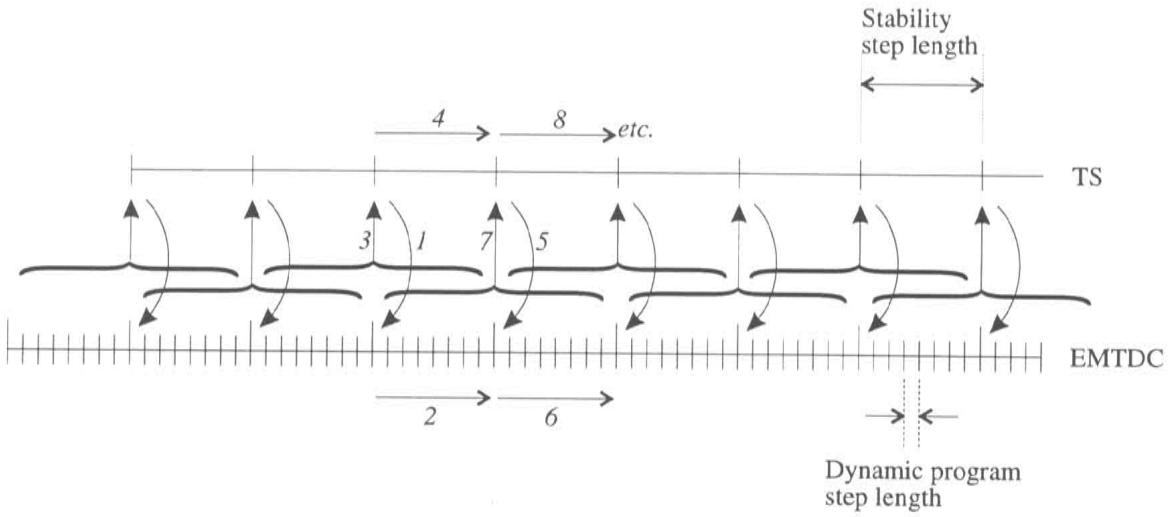

Figure 5.8 Normal interaction protocol

Following the sequential numbering on Figure 5.8, at a particular point in time, the EMTDC and TS programs are concurrent and the TS information from system 1 is passed to update the system 1 equivalent in EMTDC. This is shown by the arrow marked "1". EMTDC is then called for a length of half a fundamental period (arrow "2") and the curve fitted results over the last *full* fundamental period processed and passed back to update the system 2 equivalent in TS (arrow "3"). The information over this period is passed back to TS at the mid-point of the EMTDC analysis window which is half a period behind the current EMTDC time. TS is then run to catch up to EMTDC (arrow "4"), and the new information over this simulation run used to again update the system 1 equivalent in EMTDC (arrow "5"). This protocol continues until any discontinuity in the network occurs.

When a network change such as a fault application or removal occurs, the interaction protocol is modified to that shown in Figure 5.9. The curve fitting analysis process is also modified so as not to apply an analysis window over any point of discontinuity.

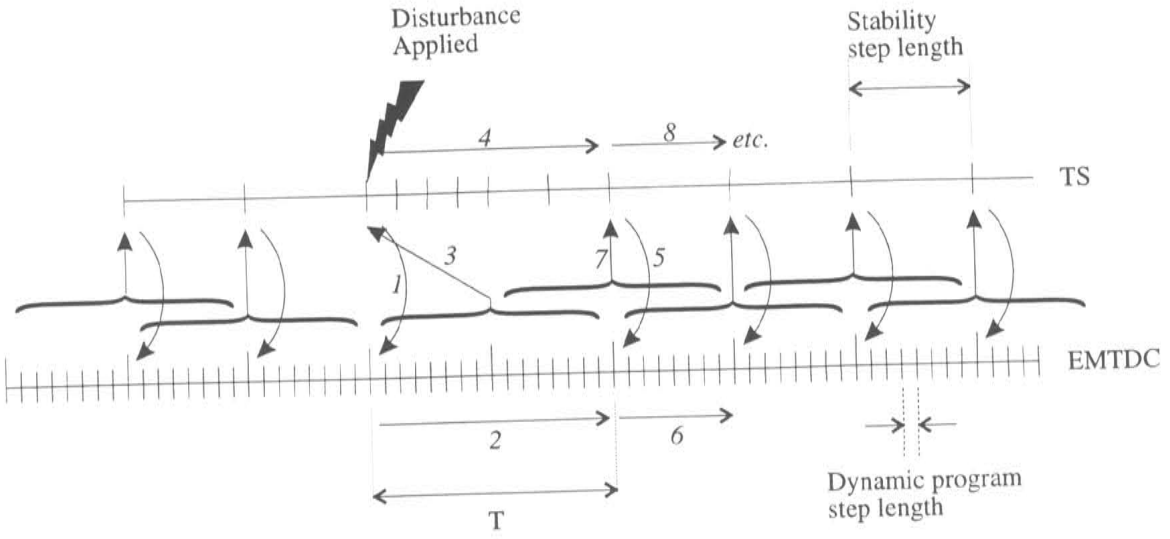

Figure 5.9 Interaction protocol around a disturbance

The sequential numbering in Figure 5.9 explains the flow of events. At the fault time, the interface variables are passed from TS to the system 1 equivalent in EMTDC in the usual manner as shown by the arrow marked "1". Neither system 1 or system 2 have yet been solved with the network change. The fault is now applied in EMTDC which is then run for a full fundamental period length past the fault application (arrow "2") and the information obtained over this period passed back to TS (arrow "3"). The fault is now also applied to the TS program which is then solved for a period until it has again reached EMTDC's position in time (arrow "4"). The normal interaction protocol is then followed until any other discontinuity time is reached.

A full period analysis after the fault is applied is necessary to accurately extract the fundamental frequency component of the interface variables as discussed in Chapter 4. The mechanically controlled nature of the *ac* system implies a dynamically slow response to any disturbance and so for this reason, it is considered acceptable to run EMTDC for a full period without updating the system 1 equivalent circuit during this time.

5.4 The Algorithm

The interfacing algorithm is shown in Figure 5.10. There are five possible states or conditions that the algorithm deals with and these are summarised in Table 5.1. The default state is "0" for the first time that the algorithm is called. This occurs once TS has reached steady state electro-mechanical equilibrium and is ready for interfacing, prior to a system disturbance.

State	Event
-1	Isolate TS network ready to interface with EMTDC
0	Initial time through interfacing routine
1	Normal interaction between TS and EMTDC
2	System network change signalled - run EMTDC for a full period past the fault and return information to TS
3	TS catching up with EMTDC after a system network change

Table 5.1 Interfacing states

Under the "0" state, EMTDC is called for a full fundamental period ahead of TS and its interfacing variables extracted and converted to positive sequence. The state is now set to "-1".

Under the "-1" state, TS is run for one half of a fundamental period and the variables at its interface location compared with those of EMTDC. This is simply to check and ensure that the data in both files is correctly set up. The TS network is then split into systems 1 and 2, and Norton equivalent circuits set up in each system. The state is now set to "1", representing normal interfacing conditions, and TS is solved until its time is concurrent with EMTDC.

Under the normal interfacing of state "1", variable information is given to EMTDC from TS to update its equivalent circuit. The equivalent circuit of system 1 in the TS model of system 2 is updated in the same way. EMTDC is then called for one half a period and the information measured over the last *fundamental period* of its simulation used to update the equivalent circuit of system 2 in TS.

In the interface data file, a time can be specified as a minimum termination time for EMTDC, after any network disturbance is cleared. Once this time is reached in the program, the interface variables of both system 2 models are compared at each TS time-step. If they correlate within a predefined tolerance over a set period, then EMTDC can be terminated and the TS representation of system 2 once again take over. During the period they are being checked, if at any time the variables are outside the specified tolerance, the checking period time is restarted.

When a network admittance change is about to occur, such as a fault being applied or removed, the interfacing routine is entered with a state value of "2". At this point in time, TS is concurrent with EMTDC. The TS interface variables are passed to EMTDC which is then run for a full period from the network discontinuity time. It is not accurate to apply the analysis window over the network discontinuity so the staggered window process must be restarted. The variables from EMTDC are passed back to TS at the time of the disturbance and the state is changed to "3".

State "3" allows TS to catch up to EMTDC before the normal interfacing procedure of state "1" recommences.

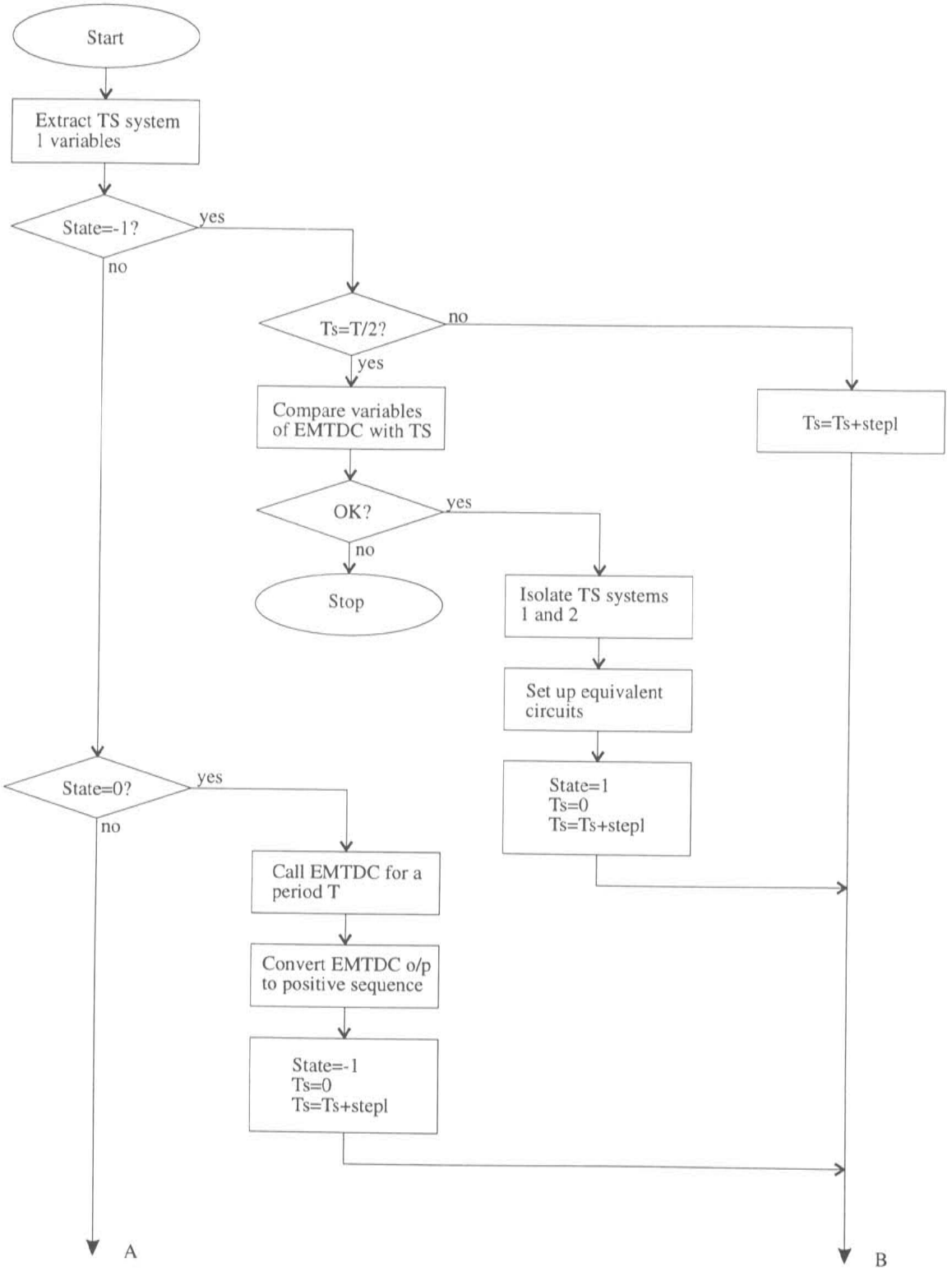

Figure 5.10 TSE hybrid algorithm

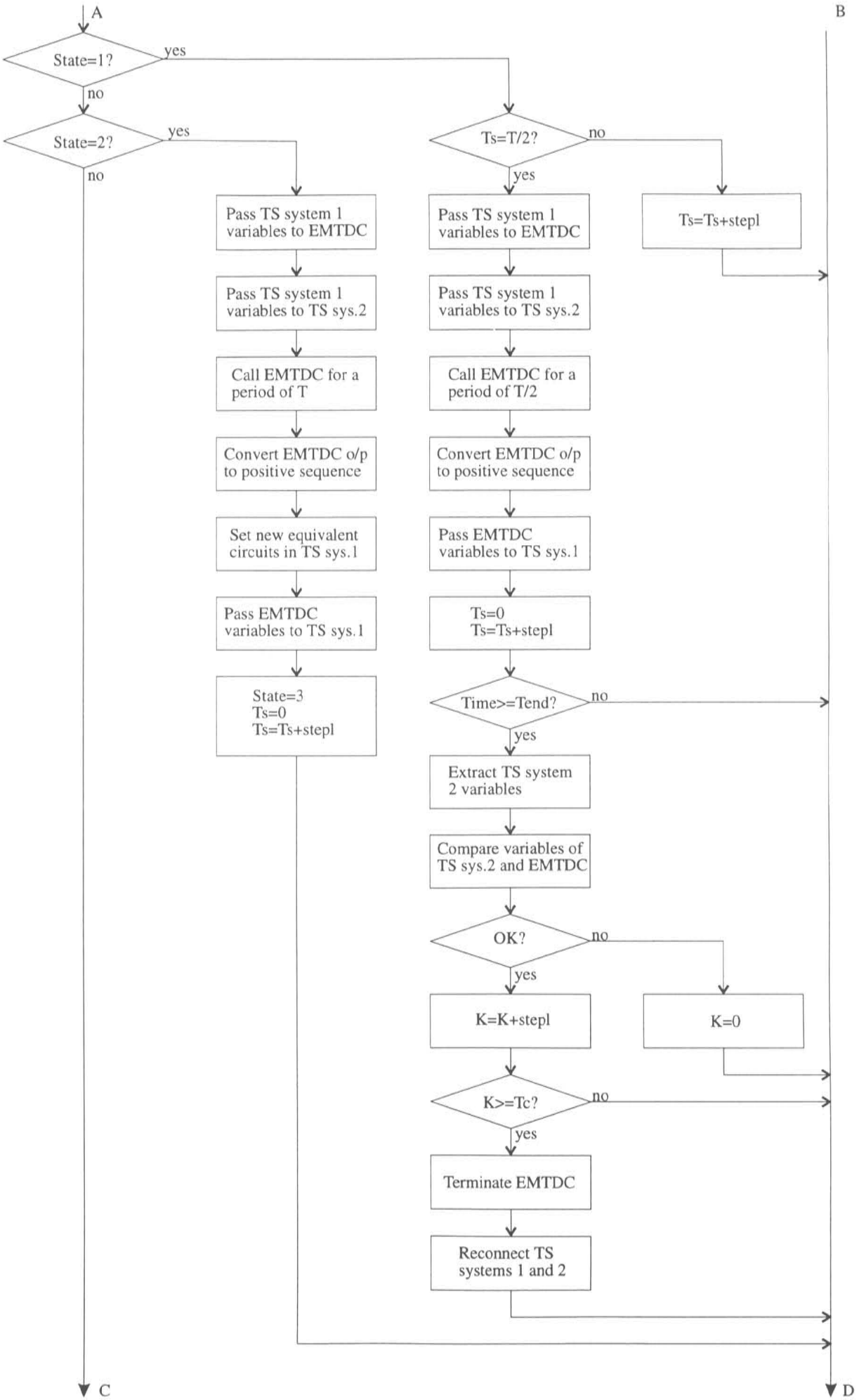
A
B
State=1?
yes
no
State=2?
yes
no
Ts=T/2?
no
yes
Pass TS system 1 variables to EMTDC
Pass TS system 1 variables to TS sys.2
Call EMTDC for a period of T
Convert EMTDC o/p to positive sequence
Set new equivalent circuits in TS sys.1
Pass EMTDC variables to TS sys.1
State=3
Ts=0
Ts=Ts+stepl
Pass TS system 1 variables to EMTDC
Pass TS system 1 variables to TS sys.2
Call EMTDC for a period of T/2
Convert EMTDC o/p to positive sequence
Pass EMTDC variables to TS sys.1
Ts=0
Ts=Ts+stepl
Ts=Ts+stepl
Time>=Tend?
no
yes
Extract TS system 2 variables
Compare variables of TS sys.2 and EMTDC
OK?
no
yes
K=K+stepl
K=0
K>=Tc?
no
yes
Terminate EMTDC
Reconnect TS systems 1 and 2
C
D

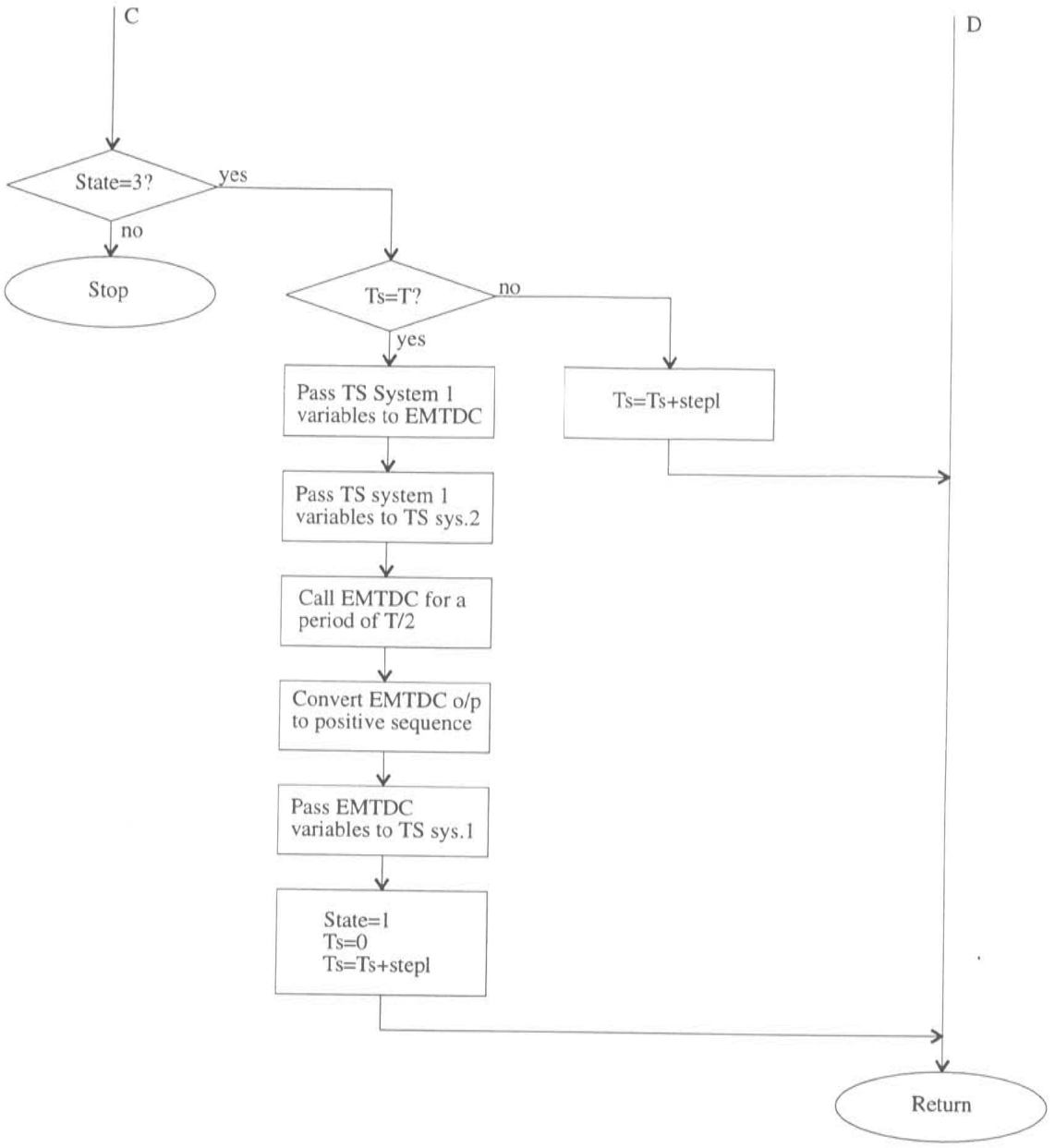

[stepl] TS program step length

[Ts] TS step length counter

[Tend] Minimum finish time for EMTDC

[K] Time counter for EMTDC and TS comparison of variables

[Tc] Time over which comparison must be within tolerance

5.5 Summary

An advanced hybrid package has been developed combining an electro-mechanical transient stability program with a detailed electromagnetic transient program. A hybrid approach is necessary because components such as HV*dc* or FACT systems often require detailed modelling, particularly when attached to weak *ac* systems. Conventional steady state or quasi-steady state representation of these devices in electro-mechanical stability programs are not sufficiently accurate, especially when disturbances occur close to their terminals. The fast dynamic responses exhibited by these types of loads require more detailed simulation, such as that possible with the three phase electromagnetic transient approach, EMTDC, incorporated in the developed hybrid. Detailed programs such as this, however, cannot model large *ac* networks due to computational expense, and therefore suffer from the need to reduce the *ac* network to a simplified equivalent.

The hybrid allows the flexibility of simulating certain components or sections of a power system in detail while simulating the rest of the system by a computationally efficient positive sequence, fundamental frequency model. In *ac-dc* systems, it offers an advantage to the *dc* system in providing the dynamic response of a large *ac* system rather than just an equivalent circuit. The hybrid also benefits the *ac* system in accurately modelling the dynamic changes that occur with the fast response of *dc* control. The hybrid has incorporated the interchanging of the detailed model with a more efficient quasi-steady state representation whenever possible. An advanced interaction protocol has also been designed for accurate interfacing of variable information between the two programs constituting the hybrid. An efficient implementation of this interfacing protocol inside the programs has been developed to allow each program to maintain separate phase reference frames.

Chapter 6

OPTIMUM INTERFACING TECHNIQUES

An inherent difficulty in hybrid interfacing is that an electro-mechanical transient stability program is generally fundamental frequency positive sequence based, while the detailed solution is invariably three phase and presents a resultant waveform which effectively models all frequencies. This has been the case with both the previous hybrid approaches of Reeve and Adapa and Heffernan *et al.* and is also the case with the programs used in the hybrid described in this thesis [Reeve and Adapa, 1988] [Heffernan *et al.*, 1981].

Transfer of information from TS to EMTDC, by its nature, is usually positive sequence at fundamental frequency, while information from EMTDC to TS on the other hand, must be reduced to pass only the information that is relevant to the TS model.

This difficulty highlights two important issues in hybrid interfacing :-

- where to locate the interface point between the two programs, and
- what information should be measured and passed between the programs

This chapter looks at both these issues, particularly in the light of previous work that has been done in these areas.

6.1 Interface Parameter Selection

The information that must be transferred from one program to the other must be sufficient to determine the power flow in or out of the interface. The generally available parameters that can be measured include the real power P, the reactive power Q, the voltage V, and the current I through the interface (Figure 6.1). Phase angle information is also required if separate phase frames of reference are to be maintained.

6.1.1 TS to EMTDC Data Transfer

The equivalent circuit of the TS modelled system in the EMTDC program consists of a source and an impedance, both of which must be three phase. From Section 5.2, the impedance is known and only the source requires updating. The TS program is simplistic in its modelling relative to EMTDC, and any interface variable can be easily read or calculated at any time-step. The choice of interface parameter to transfer was then simply

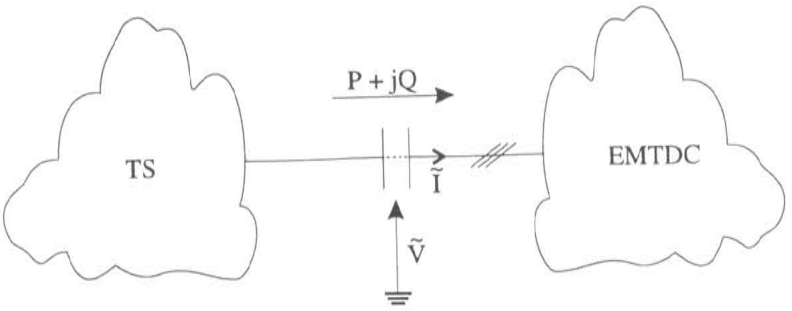

Figure 6.1 Hybrid interface

chosen to be the interface voltage and current. The positive sequence information is converted to three phase information through sequential component formulae (Section 5.2.3).

6.1.2 EMTDC to TS Data Transfer

Obtaining the required information from EMTDC requires a different approach. The parameters are now "point on wave" and require a method such as curve fitting presented in Chapter 4 to translate them. The measurements must be made at discrete points in time necessary for the interfacing transferral of data which occur at each TS time-step.

A significant difference between TS and EMTDC is that in TS, sinusoidal waveforms are assumed. EMTDC waveforms however, particularly during faults, can be very non-sinusoidal. Measurement of power flow is subject to debate, since there is no consensus on a universal definition for power when waveforms are non-sinusoidal [Emanuel, 1993]. Reactive power, for example, has two primary definitions. The Budeanu definition is accepted by the American National Standards Institute (ANSI) and the Institute of Electrical and Electronic Engineers (IEEE), while the International Electro-technical Commission (IEC) uses a different definition proposed by Fryze [IEC, 1979].

In the hybrid program proposed by Heffernan, the total *rms* real power was used as one of two interfacing parameters chosen to transfer information. The total *rms* power is made up of the fundamental power and harmonic power *ie.* :-

$$P_{rms} = P_f + P_h \tag{6.1}$$

where

P_f = fundamental *rms* power
P_h = total harmonic *rms* power

The *rms* power is very simple to extract from point oriented waveforms and Fourier transform or curve fitting methods are not necessary. It can be calculated as follows :-

$$P_{rms} = \frac{1}{N}\left[\sum_{n=1}^{N}\left(\sum_{i=a,b,c} v_i i_i\right)\right] \tag{6.2}$$

This also greatly reduces the computing time necessary for the data extraction from EMTDC.

The choice of *rms* power was made on the basis that harmonic power flow will result only from in-phase components of harmonic voltage and current. The assumption was made that if a system contains only a low resistive component, then the harmonic power flow is not significant.

This however, is not valid for every situation, and particularly at the inverter end of an HV*dc* link, the resistive component of the network is not insignificant [Bowles, 1970]. Certain harmonic frequencies in a network may also be parallel resonant or close to parallel resonance and exhibit more resistance than reactance. The presence of a transient may excite the resonant frequency and greatly affect the results. It is important, therefore, to model the fundamental power flow accurately.

Another factor to consider is that the direction of fundamental power may not necessarily be the same as the direction of harmonic power. With an HV*dc* link, while fundamental power is drawn into a rectifier, much of the harmonic power flow will be in the reverse direction. The *rms* real power measured is the difference between these two powers and so not entirely representative of the fundamental power load of the HV*dc* link. Conversely, at the inverter end the *rms* real power will include harmonic power flow into the *ac* system. This may exaggerate the amount of true fundamental power from the inverter.

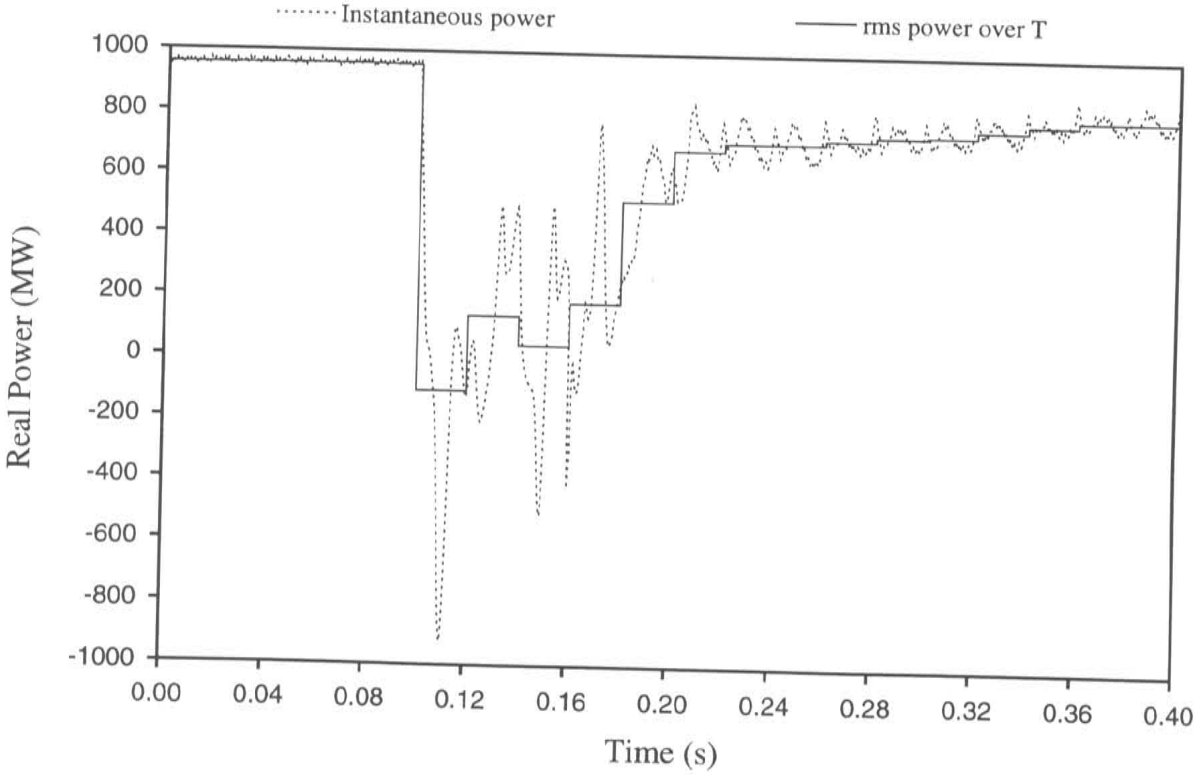

Figure 6.2 Total *rms* power

Figure 6.2 shows an EMTDC simulated result of a single phase fault at the inverter end of the CIGRE HV*dc* benchmark model [Szechtman *et al.*, 1991] (refer Appendix A.1). The instantaneous power is shown, along with the total *rms* power over discrete one cycle intervals. For hybrid interfacing purposes, data is transferred at discrete intervals equal to the stability program time-step and these are significantly larger than the interval between the discrete output points constituting the instantaneous power. The *rms* power is then taken over a fundamental period to represent its use in a hybrid situation. The fault shown in Figure 6.2 is used to compare various means of power representation in this section.

Figure 6.3 shows an analysis of the same fault comparing fundamental frequency power with the total *rms* power. The fundamental frequency power was derived using the curve fitting method in Chapter 4 to extract both fundamental voltage and current. The comparison shows that, particularly during the fault time, there exists a significant amount of P_h or harmonic *rms* power in the total *rms* power.

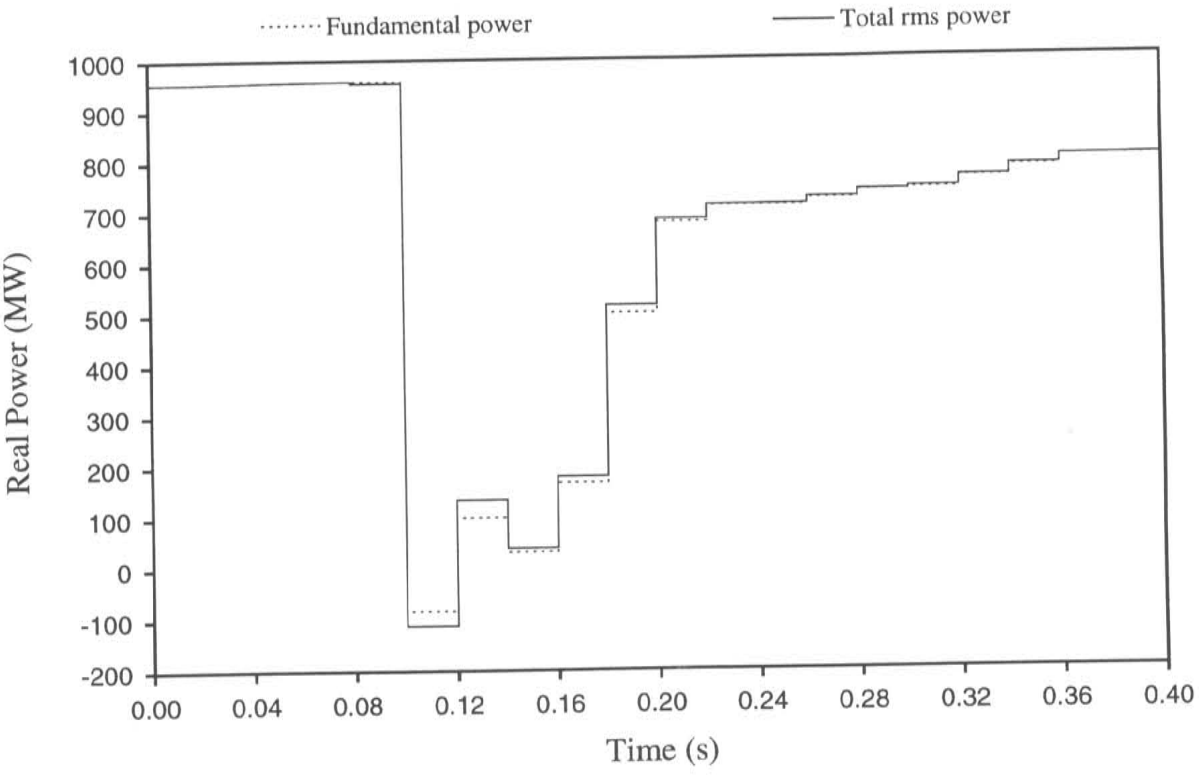

Figure 6.3 Fundamental power versus total *rms* power

The harmonic power absorbed by *ac* machines is almost entirely converted to heat loss. The effect of harmonic power on the mean torque of a machine is, in general, insignificant [Emanuel, 1990] [Arrillaga *et al.*, 1985]. These harmonic losses occur primarily in the rotor circuit but also in the stator windings and damper bars. Certain loads such as lighting and resistive heating may benefit from harmonic power, but in general it is not accurate to lump the entire *rms* real power measured into an effective rotational power of fundamental frequency.

A potentially larger problem exists when the three phase network is unbalanced. The fundamental frequency real power can then consist of positive, negative, and zero sequence components *ie.* :-

$$P_f = P_{f_{ps}} + P_{f_{ns}} + P_{f_{zs}} \tag{6.3}$$

where

$P_{f_{ps}}, P_{f_{ns}}, P_{f_{zs}}$ = positive, negative, and zero sequence components of fundamental frequency real power respectively

Negative and zero sequence powers cause additional power loss in a network and are generally useless and a liability [Emanuel, 1993]. Figure 6.4 shows the sequence composition of the fundamental *rms* power shown in Figure 6.3.

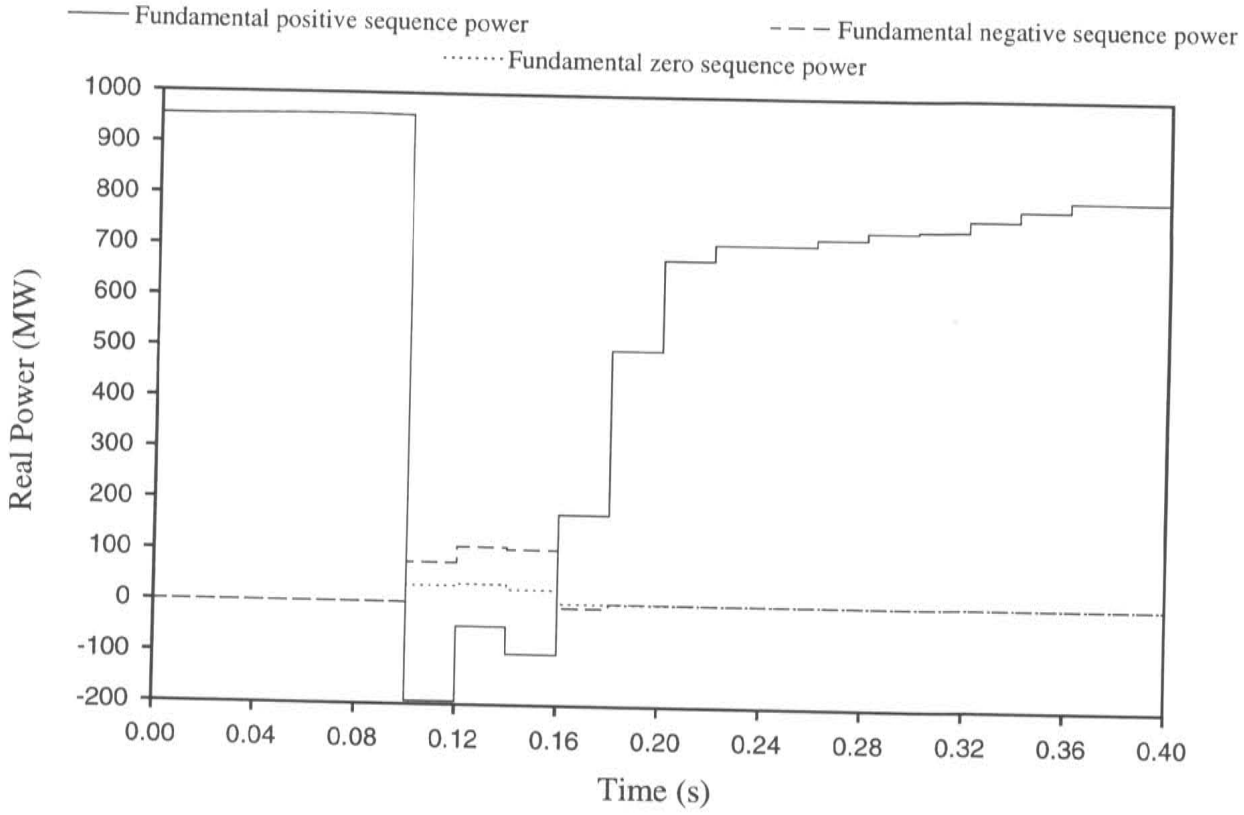

Figure 6.4 Sequence components of fundamental frequency *rms* power

Fundamental frequency negative sequence currents, in the presence of damper or armotisseur windings, can produce a braking torque which will retard the rotor [Clarke, 1950; Arrillaga *et al.*, 1985]. Damper windings, however, also serve to lower the negative sequence impedance of a machine which in turn reduces the negative sequence voltage [Kimbark, 1956]. Which of these two opposing effects is dominant depends on the

resistance of the damper windings. High resistance windings cause the braking torque to be the significant effect. The braking power of the negative sequence current is :-

$$P_b = \frac{1}{2} I_{rn}^2 R_r \tag{6.4}$$

$$\simeq I_{sn}^2 (r_n - r_p) \tag{6.5}$$

where

I_{rn} = negative sequence rotor current
R_r = rotor resistance
I_{sn} = negative sequence stator (or armature) current
r_n = negative sequence resistance of the machine
r_p = positive sequence resistance of the machine

The negative sequence resistance can be approximated from the rotor and the armature resistance *ie.* :-

$$r_n \simeq (R_s + \frac{1}{2} R_r) \tag{6.6}$$

where

R_s = armature resistance

Retardation of the rotor can also be caused by *dc* components in the armature windings. Three phase faults at or near machine terminals can cause *dc* components of short circuit armature current which can have a definite braking effect on the machine [Kimbark, 1956]. The braking power in this case is :-

$$P_b = 2 I_s^2 (r_n - r_p) \tag{6.7}$$

$$\simeq i_{dc}^2 (r_n - r_p) \tag{6.8}$$

where

I_s = the effective very low frequency value of the armature current
i_{dc} = instantaneous *dc* component of armature current

The total *rms* power then, is not always equivalent to either the fundamental frequency power nor the fundamental frequency positive sequence power. A comparison of these three powers is shown in Figure 6.5. The difference between total *rms* power and the positive sequence power can be seen to be highly significant during the fault.

The most appropriate power to transfer from EMTDC to TS is then the fundamental frequency positive sequence power. This, however, requires knowledge of both fundamental frequency positive sequence voltage and fundamental frequency positive sequence

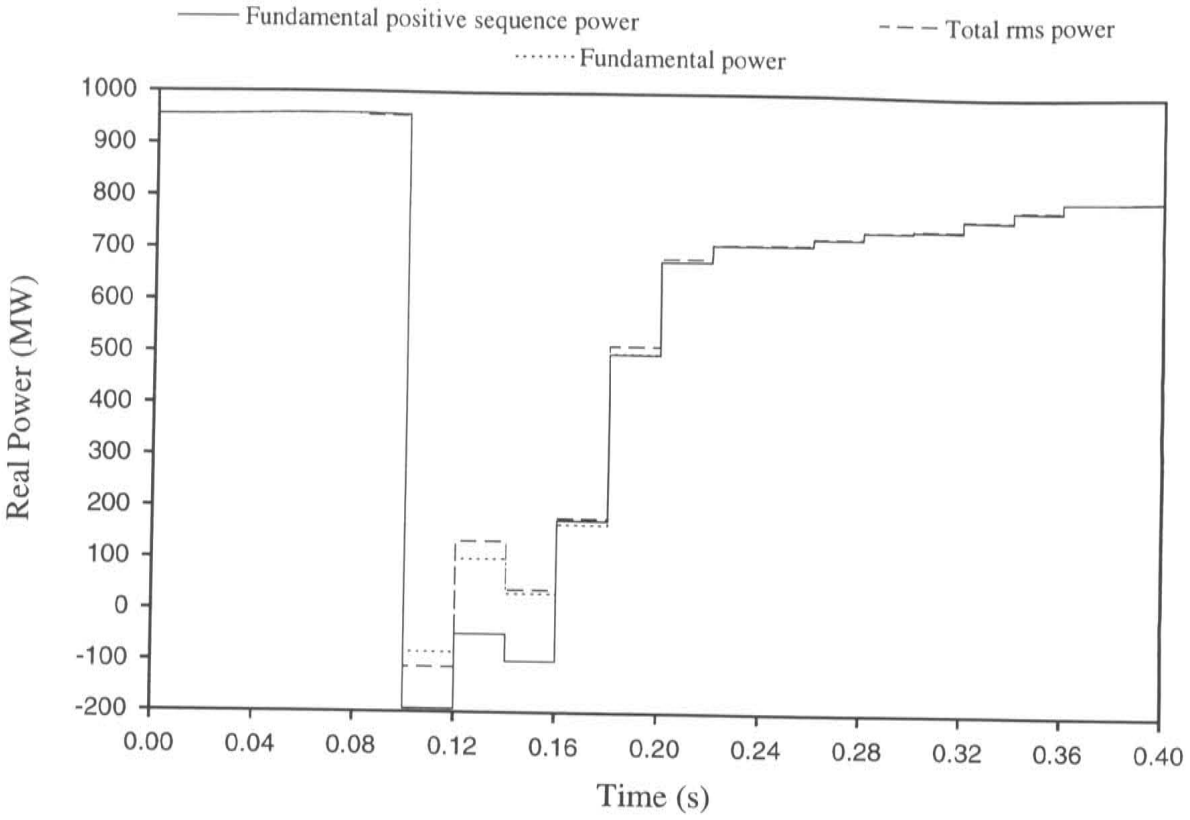

Figure 6.5 Comparison of total *rms* power, fundamental frequency power, and fundamental frequency positive sequence power

current. These two variables constitute enough information on their own and hence the use of any power variable to transfer information becomes redundant.

6.2 Interface Location

6.2.1 Converter Bus Interface

In the initial hybrid interfacing of a detailed solution with a transient stability program described by Heffernan *et al.*, the intention was to model the *ac* and *dc* solutions separately [Heffernan *et al.*, 1981]. The point of interface location was consequently the converter bus terminal. The detailed *dc* link model included all equipment connected to the converter bus, such as the *ac* filters, however every other *ac* component was modelled within the stability analysis. A fundamental frequency Thevenin equivalent was used to represent the stability program in the detailed solution and vice versa.

This concept of separating the *ac* and *dc* system modelling is an obvious one since the non-linear valve switching of the converter requires a detailed elemental analysis, while on the other hand, the stability representation is entirely adequate for the dynamically slow *ac* network. The number of interface locations is subsequently kept low, reducing

complexity of the interfacing techniques. The computational economy of the hybrid is also optimised by keeping the detailed solution to a minimum.

6.2.2 Extended Bus Interface

A different approach to hybrid analysis was proposed by Reeve and Adapa where the interface location was extended out from the converter bus into the *ac* system [Reeve and Adapa, 1988]. Reeve and Adapa maintained that, particularly for weak *ac* systems, a fundamental frequency equivalent representing the *ac* system was not sufficient at the converter terminals of the detailed *dc* solution. Other frequencies present in the detailed *dc* solution are not taken into account.

To counter this inadequacy, it was suggested that the interface location be moved outward from the converter into the *ac* system. The extent of the *ac* system to be included in the *dc* system depends on two factors, phase imbalance and waveform distortion.

As more of the *ac* system was encompassed in the detailed solution however, it was noted that the number of interface buses will generally increase.

A test system was devised by Reeve and Adapa to demonstrate the need for an extended interface rather than an interface at the converter terminal bus. The *ac* system was designed with an effective short circuit ratio at the inverter terminal of 3.0. A solid three phase short circuit fault was applied at the inverter bus and the results analyzed. A benchmark test case was performed with the entire analysis in EMTP while two other cases were compared with this benchmark, one interfacing at the converter bus and the other at an extended bus. The results from Reeve and Adapa are shown in Figures 6.6 and 6.7.

Figure 6.6 shows the inverter *ac* bus voltage for the three test cases. Cases (i) and (iii) are almost identical and represent the benchmark EMTP case and the hybrid case with the extended interface respectively. The peak recovery over-voltage in these cases is $1.4pu$. Case (ii) representing the hybrid solution with the converter bus interface shows more overall distortion and prolonged effects after the fault removal. The peak over-voltage in this case is $2.06pu$.

The *ac* short circuit currents to the fault are shown in Figure 6.7. Similarly to the voltage waveforms, the hybrid case with the converter bus interface (case (ii)) shows significantly different results than the benchmark and the extended interface cases (cases (i) and (iii) respectively). The over-current in case (ii) reaches $5.43pu$ as opposed to $6.36pu$ for cases (i) and (iii).

From the results shown, the authors claim that use of the converter bus is clearly inappropriate since the difference in results between the two interface location tests could be important for critical cases of transient stability.

6.2.3 Optimum Interface Bus Location

Although the concept of extending the interface location further out into the *ac* system has its advantages, it also suffers many disadvantages. The concept is proposed in particular for weak *ac* systems. A weak *ac* system however, is likely to have any major generation capability far removed from the converter terminal bus, as local generation serves to

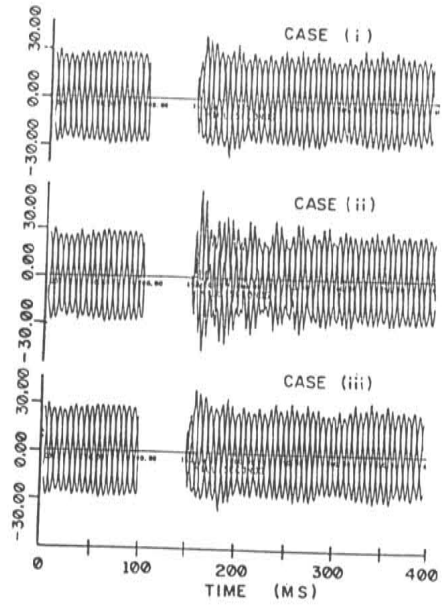

Figure 6.6 Inverter *ac* voltage
[Reeve and Adapa, 1988]

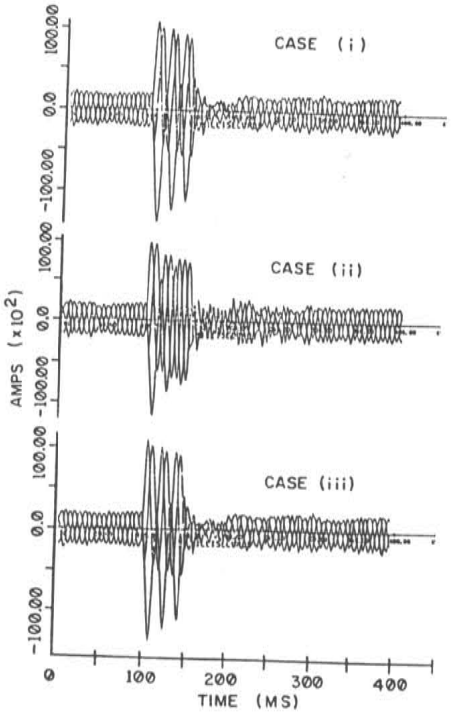

Figure 6.7 Inverter *ac* current
[Reeve and Adapa, 1988]

enhance system strength. If the generation is indeed far removed out into the *ac* system, then the distance required for an interface location to achieve considerably less phase imbalance and waveform distortion is also likely to be significant.

The primary advantage of a hybrid solution is in accurately providing the *dc* dynamic response to a transient stability program, and in efficiently representing the dynamic response of a considerably sized *ac* system to the *dc* solution. Extending the interface some distance into the *ac* system where the effects of a system disturbance are almost negligible diminishes the hybrid advantage. If a sizeable portion of the *ac* system requires modelling in detail before an interface to a transient stability program can occur, then one might question the use of a hybrid solution at all and instead use a more conventional approach of a detailed solution with *ac* equivalent circuits at the system cut-off points.

Another significant disadvantage in an extended interface is that *ac* systems may well be heavily interconnected. The further into the system that an interface is moved, the greater the number of interface locations required. The hybrid interfacing complexity is thus increased and the computational efficiency of the hybrid solution decreased. The requirement for a detailed representation of a significant portion of the *ac* system serves to decrease this efficiency, as does the increased amount of processing required for variable extraction at each interface location.

The difficulties and disadvantages posed by an extended interface bus demand a re-examination of the converter terminal bus as the interface location. The advantages of using the converter bus are clear :-

- The detailed system is kept to a minimum
- Interfacing complexity is low
- Computational expense is minimised
- Converter terminal equipment such as filters, synchronous condensers, SVC's *etc.* can still be modelled in detail

Reeve and Adapa rightly pointed out that the major drawback of the detailed solution is in not seeing a true picture of the *ac* system, since the equivalent circuit is fundamental frequency based. Waveform distortion and imbalance also make it difficult to extract the fundamental frequency information necessary to transfer to the stability program.

The problem of waveform distortion for transfer of data from EMTDC to TS is dependent on the accuracy of the technique for extraction of interfacing variable information. If fundamental frequency quantities can be accurately measured under distorted conditions, then the problem is solved. Chapter 4 of this thesis described an efficient curve fitting algorithm which was used to analyze various types of waveform disturbances. It was shown that using the technique described, fundamental frequency quantities *can* be accurately measured under a assortment of waveform disturbing effects.

A second problem involves the effects of waveform distortion on the detailed solution. A simple fundamental frequency equivalent circuit is insufficient to present the correct impedance of the *ac* system at other frequencies to the converter.

Reeve and Adapa countered this second problem by representing more of the *ac* system in detail through use of the extended interface bus. The impedance at the converter bus was

then more accurate for other frequencies and not just for the fundamental. The difficulties with an extended interface bus have already, however, been made clear. An alternative solution is to present a fully frequency dependent equivalent circuit of the *ac* system at the converter terminal instead of just a fundamental frequency equivalent. A frequency dependent equivalent prevents the necessity of modelling any significant portion of the *ac* system in detail yet still provides an accurate picture of the system impedance across its frequency spectra. Frequency dependent equivalents can be easily derived by such methods as that proposed by Watson [Watson *et al.*, 1985].

To validate the necessity of a frequency dependent equivalent, a test system based on that devised by Reeve and Adapa was used to show the unsuitability of the converter bus. This is shown in Figure 6.8. The inverter effective short circuit ratio was reduced even further to 2.0 providing an even weaker *ac* system connected to a *dc* link. The *dc* link was represented by the CIGRE benchmark model [Szechtman *et al.*, 1991]. Data for the test system can be found in Appendix A.2.

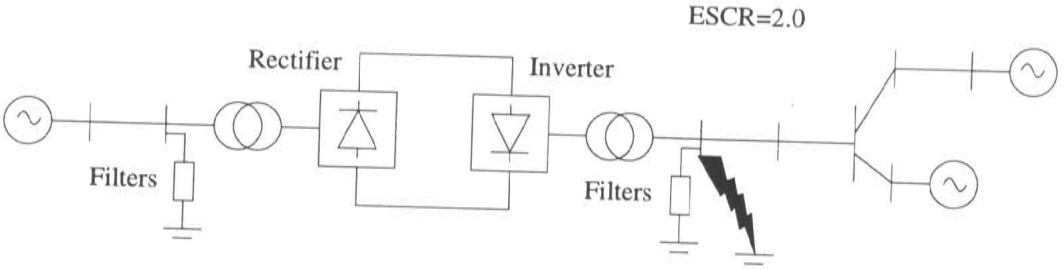

Figure 6.8 Test System

Similarly to Reeve and Adapa, a three phase solid short circuit fault was applied at the inverter terminal. Three cases were investigated, the first being the entire system represented by the detailed solution. The second and third cases were the hybrid solution interfaced at the converter bus, one case with a fundamental frequency Thevenin representation of the stability program in the detailed solution, and the other with a frequency dependent equivalent.

The inverter terminal voltage results for the three cases are shown in Figure 6.9. The benchmark EMTDC case and the frequency dependent equivalent case are identical. The fundamental frequency equivalent case (Figure 6.9(b)) shows more distortion and prolonged effects from the disturbance than the benchmark EMTDC case, similar to the results shown by Reeve and Adapa.

The inverter *ac* current results are shown in Figure 6.10. These too show a significant difference between the fundamental frequency equivalent case (Figure 6.10(b)) and the benchmark EMTDC solution. The over-currents during the fault are less for the fundamental frequency equivalent case, while the distortion is again more evident and

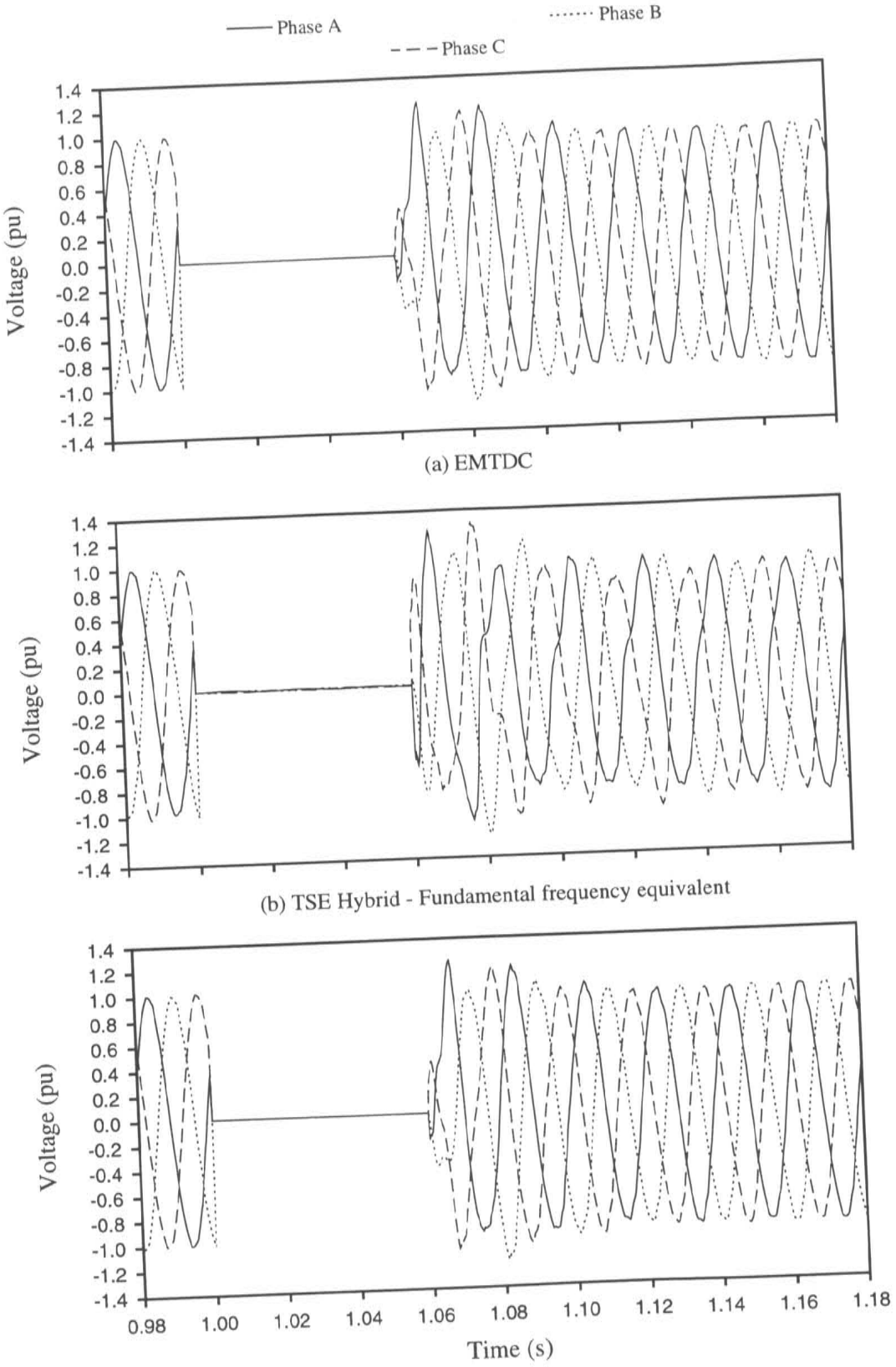

(a) EMTDC

(b) TSE Hybrid - Fundamental frequency equivalent

(c) TSE Hybrid - Frequency dependent equivalent

Figure 6.9 Inverter *ac* voltage

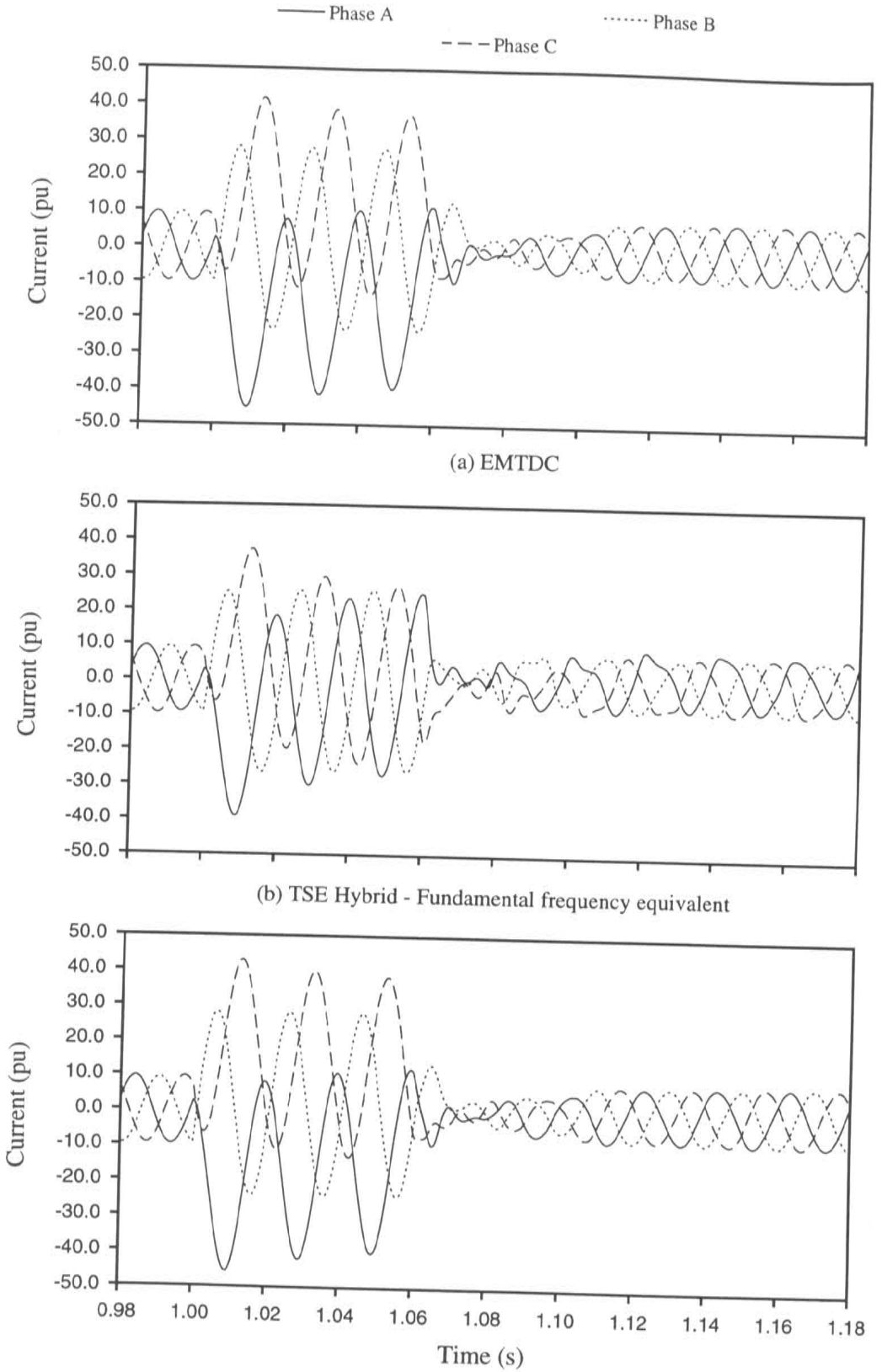

(a) EMTDC

(b) TSE Hybrid - Fundamental frequency equivalent

(c) TSE Hybrid - Frequency dependent equivalent

Figure 6.10 Inverter *ac* current

prolonged. The case using a frequency dependent equivalent for the *ac* system equivalent in EMTDC is again identical to the benchmark EMTDC solution.

These results correlate well with those by Reeve and Adapa and show the inadequacy of a fundamental frequency equivalent at the converter terminal. Additionally the results show that using a frequency dependent equivalent is also entirely adequate for presenting the correct effects of waveform distortion to the converter terminal. A frequency dependent equivalent offers an alternative solution to the extended interface bus proposed by Reeve and Adapa. This alternative is easier to create and implement, more computationally efficient, and just as accurate in providing a correct impedance at all frequencies to the converter terminal.

6.3 Summary

This chapter investigated two critical aspects of hybrid interfacing, the interfacing parameters passed between the two programs, and the location at which interfacing should occur. The transfer of information from TS to EMTDC is relatively simple, from EMTDC to TS however, information must be selectively filtered to pass only the relevant fundamental frequency positive sequence data. A previous approach using *rms* power was shown to be arguably inappropriate, particularly during unbalanced faults. Any meaningful representation for fundamental frequency power can only come from a knowledge of both $\tilde{V}$ and $\tilde{I}$, also at fundamental frequency. These parameters represent enough information on their own and so the use of power as an interface parameter becomes redundant.

The previous approaches of where to locate the interfacing were then analyzed. An extended interface out into the *ac* system gave some advantages over a converter terminal interface but it also lessened the usefulness of a hybrid solution. With an interface at the converter terminal, a frequency dependent equivalent was offered as an alternative approach to obtain the same merits as an extended interface without the inherent disadvantages. Results were shown to confirm the converter terminal as an appropriate location when a frequency dependent equivalent is used.

Chapter 7

HYBRID PROGRAM STUDIES

The previous two chapters have described a hybrid solution to *ac-dc* power systems, allowing detailed representation of a *dc* system while maintaining a full dynamic representation of the *ac* system. This hybrid solution is now applied to a test system and subjected to two different disturbances to determine the system response.

The test system is modelled both entirely in the transient stability program TS, and in the electromagnetic transient program EMTDC for comparison purposes. The *dc* system in the TS only solution is modelled using quasi-steady state equations as outlined in Chapter 2, while the hybrid solution uses EMTDC to model the *dc* system in elemental detail.

The inherent differences in these modelling approaches are clearly shown in the results and are explained in the course of this chapter.

7.1 The Test System

The test system selected for these studies consists of a two-terminal 1000 MW mono-polar HV*dc* link connected on the inverter side to a simple *ac* system, and on the rectifier side to a more complex *ac* system incorporating a number of generating buses.

The HV*dc* system is based on the CIGRE benchmark model which is designed to promote comparison between various simulation tools and in particular to investigate different HV*dc* control strategies [Szechtman *et al.*, 1991]. The link consists of two phase shifted six pulse Graetz bridges at both the inverter and rectifier terminals giving an overall conventional twelve pulse configuration. The nominal *dc* line voltage is 500 kV while the *dc* current is 2000 A. The parameters of the *dc* line between the converter terminals are typical of that for a medium to long cable.

The inverter *ac* system is identical to that in the CIGRE benchmark case and is a simple R-L-L equivalent circuit system. Filters on the *ac* side are included and are of the damped-arm type. A capacitor bank is also provided to sufficiently meet the reactive power demands of the inverter terminal. The inverter *ac* system short circuit ratio, including the converter terminal filters, is 2.5. The HV*dc* link is shown in Figure 7.1 along with the inverter side *ac* system representation.

The rectifier *ac* system is a simplified portion of the New Zealand South Island system and is shown in Figure 7.2. The *ac* system contains four generating buses in an interconnected loop composed of six buses in total. Double circuit transmission lines exist

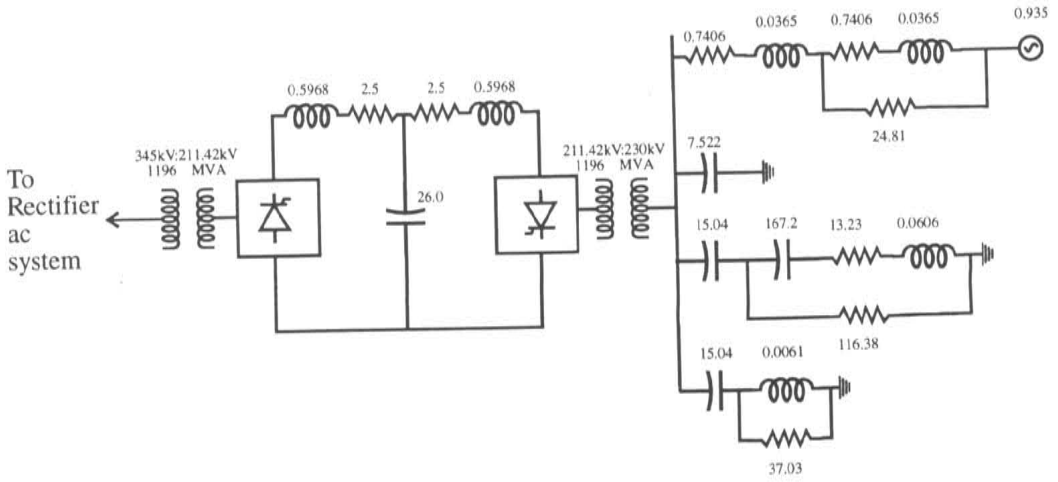

Figure 7.1 Test system HV*dc* link and inverter *ac* system

between Roxburgh and Clyde, and Clyde and Twizel, while single circuit lines connect the rest of the system. Loads representing further system connections are present at both Twizel and Roxburgh. Each generator has associated with it both an automatic voltage regulator (AVR) and a speed governor. Details of the test system parameters are outlined in Appendix A.3.

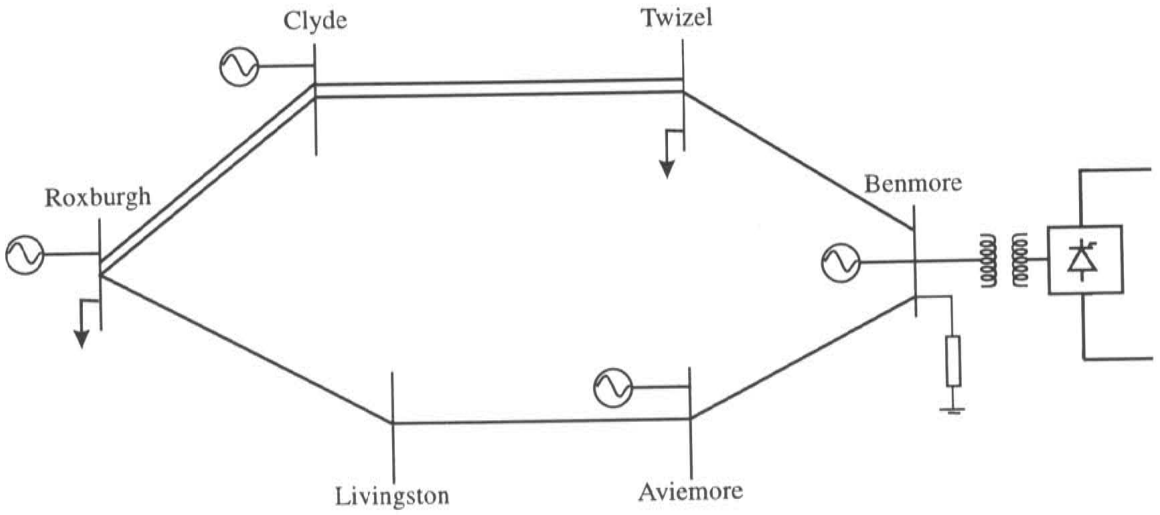

Figure 7.2 Test system rectifier *ac* system

The converter rectifier terminal also has a set of filters as per the CIGRE benchmark model and with these, the short circuit ratio is calculated to be 2.7.

7.1.1 HV*dc* Controls

The HV*dc* control system for TS is largely inherent in the program, with one of the two terminals specified in constant current mode, and the other in constant voltage at a specified firing order. For the test system, the rectifier is specified under constant current control

and the inverter under minimum gamma control. Under a fault situation, the mode of these terminals may be swapped if the rectifier *dc* voltage falls below that of the inverter.

Electro-mechanical stability programs, including TS, are somewhat limited in their simulation of abnormal operating conditions. In TS for example, an abnormal operating condition exists when the commutation angle exceeds 60 degrees. If this occurs at the inverter terminal, the inverter is simply bypassed. The rectifier terminal is kept under operation and maintains the current to at least 30% of its nominal setting. After a set period, if the problem causing abnormal operation has been removed, the inverter is re-started and the power ramped back up to normal using current control.

If abnormal operation occurs at the rectifier terminal, the rectifier is blocked, the inverter bypassed, and the entire link is shut down for a set period. Once this period has elapsed and the problem causing abnormal conditions removed, the rectifier is then de-blocked and the *dc* current ramped up to 30% of its nominal value. The inverter terminal is then re-started and the power ramped back up to normal.

In the detailed EMTDC program, the HV*dc* controls are completely user definable and can be specified down to actual firing orders instead of current settings.

The TS program is only one example of transient stability programs available, many of which can model *dc* controls in more comprehensive detail. For this reason, the EMTDC controls were restricted to model the same functionality as that in TS to obtain a fair comparison in the results. Shut-down and start-up procedures around a fault were also included in EMTDC to match the TS program constraints. The rectifier control system is again constant current while the inverter control system is minimum gamma.

The constant current control on the rectifier seeks to maintain the *dc* current at its set value by controlling the ordered firing angle (alpha). If the *ac* voltage at the rectifier terminal falls, then the firing angle decreases to maintain the rectifier *dc* voltage constant and hence the voltage profile between the rectifier and inverter, and consequently the *dc* current. A minimum firing angle of 3 degrees forms the limit the rectifier can control to, and when this is reached, the rectifier can no longer maintain a constant *dc* voltage if the *ac* voltage continues to decrease.

The inverter is designed for minimum gamma control which ideally maintains a constant inverter *dc* voltage at minimum firing angle. This provides the least reactive power demand on the inverter *ac* system.

7.1.2 Steady State Solution

The test system in the steady state has the rectifier *ac* system bus voltage magnitudes and angles as shown in Table 7.1. The *dc* steady state conditions are shown in Table 7.2.

7.1.3 Frequency Dependent Equivalent Circuit

The hybrid TSE program requires a frequency dependent equivalent circuit to represent the rectifier *ac* system in the EMTDC *dc* system model. The necessity for a frequency dependent equivalent was outlined in Chapter 6. The *dc* system requires an accurate picture of the *ac* impedance at all frequencies, not just the fundamental.

Bus	$\|V\|_{pu}$	$\theta°$
Aviemore	1.015	1.338
Benmore	1.000	0.000
Clyde	1.043	6.479
Roxburgh	1.042	6.338
Livingston	1.024	2.415
Twizel	1.015	1.564

Table 7.1 Rectifier *ac* system steady state busbar voltages

	Rectifier	Inverter
V_{dc}	500 kV	490 kV
I_{dc}	2 kA	2 kA
α	17.65°	15°
P_{dc}	1000 MW	980 MW
Q_{dc}	583 MVAr	545 MVAr

Table 7.2 Steady state *dc* conditions

The equivalent circuit for the rectifier *ac* test system used in this chapter was based on a model by Hingorani and developed by Watson [Hingorani and Burbery, 1970] [Watson *et al.*, 1985]. The frequency dependent equivalent circuit is shown in Figure 7.3. Table 7.3 lists the component values for the circuit. A graph of the impedance magnitude of the actual rectifier *ac* system based on its modelled parameters, and the frequency dependent equivalent is given in Figure 7.4. It can be seen that the equivalent gives a very good match to the impedance of the actual system.

	$R\ (\Omega)$	$L\ (H)$	$C\ (\mu F)$
Arm 1	13.6	0.030883	0.3031
Arm 2	6.02	0.048338	0.7987
Arm 3	25.1	0.388620	0.1369
Arm 4	0.50	0.079359	1.8988
Arm 5	17.0	0.092674	-
Series R	1.2	-	-

Table 7.3 Frequency dependent equivalent circuit parameters

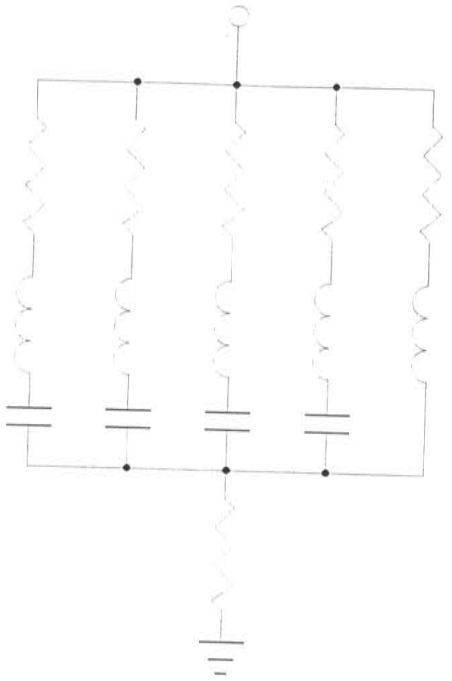

Figure 7.3 Frequency dependent equivalent

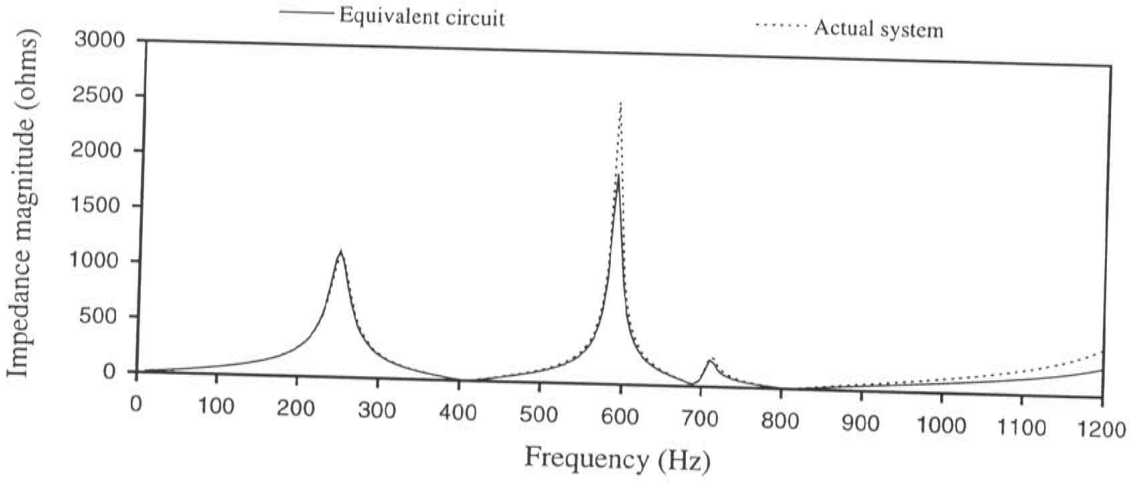

Figure 7.4 Frequency dependent equivalent

7.2 Minor Disturbance

The first transient disturbance applied to the test system consisted of a switching operation involving the shunt capacitor at the rectifier bus. A minor disturbance such as this was useful to confirm that the interfacing in TSE was performing as required and that the two *dc* models, both the quasi-steady state (QSS) and the EMTDC version, were compatible

under non-severe conditions.

The disturbance simply consisted of switching the shunt capacitor out at a certain time. The purpose of the capacitor is to provide reactive MVAr's, necessary for the operation of the HV*dc* link. The removal of the capacitor represents a sudden shortage of MVAr's and hence a consequential *ac* voltage drop at the rectifier terminal.

First of all, the switching operation was modelled using just the TS program with its QSS version of the HV*dc* link. The rectifier *ac* generating bus voltage magnitudes and angles are shown in Figure 7.5. The voltage magnitude drop is evident on all the generating buses in the *ac* system, as is the eventual return to nominal steady state conditions through the action of the generator controllers. The transient disturbance is also evident on the bus voltage angles (which are relative to the reference bus, Clyde) at particularly Benmore and Aviemore.

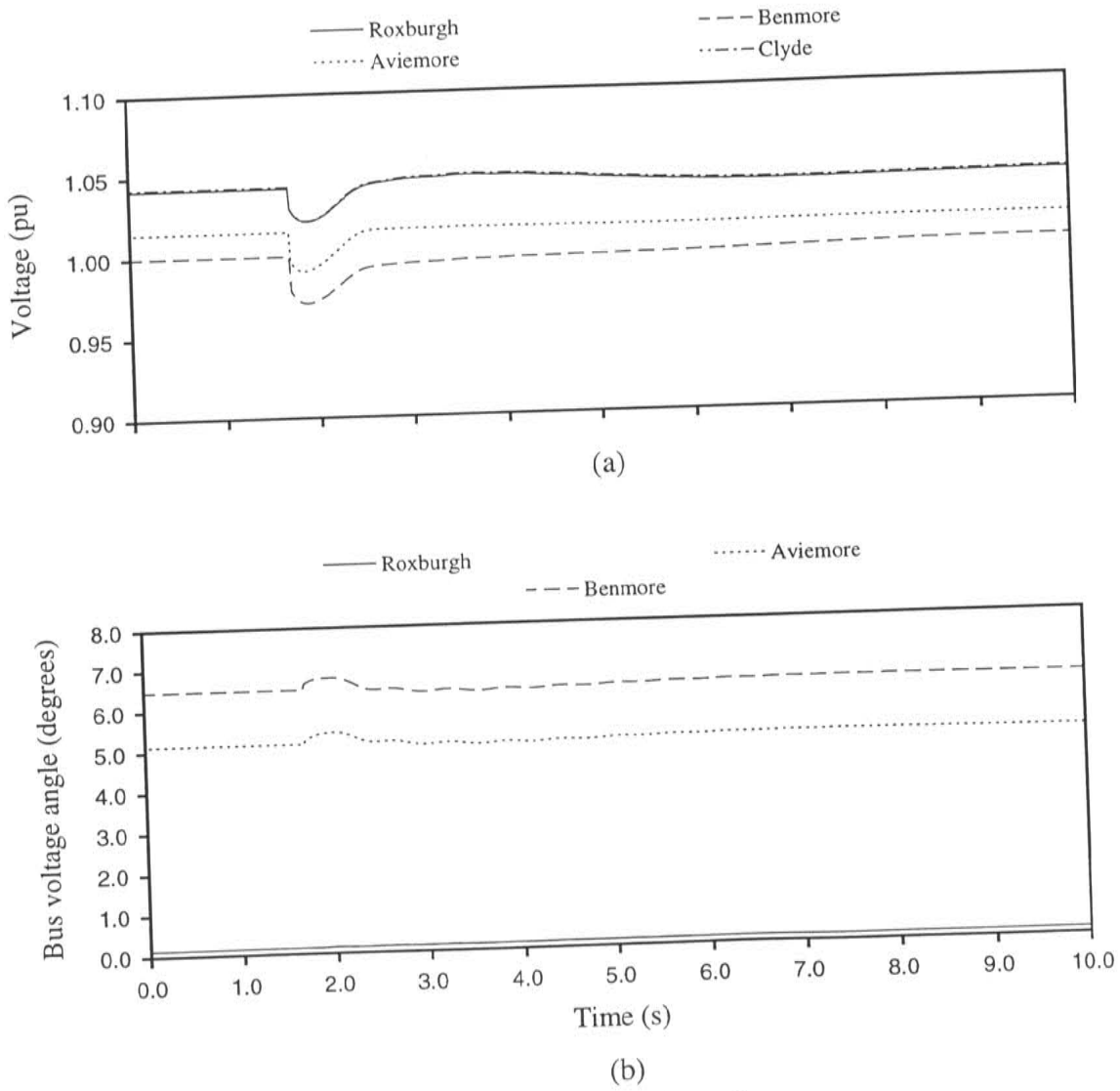

Figure 7.5 TS rectifier *ac* system bus voltages

The rectifier *dc* conditions are shown in Figure 7.6. The drop in *ac* voltage magnitude is countered by the rectifier firing angle change to maintain constant current as required.

The minimum firing angle (set at 3 degrees) is not reached and so the *dc* voltage and current (and hence *dc* real power) are not affected.

The firing angle returns to its pre-disturbance value as the *ac* voltage at the rectifier bus slowly returns to its nominal $1pu$ value. The reactive power required by the *dc* link is dependent on the firing angle and consequently as the firing angle decreases, so does the reactive power requirement. This aids in the recovery of the *ac* voltage.

The generator field voltages are shown in Figure 7.7(a). The AVR limit at Aviemore is evident, as is the controllers attempt to maintain their set bus voltage magnitudes. The Benmore generator at the rectifier bus, as expected, is the most affected by the disturbance and a new steady state value is eventually approached. The relative machine angles in Figure 7.7(b) also shows the effect of settling to this new steady state condition at Benmore.

The same switching operation was then applied to the hybrid TSE program which modelled the HV*dc* link in EMTDC. The EMTDC model uses the frequency dependent equivalent for the rectifier *ac* system described in Section 7.1.3, with the source value controlled by TS. The EMTDC model also passes information on the *dc* link requirements to TS at the interface in the hybrid manner described in Chapter 5.

The link model was first brought up to steady state operation on its own and a snapshot taken. This snapshot was then used to interface with TS at time $t = 0$, before the switching operation at time $t = 1.7sec$. The same TS data file as that used for the TS only simulation was used, and in addition, an interface data file was also read (refer Section 5.1). The voltage magnitude at Benmore, the rectifier terminal bus, is shown in Figure 7.8(a) and compared with the same terminal voltage from the TS only solution. The voltage angles are compared in Figure 7.8(b) and the rectifier firing angle in Figure 7.8(c). All three comparisons show excellent correlation between the two models. Figures 7.8(a) and 7.8(b) compare "TS generated" variables between TS only and the TSE hybrid. The firing angle comparison compares the "EMTDC generated" firing angle from TSE with that of the QSS model from the TS only solution. The more transitory nature of the low level firing angle control from EMTDC is evident.

The pre-fault and post-fault steady state values between the compared results show the validity of the two models with respect to each other. The *dc* conditions generated by the EMTDC model in TSE are shown in Figure 7.9 and again show almost identical results to that of the QSS model in TS. The time scale in both figures is zoomed in to show the true nature of the *dc* waveforms, and the change in particularly the *dc* voltage waveform as the capacitor is removed.

The *dc* voltage takes a slight momentary dip at the instant of switching since the firing angle in EMTDC, unlike that of TS, cannot react instantly to the drop in *ac* voltage. This consequently causes the current to have a transient dip immediately following the switching operation. The average *dc* voltage very quickly recovers however, to its nominal value and hence also restores the *dc* current.

The real power comparison between models is shown in Figure 7.10, with both curves derived from the positive sequence, fundamental frequency voltage and current at the interface location. The time scale is again zoomed in around the switching point. The results show the effect of the non-instantaneous change in the firing angle of EMTDC at

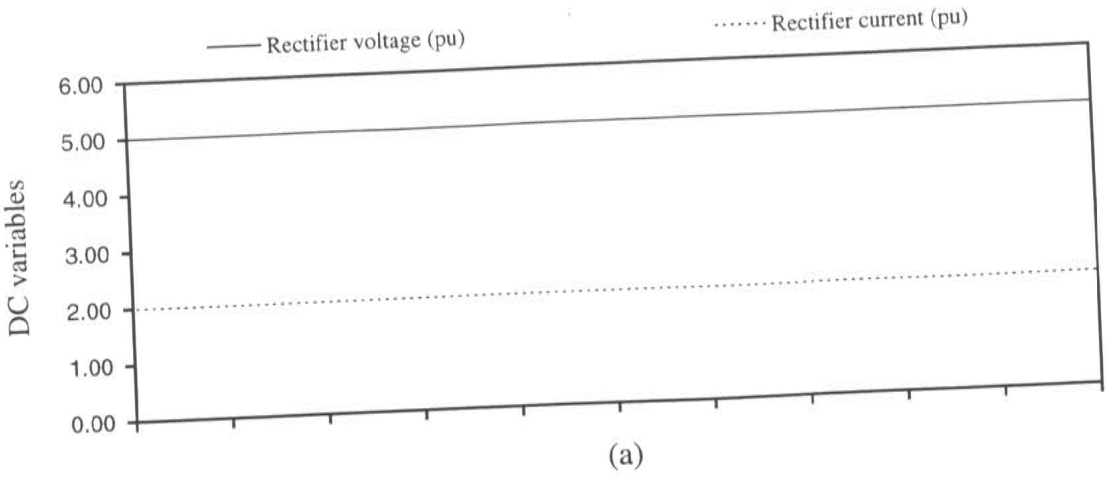

(a)

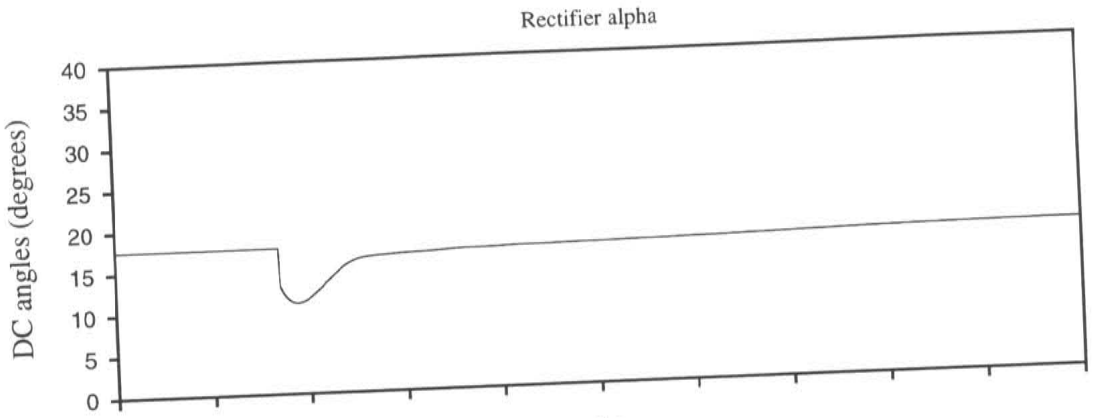

(b)

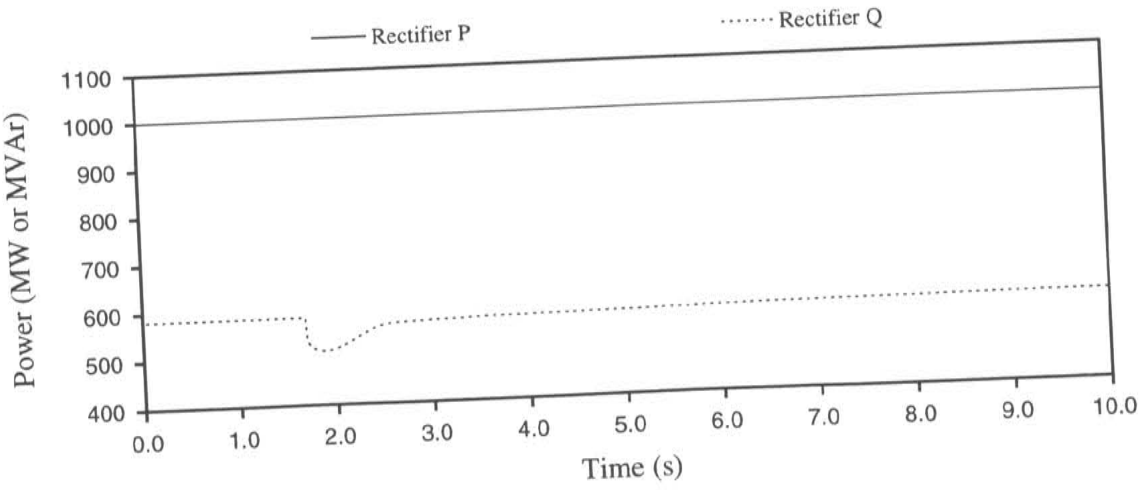

(c)

Figure 7.6 TS rectifier terminal *dc* parameters

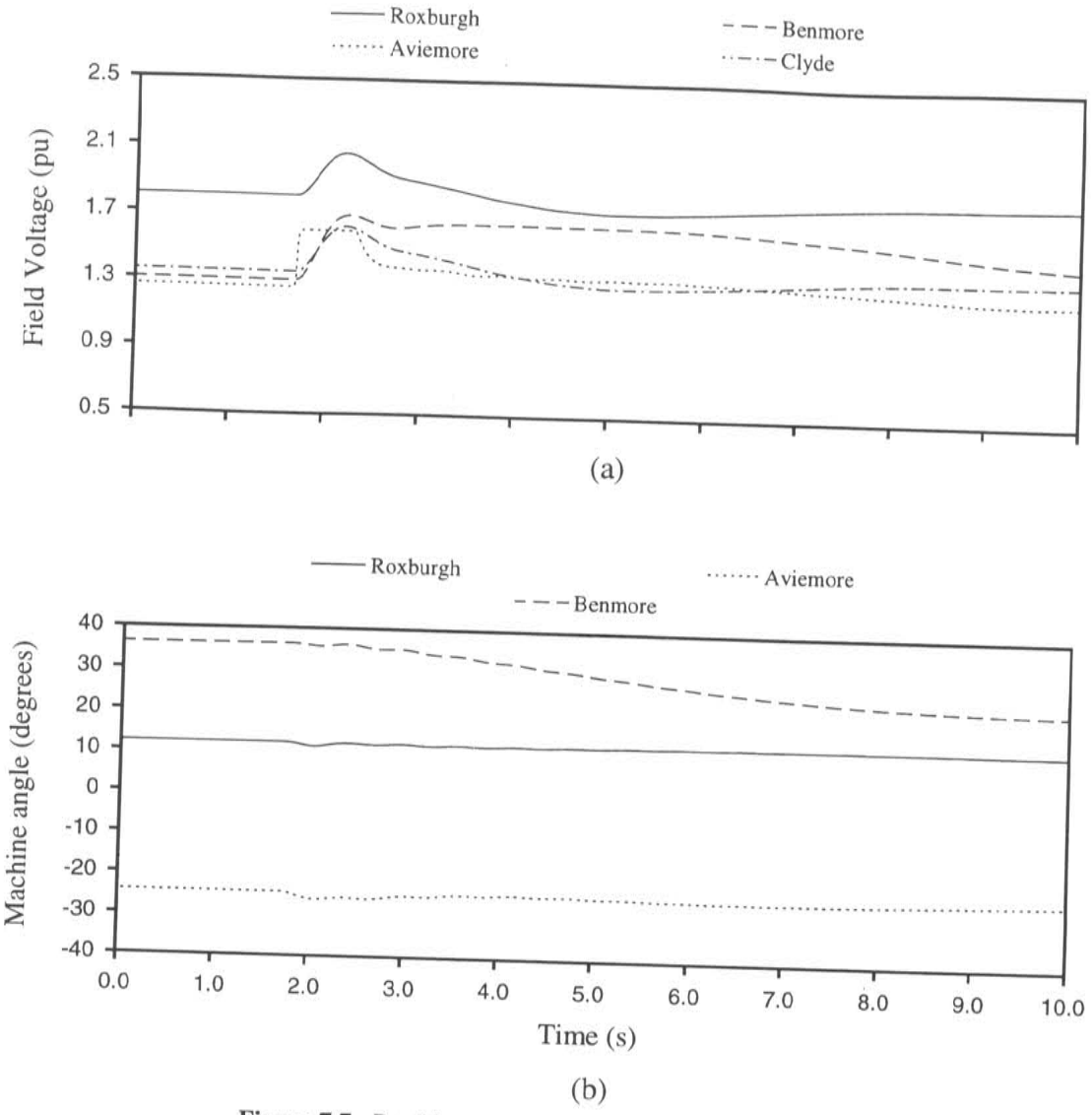

Figure 7.7 Rectifier *ac* system generator parameters

the time of switching the capacitor out. The momentary dips in *dc* voltage and current combine to give a consequential dip in real power input to the link. A slight overshoot of the firing angle is also evident before the real power stabilises. Once the gradient of the required change in firing angle control lessens, the real powers between the models are effectively matched.

The transient stability program TS simply selects a firing angle to match the *dc* and *ac* solutions at the required time step. As long as the firing angle is above its set minimum limit, the *dc* voltage and current at the rectifier are maintained constant without fluctuation.

Reactive power from both TS and TSE is shown in Figure 7.11. Like the real power, this is derived from the complex positive sequence, fundamental frequency voltage and current at the interface location. The reactive power also displays a distinct similarity to the real power. Since at the instant of the capacitor switching in EMTDC, the firing angle does not immediately change, the reactive power requirement is higher than for the TS program QSS solution. The overshoot in the firing angle reacting to the disturbance is

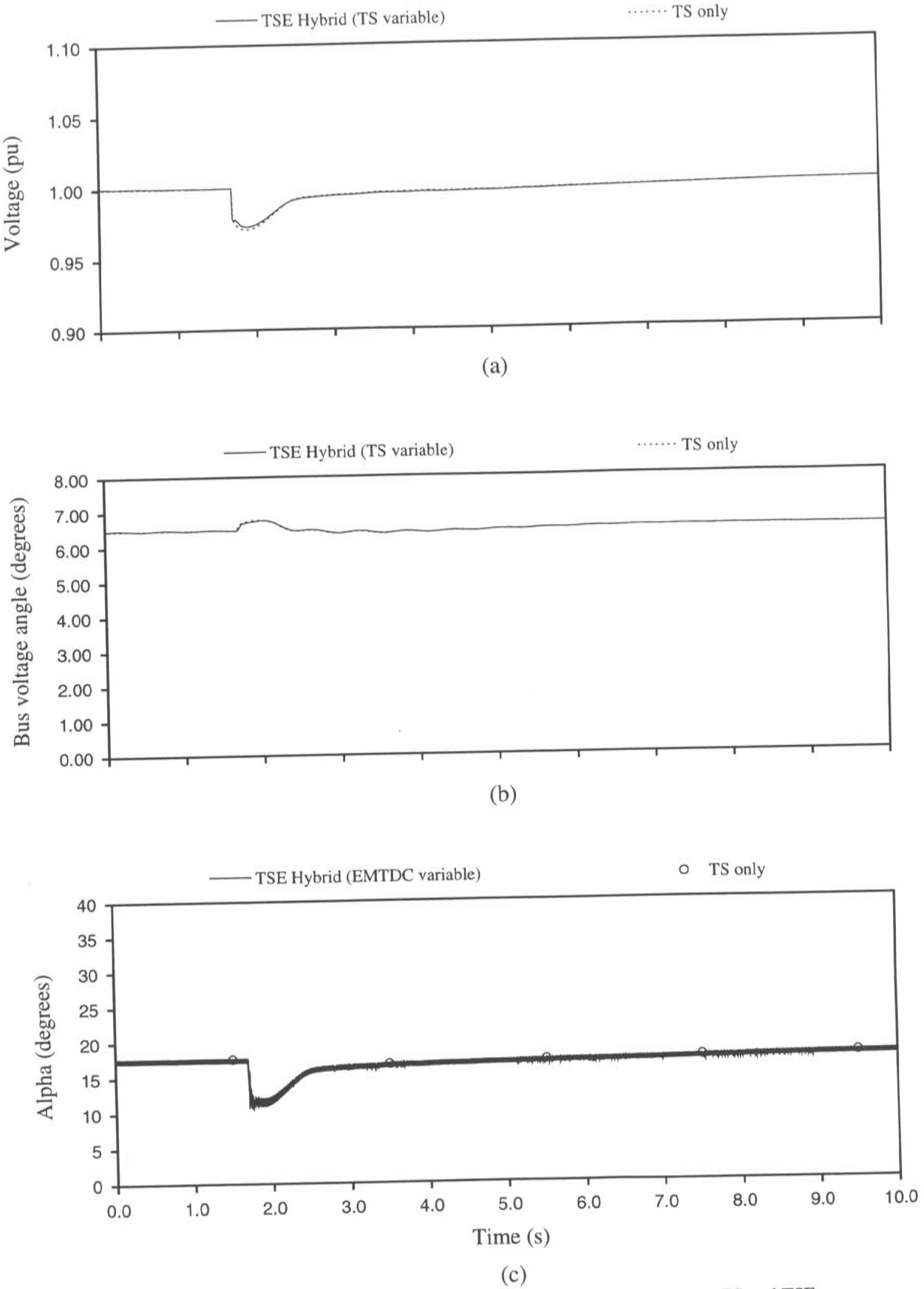

Figure 7.8 Comparison of rectifier terminal *ac* bus voltage and *dc* firing angle between TS and TSE solutions

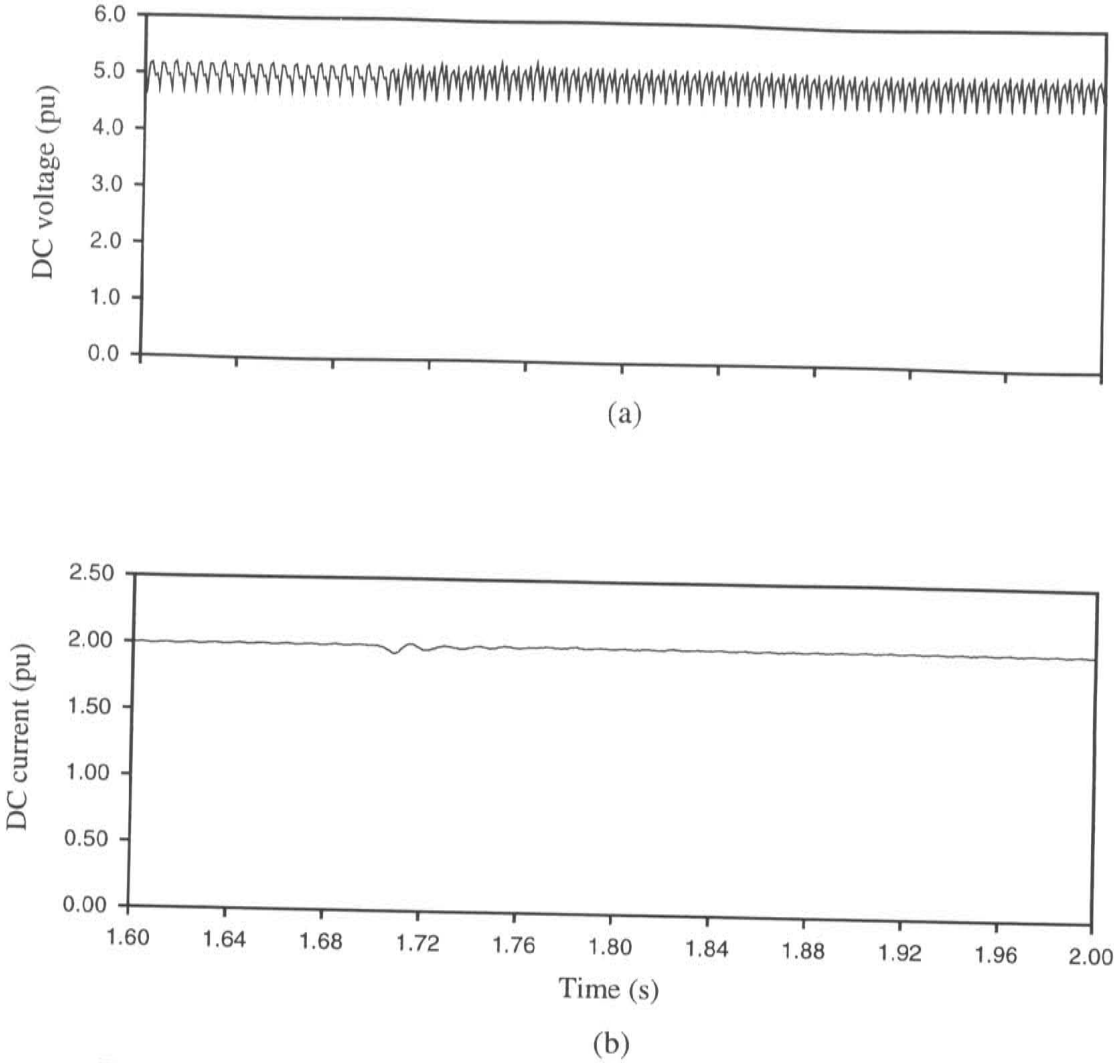

Figure 7.9 TSE-EMTDC model *dc* current and voltage at the rectifier terminal

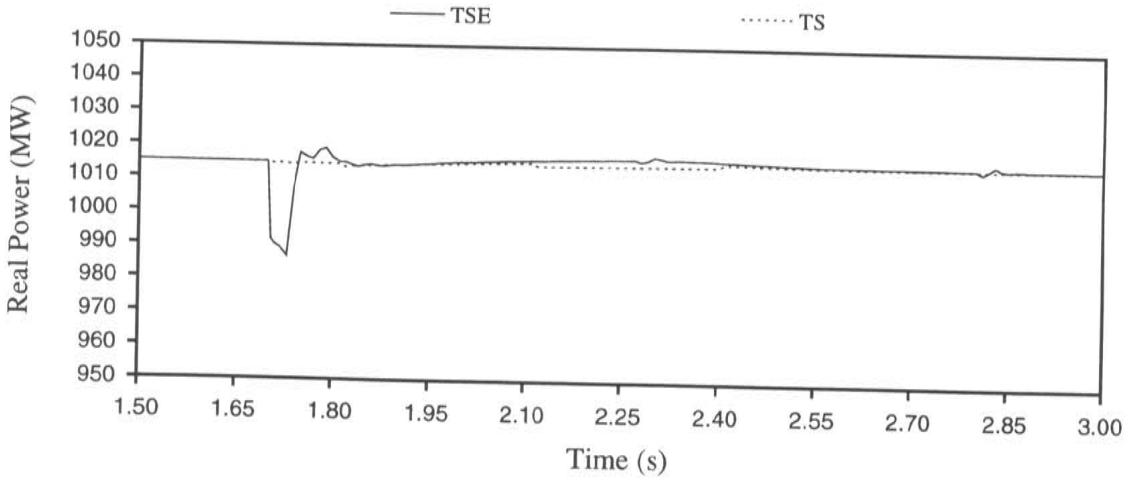

Figure 7.10 Comparison of real power across interface between TS and TSE solutions

also visible. As the firing angle settles however, the solutions converge.

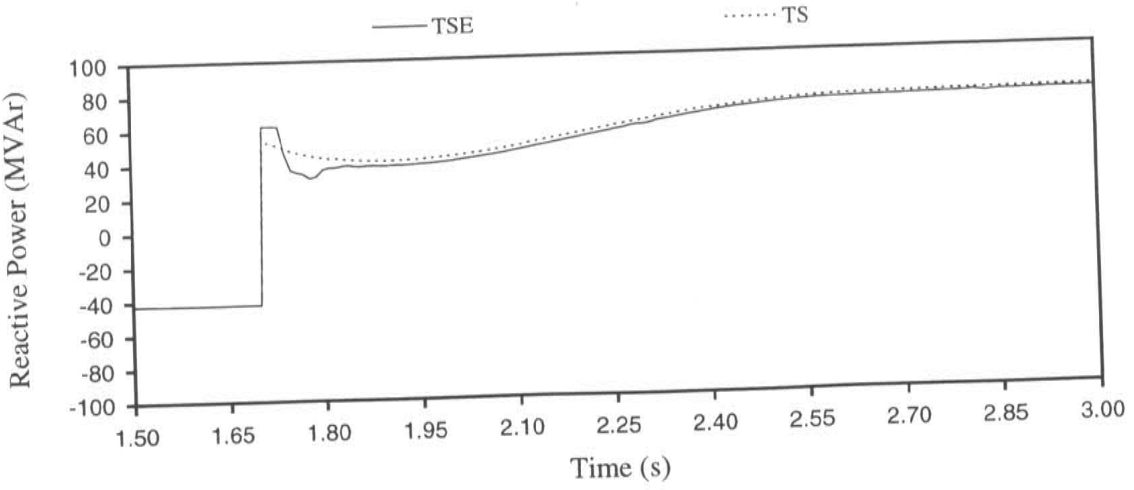

Figure 7.11 Comparison of reactive power across interface between TS and TSE solutions

The comparison of the hybrid TSE with the transient stability program TS for the removal of the shunt capacitor showed the effectiveness and validity of the hybrid approach. For a minor disturbance, the results were very much the same between both the EMTDC and the QSS *dc* models. The electromagnetic transient nature of the EMTDC *dc* model was evident as was the more detailed model of the *dc* controls. The effect of simulating the controls down to actual effective firing orders with realistic time constants produced transient fluctuations in *dc* variables around a disturbance that were not evident in the TS program QSS solution. There are other inherent differences between the two *dc* models. One is based on effectively steady state equations, while the other is an elemental model of resistance, inductance and capacitance. The elemental model can simulate thyristor resistance, snubber circuits, bus and assembly impedances, transformer winding resistances *etc*. In the QSS model however, the equations rely on a specified commutation impedance. Commutation reactance and resistance must be estimated and assumed to be kept constant. In complex systems however, there is no way of accurately determining these values.

7.3 Major Disturbance

In this section, a major disturbance was applied to the test system to examine the differences between the simulation approaches. A three phase fault was applied at the rectifier *ac* system terminal and cleared in three cycles. Various *ac* fault types have differing severities, however a three phase fault at a converter terminal is the most severe in blocking all power flow [Meredith, 1983].

An *ac* system fault was chosen since *dc* faults may not be as disruptive to an *ac* system as *ac* faults.

Faults on a *dc* system seldom exceed $3pu$ (on two terminal systems) and can be extinguished rapidly since the rectifier terminal is the only contributor to the current and

is generally under constant current control. The only fault current is then the capacitive discharge of the line and any current overshoot caused by the rectifier control circuit time delay. Any overshoot current is also limited by the inductive time constants of the *dc* circuit.

The rectifier terminal was selected above the inverter since rectifier faults are often worse for transient stability. An inverter fault still allows generation at the rectifier to supply line losses and local load. A rectifier fault however, especially near generators, more totally blocks both *ac* and *dc* power. This results in greater transient acceleration of the generators.

It is widely accepted that positive sequence transient stability programs are only useful for an *approximate* analysis of unbalanced faults. An accurate analysis requires a detailed three phase model and this is sometimes essential to correctly predict transient stability [Meredith, 1983]. A hybrid approach is naturally then highly applicable to unbalanced faults. This section shows that a hybrid approach is also necessary and applicable for accurate simulation of balanced faults.

The analysis performed in this section consists of :-

- The transient stability program TS on its own with a quasi-steady state (QSS) representation of the *dc* link

- The electromagnetic program EMTDC on its own using a detailed three phase elemental analysis of the *dc* link, and

- The hybrid program TSE, combining a TS *ac* system with an EMTDC *dc* system representation.

The EMTDC representation of the *dc* system in both the hybrid and the EMTDC only approach, use a frequency dependent equivalent to represent the rectifier *ac* system. In the hybrid case, the source value of the equivalent circuit is modified using results from the TS program, while in the EMTDC only case, the source value is fixed. The EMTDC only case was included since this is a conventional approach when a detailed representation of the *dc* link is required. This allows an excellent comparison of both electromagnetic and electro-mechanical based solutions, to the hybrid TSE program.

7.3.1 The TS-(QSS) Response

The analysis using the transient stability program TS with a QSS representation of the *dc* link is shown in Figures 7.12 to 7.17. At time $t = 1.7sec$ the 3 phase fault is applied and then subsequently cleared 3 cycles later. Figures 7.12(a) and 7.12(b) show the generating bus voltage magnitudes and angles (angles relative to the reference bus Clyde). The effect at the fault terminal is particularly evident as the voltage magnitude drops to zero and the voltage angle rises nearly fifty degrees. The return to a stable voltage angle can also be seen, with an initial oscillation due to the generator controllers eventually decaying away.

Figures 7.13 and 7.14 display the effect of the fault on the *dc* variables at each

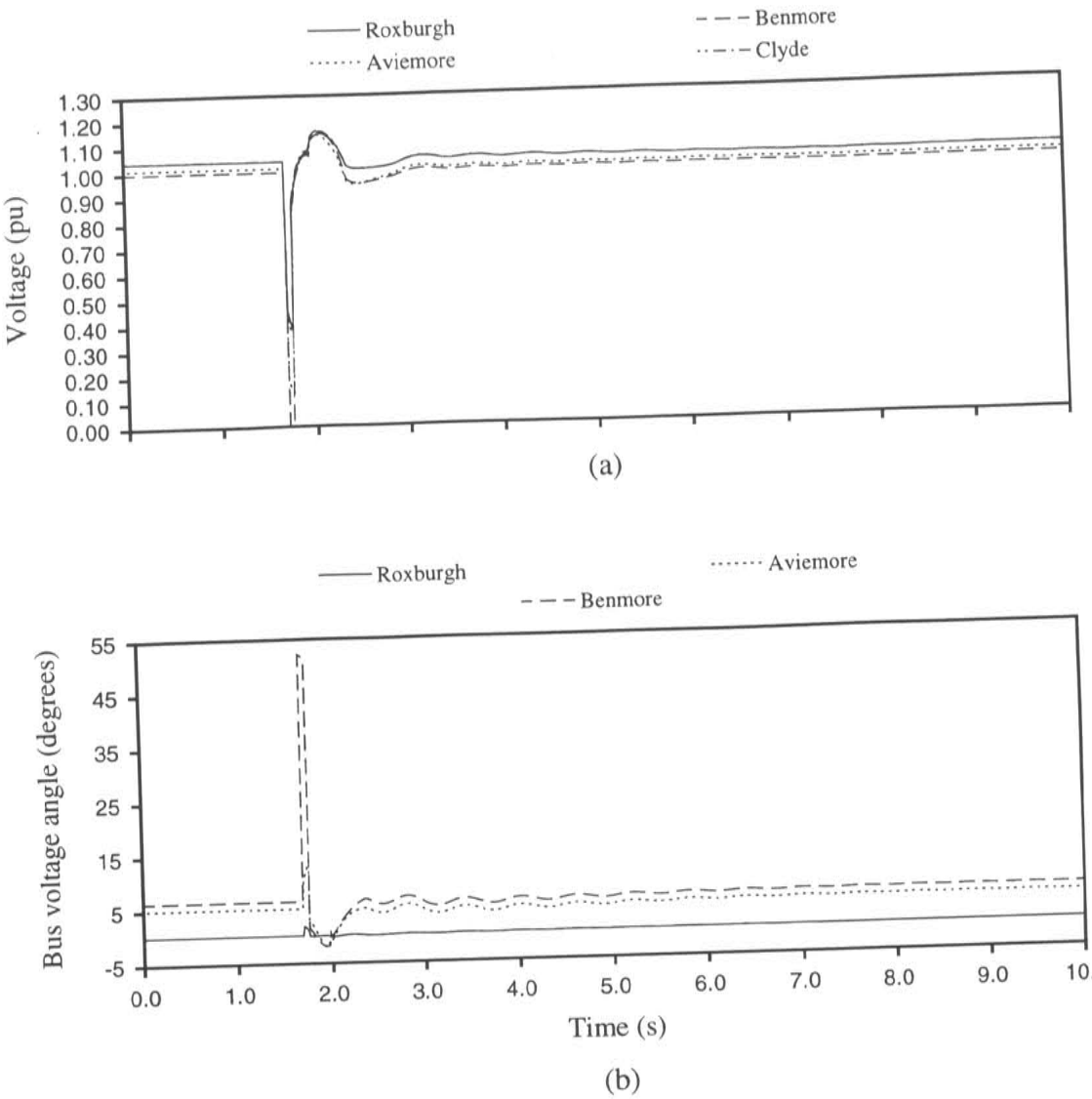

Figure 7.12 Rectifier *ac* voltage

terminal of the link. At the instant of the fault, the rectifier terminal is blocked and the inverter terminal bypassed as per the shutdown logic in TS (Section 7.1.1). Once the fault is removed, the rectifier terminal is unblocked and the *dc* current through the rectifier ramped to 30% of its nominal value. The inverter terminal is then un-bypassed and the *dc* real power ramped back up to its nominal value. The sequence of events surrounding the fault and the corresponding *dc* link logic is summarised in Table 7.4.

The machine response to the fault is shown in Figure 7.15. The field voltages and machine angles vary and oscillate through the response of the AVR but eventually settle back to steady state values. The Aviemore field voltage response is somewhat different than the other generators due to its larger forward regulator gain and lower upper field voltage limit.

To fully correlate the change in the *dc* and *ac* variables, a closer examination of the period from just prior to the fault to a short time after is required. Figures 7.16 and 7.17 show the main *ac* and *dc* variables at the rectifier and inverter terminals from the period

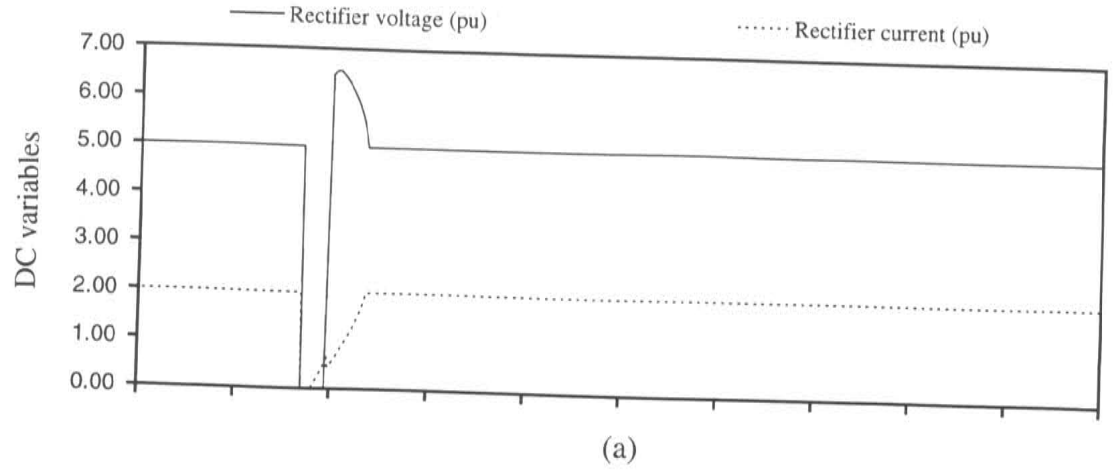

(a)

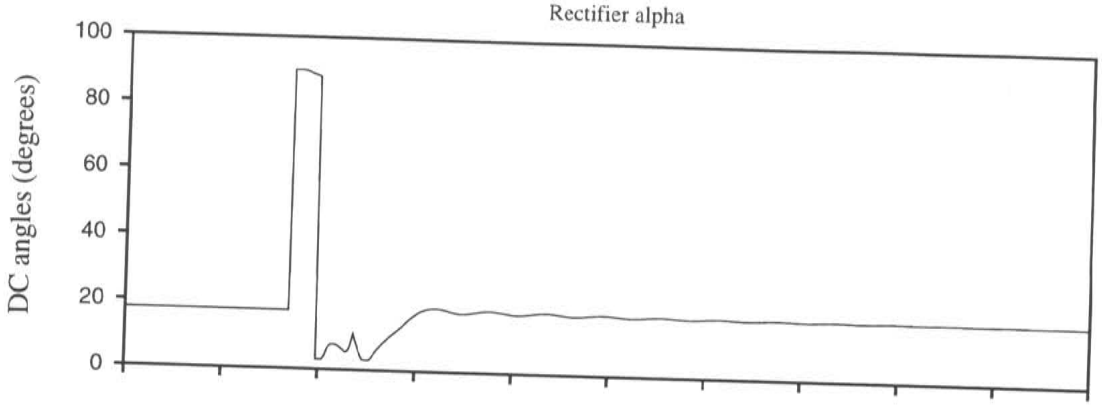

(b)

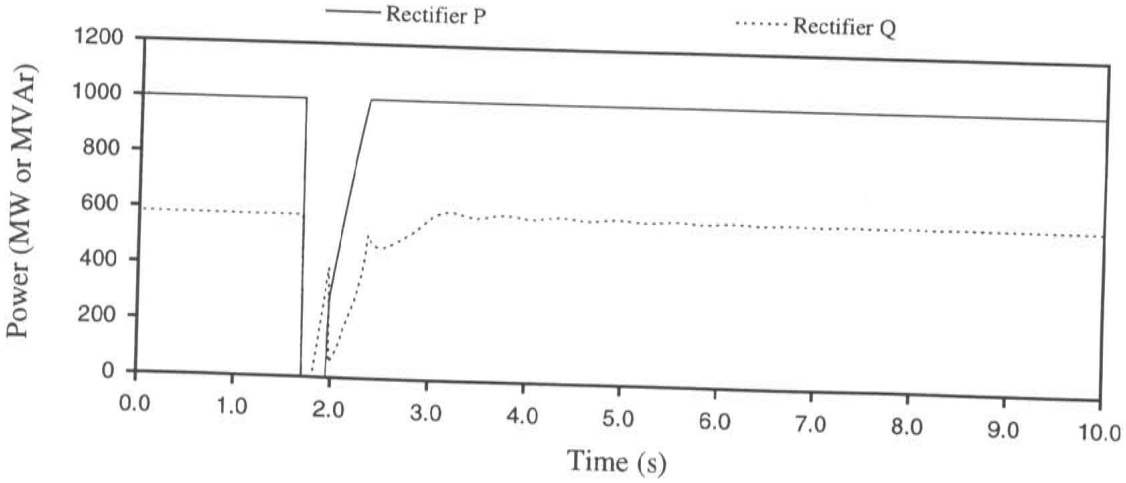

(c)

Figure 7.13 Rectifier *dc* variables

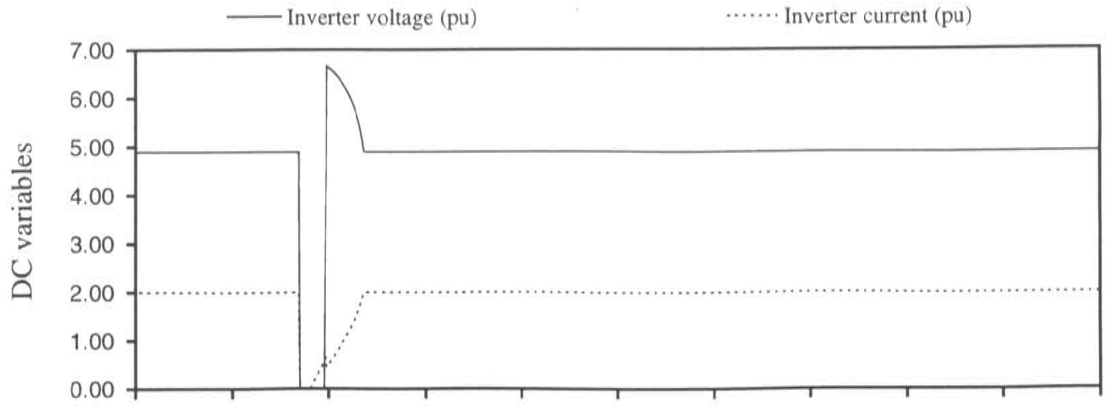

(a)

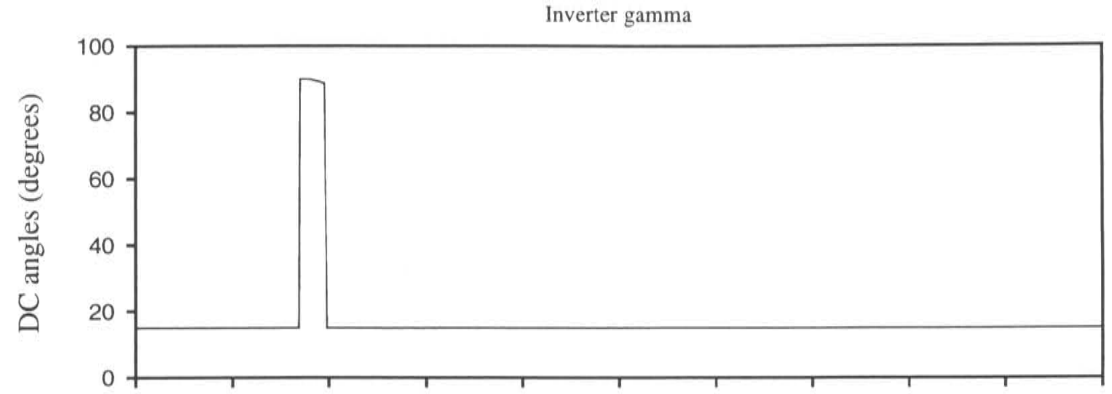

(b)

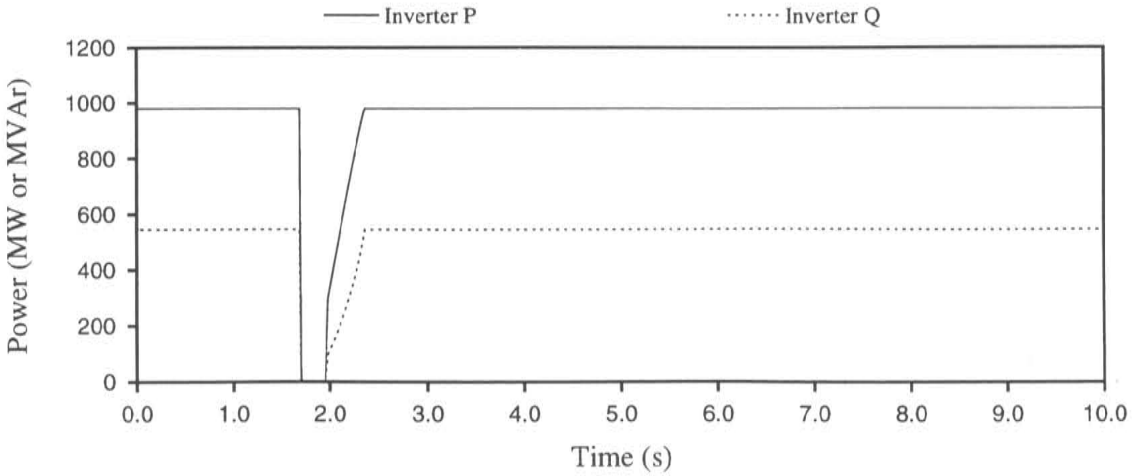

(c)

Figure 7.14 Inverter *dc* variables

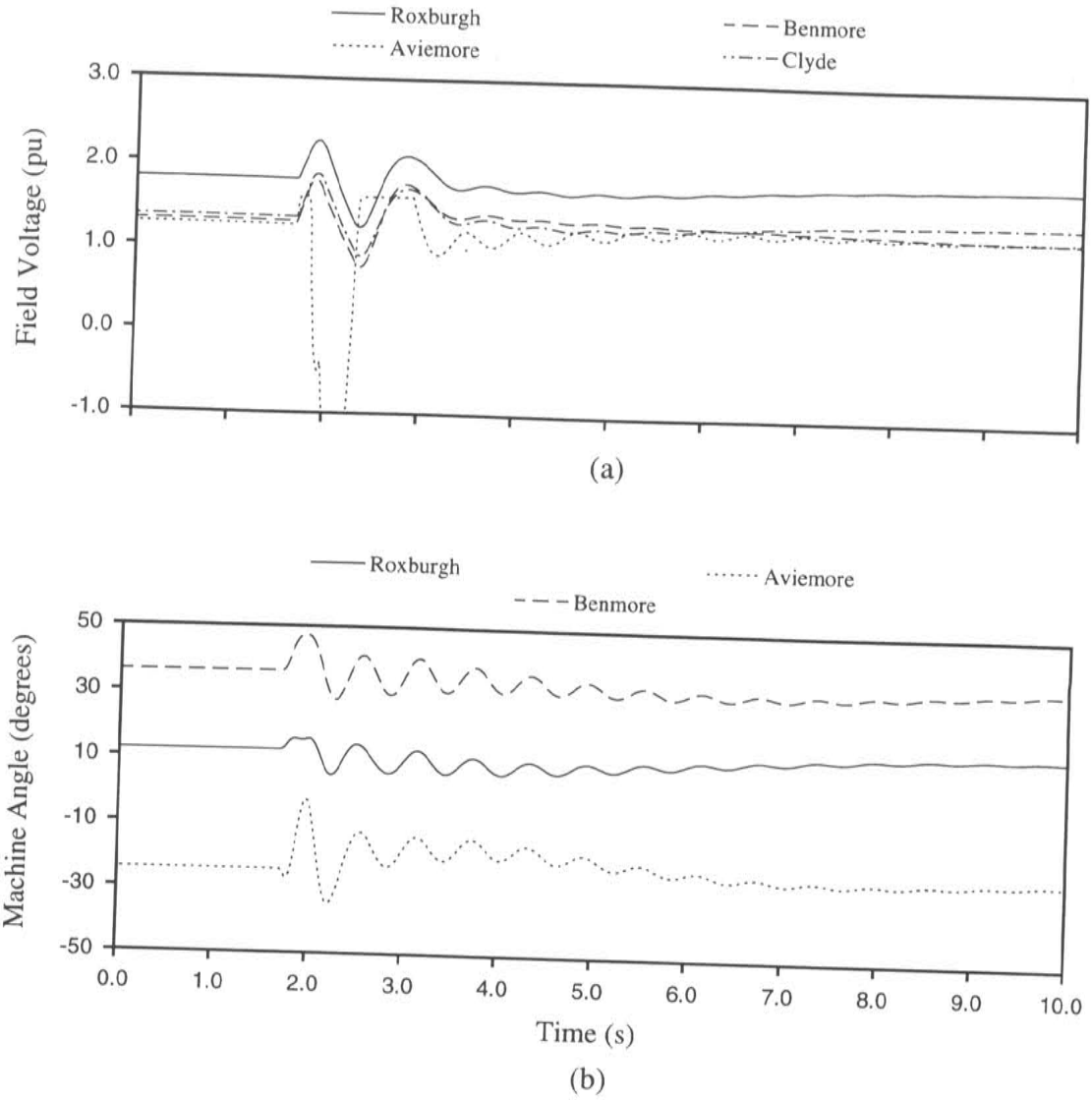

Figure 7.15 Rectifier *ac* system machine response

$t = 1.5sec$ to $t = 3sec$.

Figure 7.16(a) displays the *ac* voltage at both converter terminals. At the rectifier, the *ac* voltage drops to zero for the duration of the fault and then begins to recover. A sharp increase in *ac* voltage is seen at $t = 1.97sec$ as the inverter terminal is switched on and the link begins to power ramp to its nominal setting. This sudden change in rectifier *ac* voltage is caused by the sudden drop in reactive MVAr's required by the link (Figure 7.17(c)) as the *dc* voltage steeply rises (Figure 7.16(b)) and the rectifier firing angle rapidly drops (Figure 7.16(c)). The rectifier *dc* current (Figure 7.17(a)) which had at $t = 1.97sec$ risen to 30% nominal value, correspondingly dips suddenly as the inverter is re-started, and then rises to full nominal value as a function of the link power ramping. During this power ramp period to $t = 2.35sec$ (Figure 7.17(b)), the rectifier *ac* voltage is affected by both the generator controllers and particularly at this stage, the reactive MVAr requirements of the rectifier terminal. The *dc* voltage at the rectifier returns to its nominal value over this power ramp period from a high point caused by the low *dc* current and the high *ac* voltage.

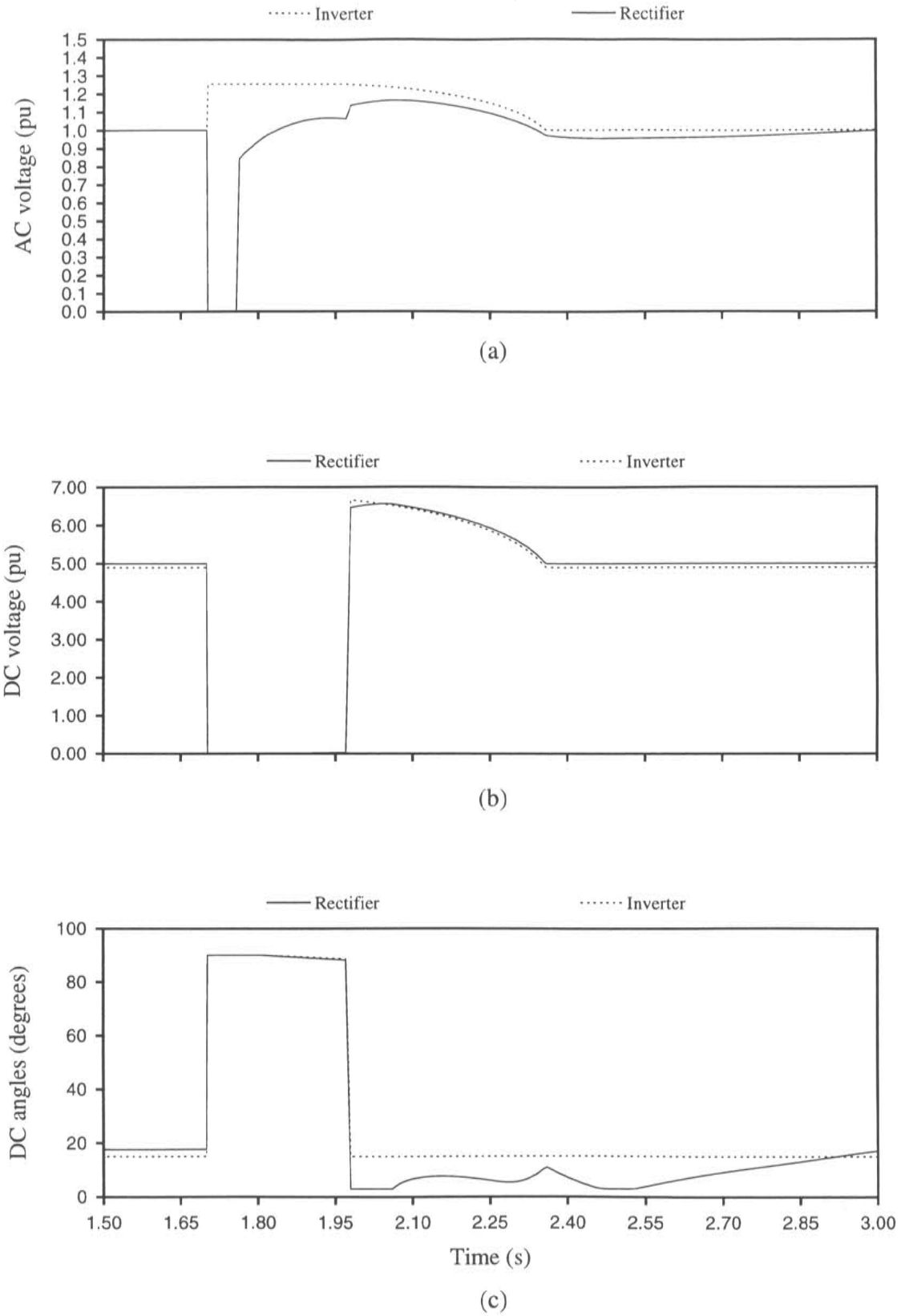

Figure 7.16 Rectifier *ac* voltage, *dc* voltage, and firing angle

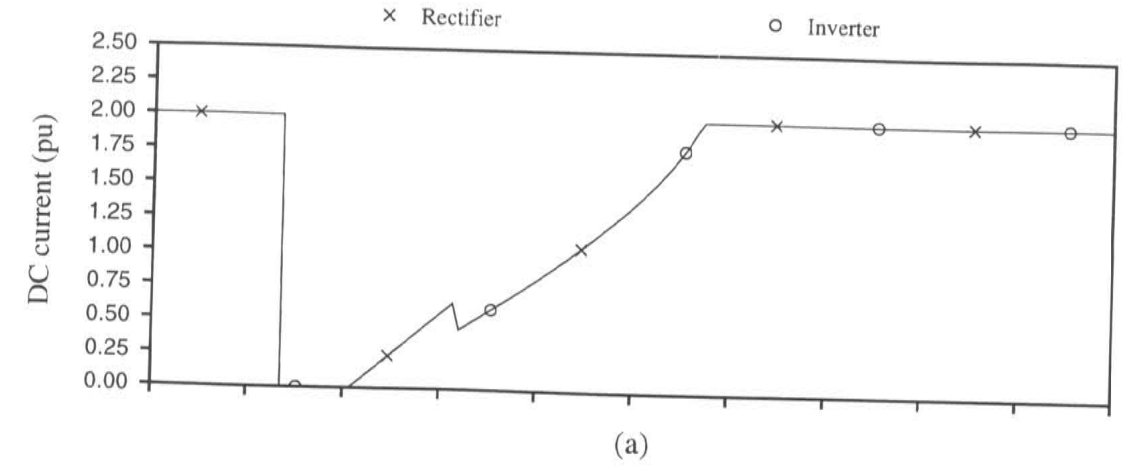

(a)

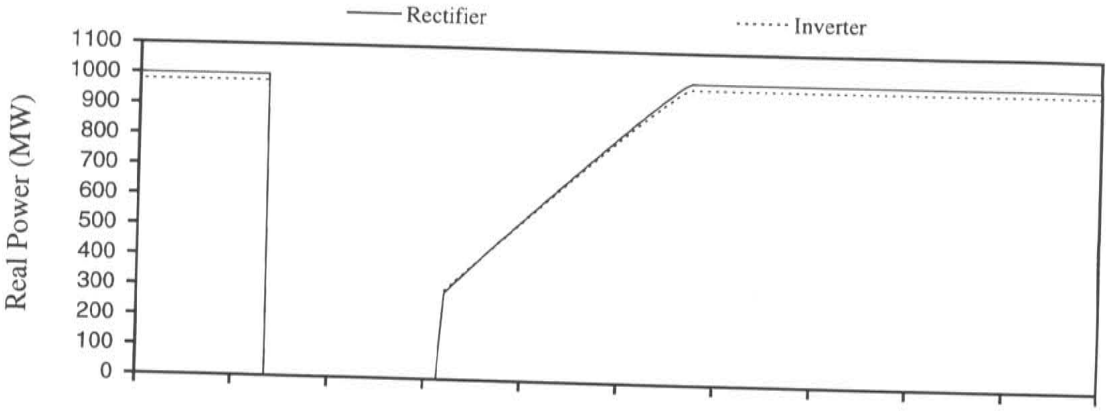

(b)

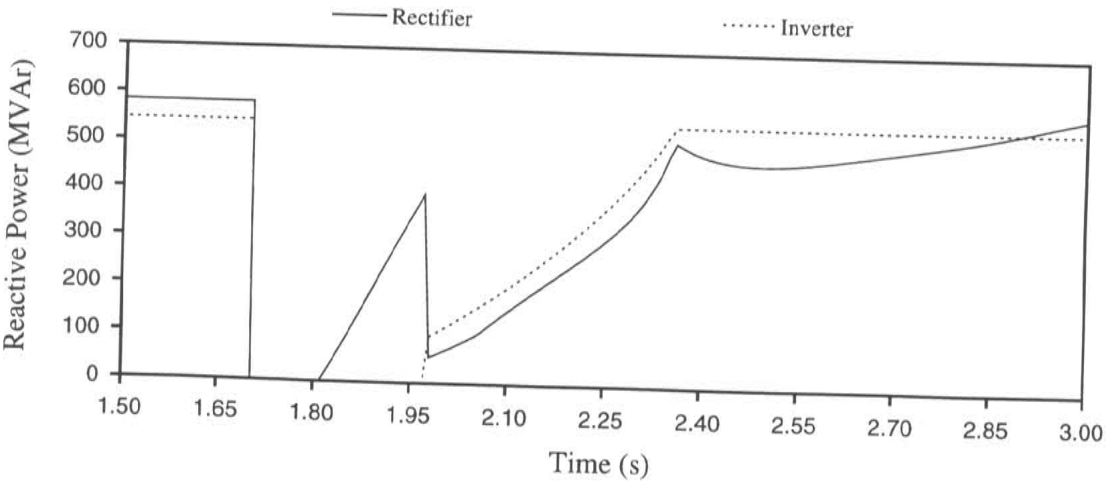

(c)

Figure 7.17 Rectifier *dc* current, real power, and reactive power

Time (seconds))	Event(s)
1.70	3 phase fault applied at rectifier *ac* terminal Rectifier *dc* terminal blocked Inverter *dc* terminal bypassed
1.76	3 phase *ac* fault removed
1.81	Rectifier *dc* terminal unblocked Rectifier *dc* current ramped to 30% of nominal value
1.97	Inverter *dc* terminal un-bypassed Rectifier and inverter now power ramped to nominal power level
2.35	Nominal *dc* link power reached

Table 7.4 Sequence of fault related events

The rectifier firing angle meanwhile, varies itself to maintain the voltage profile between rectifier and inverter giving the required *dc* current for the specified power ramp. From $t = 2.35sec$ on, the rectifier firing angle varies as a function of the *ac* voltage as does the reactive power requirement at the rectifier, which is determined by both *ac* voltage and firing angle.

The inverter response is much simpler. At the fault application, the link is shut down and the inverter *ac* voltage rises as a consequence of the sudden removal of reactive MVAr's required by the link. When the inverter is re-started at $t = 1.97sec$, the *ac* voltage returns to its nominal $1pu$ value as a function of the rising MVAr's once again required by the inverter terminal (Figure 7.17(c)).

When the *dc* link current flows back through the inverter bridges instead of the bypass valves (at $t = 1.97sec$), the inverter *dc* voltage rises steeply to a high value, similar to the rectifier, caused again by the high *ac* voltage and low *dc* current. The inverter firing angle is under constant firing angle control for simplicity of analysis at the rectifier, and hence with no control mode change, the firing angle at the inverter remains at its minimum value (15 degrees) while the inverter terminal is switched on.

7.3.2 The EMTDC Response

The test system was then modelled in EMTDC with a fixed, frequency dependent equivalent representing the *ac* system. Computational expense effectively prohibits the modelling of the entire *ac* system particularly with the requirement of the settling of rotor angles in multiple generators. The EMTDC model has an entirely different output than that of TS in that it models point on wave effects rather than magnitudes. The EMTDC modelling emphasis is on the HV*dc* link dynamics while the TS emphasis is on the *ac* system dynamics.

Comparisons between the two programs show reasons why these separate modelling techniques are *both* utilised in *ac-dc* system studies. TS cannot describe adequately the

operation of the *dc* link and EMTDC similarly cannot describe to any accurate degree the entire *ac* system operation. The benefits of the combined TS-EMTDC approach in the next section are then all the more obvious.

The EMTDC plots shown in Figures 7.18 to 7.19 are of the rectifier *dc* variables and also show the relevant TS variable for comparison. The time period of the plots is from just prior to the fault at $t = 1.5sec$ to $t = 3sec$. This period in itself is very large in terms of computational time required for EMTDC simulation compared with that of TS for the same period (an order of nearly 100 times longer).

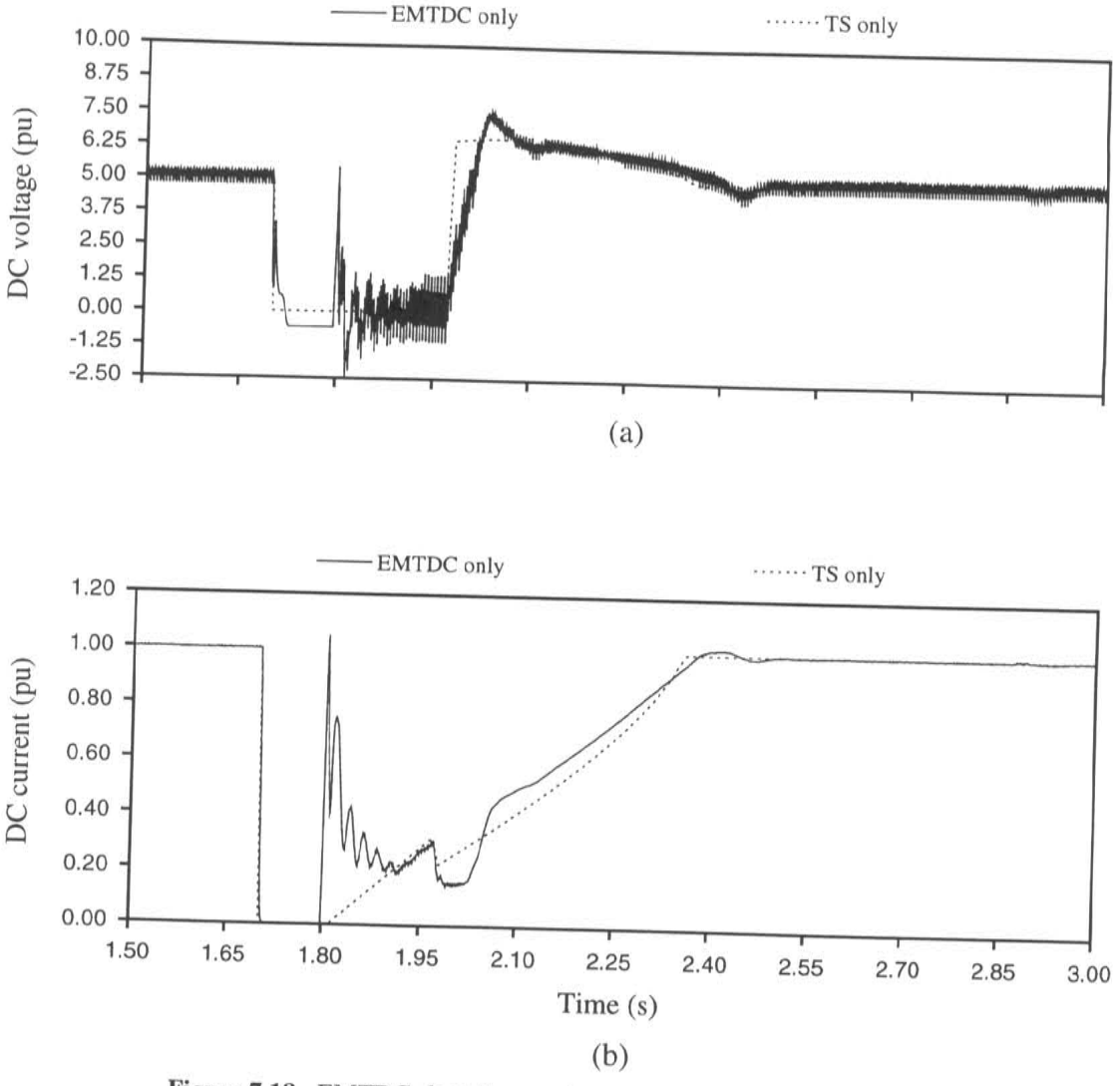

Figure 7.18 EMTDC *dc* voltage and current compared with TS

At $t = 1.7sec$, the fault is applied and both the *ac* voltage (Figure 7.19(a)) and *dc* current (Figure 7.18(b)) through the rectifier bridges drop to zero. The *dc* voltage measurement (Figure 7.18(a)) is affected by the inductive-capacitive nature of the *dc* cable. Through a telecommunication delay, the inverter is bypassed a few milliseconds after the rectifier is blocked. The net effect of this, and in particular the sudden withdrawal of the voltage source at the rectifier, is to create a small negative voltage across the rectifier bridges. The difference between the *dc* current measured and the *dc* current ordered causes

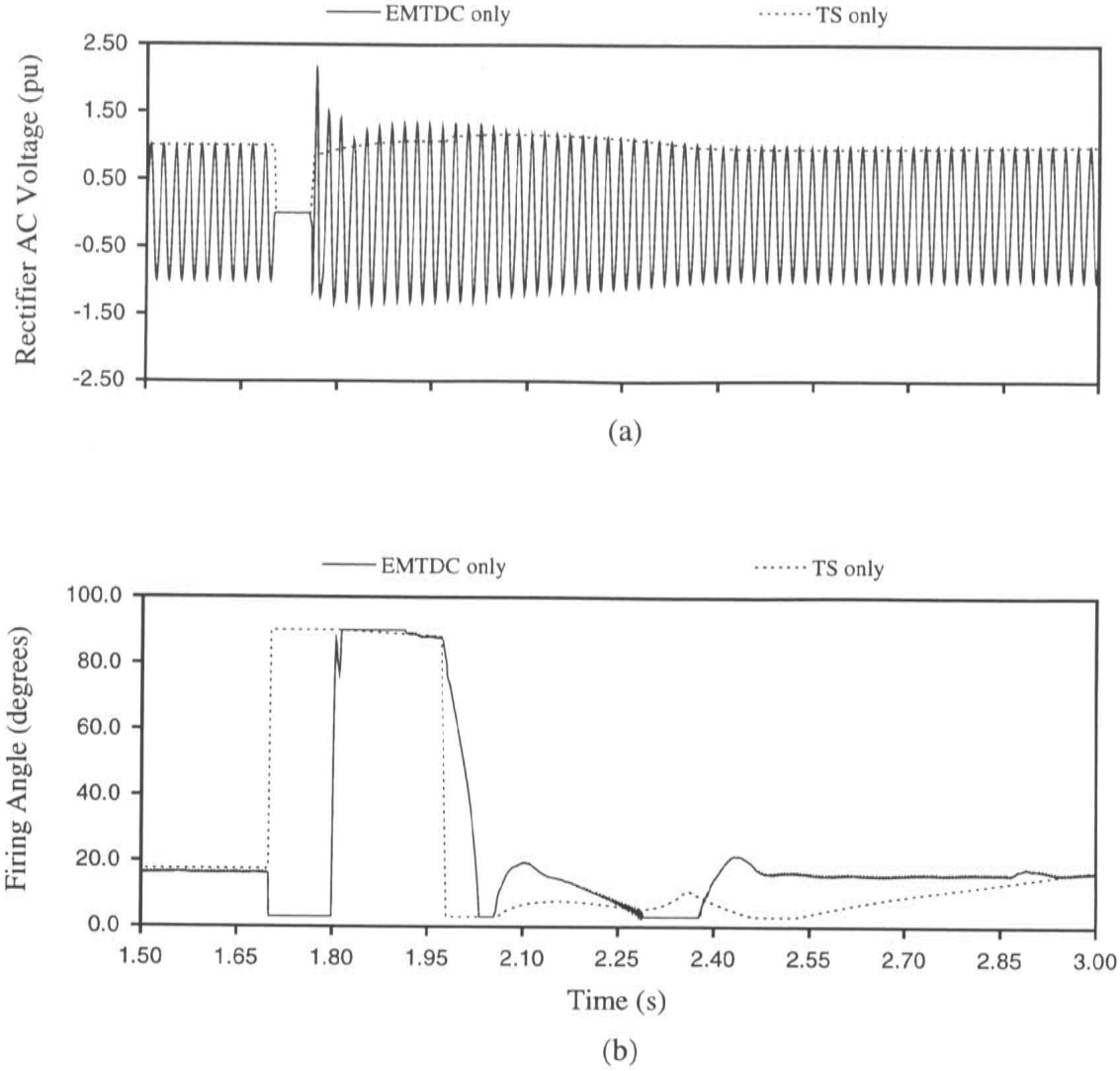

Figure 7.19 EMTDC *ac* voltage and *dc* firing angle compared with TS

the ordered alpha (Figure 7.19(b)) to immediately drop to zero. In the TS case, the ordered alpha is automatically sent to 90 degrees to await the unblocking of the rectifier. While the rectifier is blocked however, the value of alpha ordered is immaterial.

When the fault is cleared at $t = 1.76sec$, the *dc* terminals remain inoperative but the *ac* voltage overshoots and remains high until the full power to the link is restored. The equivalent of the *ac* system uses a fixed voltage source behind a frequency dependent equivalent. When the fault is cleared, the *dc* link is still off and consequently the current drawn through the equivalent impedance is less. This partially creates the over-voltage condition, along with the inductive nature of the *ac* system presented with a sudden change at the rectifier terminal. The *ac* filters at the rectifier terminal will also create an inrush current (limited by the series inductance) as they once again charge to their nominal capacitive voltage.

At $t = 1.8sec$ the rectifier is unblocked, and a few milliseconds later the inverter terminal un-bypassed. In this condition, the *dc* cable looks capacitive and consequently a high current overshoot occurs. This current is more than the current ordered through

the controller hence the firing angle alpha, instead of immediately beginning a slow move down from 90 degrees to raise the rectifier voltage and start the current ramp, actually maintains itself at 90 degrees for around another $100msec$. The inrush current into the cable is then finally exceeded by the ordered current, and the link current finishes its ramp to 30% nominal as required. This is completed at $t = 1.97sec$.

As alpha moves down from 90 degrees to control the final part of the current ramp, the rectifier voltage, previously oscillatory due to the inrush current, settles to its low but positive value. The *ac* voltage during this time is still high but is gradually falling as the *dc* link begins to take load.

The inverter is re-started at $t = 1.97sec$. The link current dips as in the TS-(QSS) case, however the dip in EMTDC is maintained for a longer period (approximately $50msec$) and is lower than that in the TS-(QSS) case. In EMTDC, alpha cannot instantly change and instead requires this period of the dip length to vary from near 90 degrees to minimum. As the firing angle decreases, the rectifier *dc* voltage is increased, but accordingly slower than the TS-(QSS) case.

The *dc* voltage overshoots, similar again to TS-(QSS), but to an even greater extent. This is due both to the *ac* rectifier voltage which is still high, and the inability of alpha to instantly reverse direction. The *dc* voltage overshoot also causes the *dc* current to ramp faster and overtake the TS-(QSS) ramp rate.

At the end of the power ramp, the *ac* voltage has returned to nominal $1pu$ and after a small oscillatory settling of controllers, so does the *dc* voltage and current. The firing angle (alpha) is still different between the EMTDC and TS-(QSS) cases since in the TS-(QSS) case, the *ac* voltage is actually low until approximately $t = 3sec$ and consequently, alpha also must be lower to maintain the rectifier *dc* voltage constant. As the generator controllers in the *ac* system of the TS-(QSS) case react to the re-introduction of the *dc* load, the rectifier *ac* voltage returns to its nominal value. The firing angle, alpha, consequently does the same.

7.3.3 The TSE Hybrid Response

The EMTDC and TS only cases showed results that were quite different in aspects of their response to the balanced three phase *ac* fault introduced. The physical *dc* control limitations, the *dc* cable characteristics, and the *ac* filter characteristics in EMTDC, combined with the generator controllers in TS, produced different dynamic responses during the fault and subsequent recovery. Significant differences in every variable are then possible at some stage during the fault and recovery process including real and reactive power requirements. In some situations this may even be enough to affect the transient stability of either the *dc* system or the *ac* system recovery. Even if the stability of the systems are not adversely affected, the recovery predicted is unlikely to show a totally realistic response without the electromagnetic transient modelling of the *dc* system and the electro-mechanical modelling of the *ac* system.

To achieve this simultaneous accurate dynamic modelling of both *ac* and *dc* systems, the TSE hybrid, described in Chapter 5, was used to simulate the three phase fault. An EMTDC solution was used to model the HV*dc* link while a TS solution was used for

the *ac* system. These two solutions interacted throughout the simulation time to combine the true dynamic responses of both the HV*dc* link and the *ac* system generators. The hybrid TSE simulation results are shown in Figures 7.20 to 7.27. Figure 7.20 shows the *ac* voltage magnitude and phase and Figure 7.21 the machine field voltages and rotor angles. These two figures derive their data from the TS part of the hybrid.

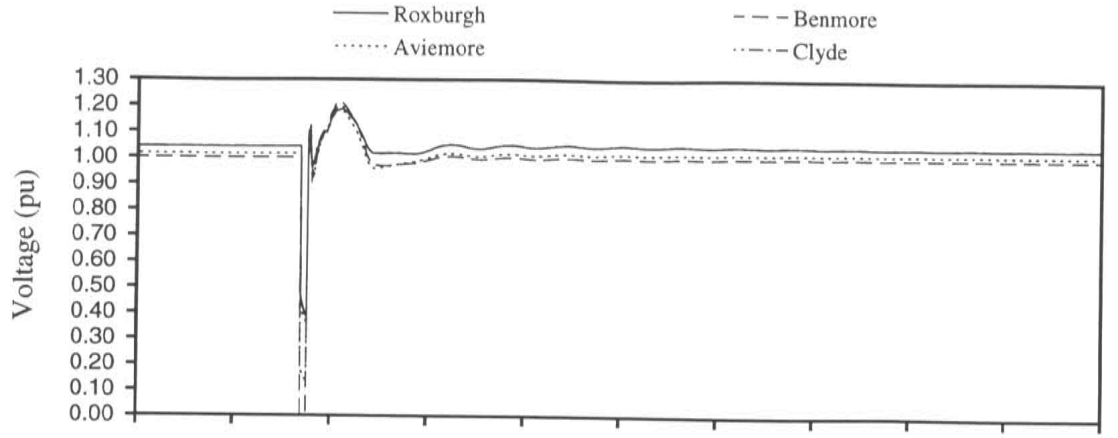

(a)

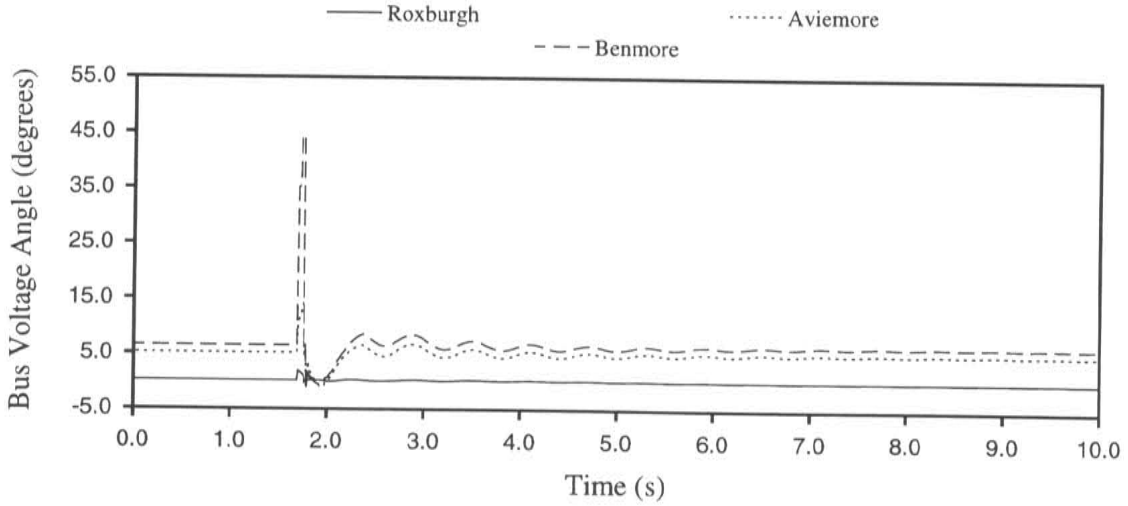

(b)

Figure 7.20 Rectifier *ac* voltage - TSE (TS variable)

The TSE hybrid solution is compared with both the previous TS and EMTDC only solutions in Figures 7.22 to 7.27. The rectifier *ac* voltages are compared in Figure 7.22. Figure 7.22(a) shows the TS only bus voltage compared with the TS variable from the TSE hybrid solution, while Figures 7.22(b) and 7.22(c) display the EMTDC variable from the EMTDC and TSE solutions respectively.

In Figure 7.22(a) there are 3 distinct sections of difference between the TS and TSE solutions. The first is the transient overshoot evident in the TSE solution. This results from the over-voltage transient in the EMTDC solution caused by the elemental type modelling of components, and in particular, the inductive nature of the *ac* system.

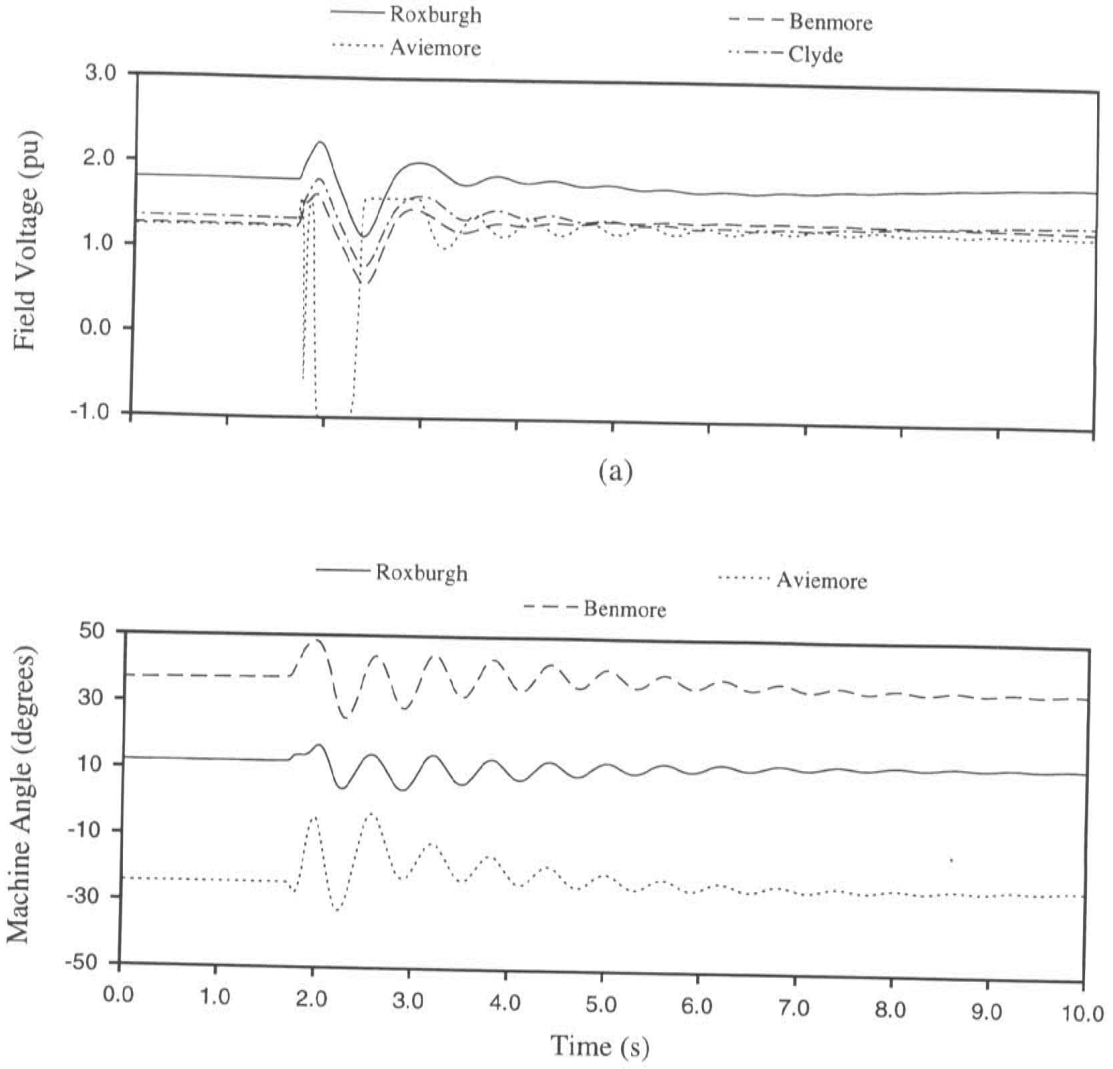

Figure 7.21 Machine variables - TSE (TS variables)

The effect of the overshoot on the generators contributes to the second section of difference is between time $t = 1.8sec$ to approximately $t = 1.91sec$ when the TSE *ac* voltage is lower than that of TS but rises steeper and subsequently slightly exceeds the TS *ac* voltage.

The last section from time $t = 1.91sec$ to $t = 2.8sec$ shows a higher TSE *ac* voltage but eventually at the end of this time period, the two voltages once again coincide through the actions of the generator controllers.

Figures 7.22(b) and 7.22(c) show a significant difference only between the fault removal and time t=2.1s. The EMTDC waveform, with its *fixed* source value, displays a higher *ac* voltage over this period while the link is regaining full load. The TSE waveform shows the behaviour of the *ac* generators as supplied by TS. The *ac* voltage in TSE is slightly lower than that of EMTDC over the period $t = 2.4sec$ to $t = 3.0sec$ for this reason.

The rectifier *dc* current of all 3 solutions is shown in Figure 7.23 while a *dc* voltage

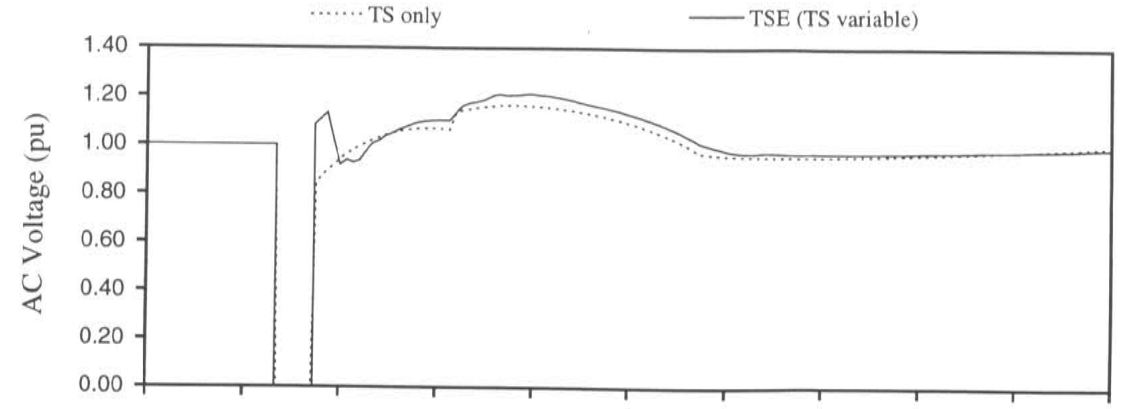

(a)

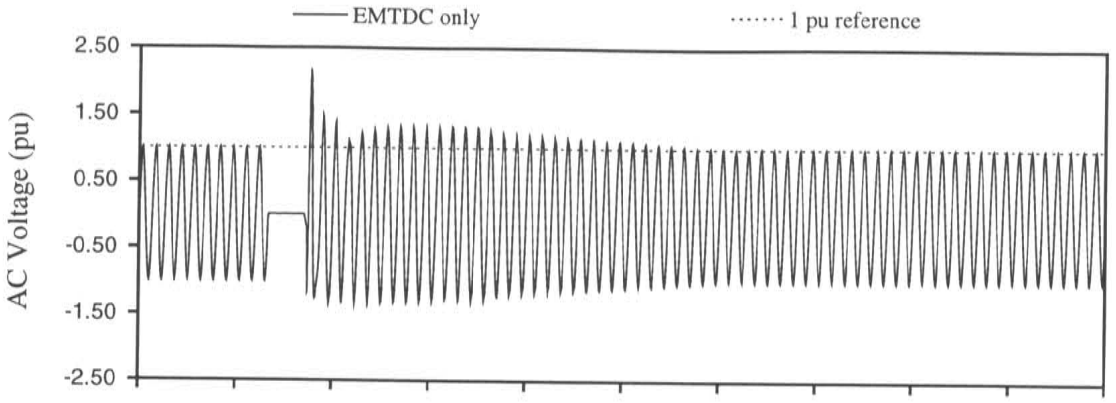

(b)

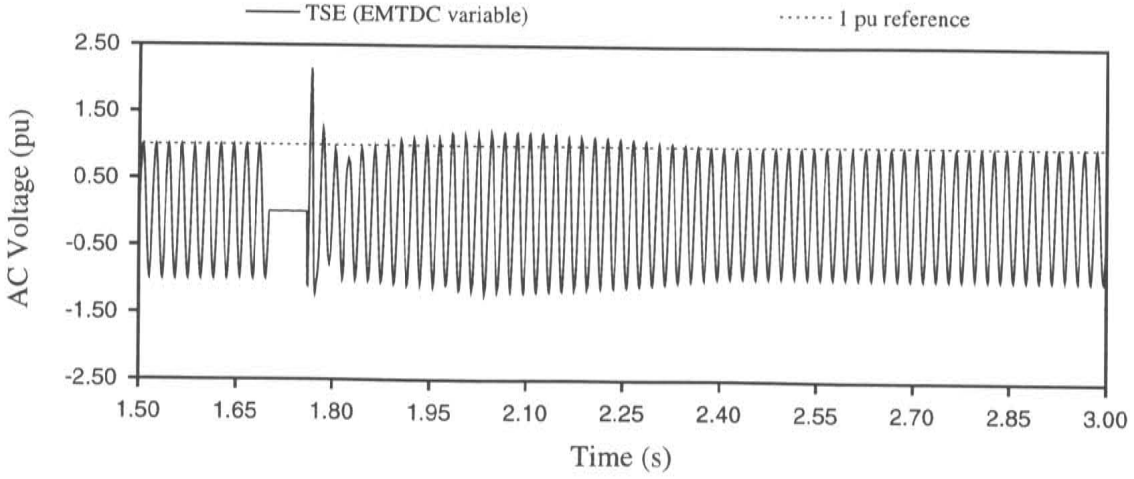

(c)

Figure 7.22 Rectifier *ac* voltage comparisons

comparison is shown in Figure 7.24. The TSE current is very similar to that of EMTDC except over the period from time $t = 2.03sec$ to $t = 2.14sec$ when the TSE *dc* current climbs slower than that of EMTDC to its position of power ramping. The TSE solution has a smaller *dc* voltage overshoot but a higher overall *dc* voltage over this period. This can also be seen in the firing angle alpha shown in Figure 7.25 with alpha remaining at a minimum value longer than TS and hence causing this higher voltage. This is due to the lower *ac* voltage at the rectifier requiring a lower firing angle to maintain the *dc* voltage required for the ordered current. Since alpha is at its minimum value, the *dc* current in TSE is slower to respond to its ordered value.

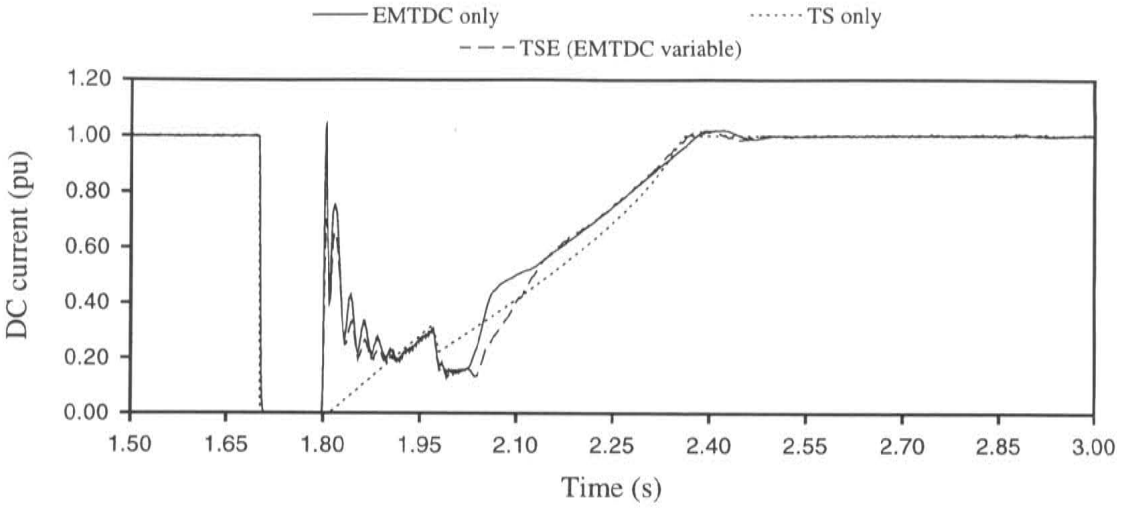

Figure 7.23 Rectifier terminal *dc* current comparison

The slightly lower *ac* voltage in TSE compared with EMTDC also causes the firing angle to be lower further on in time. As the *ac* voltages of EMTDC and TSE move together, so do the firing angles.

The *ac* current across the interface is shown in Figure 7.26 for both EMTDC and TSE. Similar to the *ac* voltage, during the fault recovery, the *ac* current in TSE is less since the *ac* system equivalent is not fixed but varies according to the information supplied by TS.

The fundamental, positive sequence, real and reactive power flows were also monitored across the interface converter bus in both TS and TSE and are shown in Figure 7.27. The main differences in real power occur during the link power ramp. The difference is almost a direct relation to the *dc* current difference between TS and TSE shown in Figure 7.23. The oscillation in *dc* voltage and current as the rectifier terminal is de-blocked is also evident.

As for the reactive power Q, prior to the fault, a small amount is flowing into the system due to a surplus MVAr's at the converter terminal. The fault reduces this power flow to zero. When the fault is removed and the *ac* voltage overshoots in TSE, the reactive MVAr's also overshoot in TSE and since the *dc* link is shut down, a considerable amount of reactive power flows into the system.

The differences and cross-over points between reactive power from TS to that of

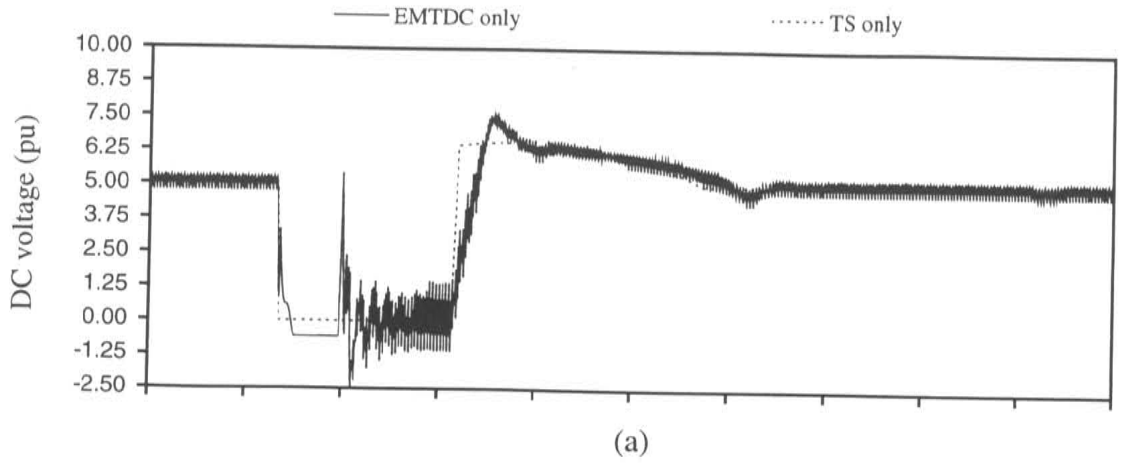

(a)

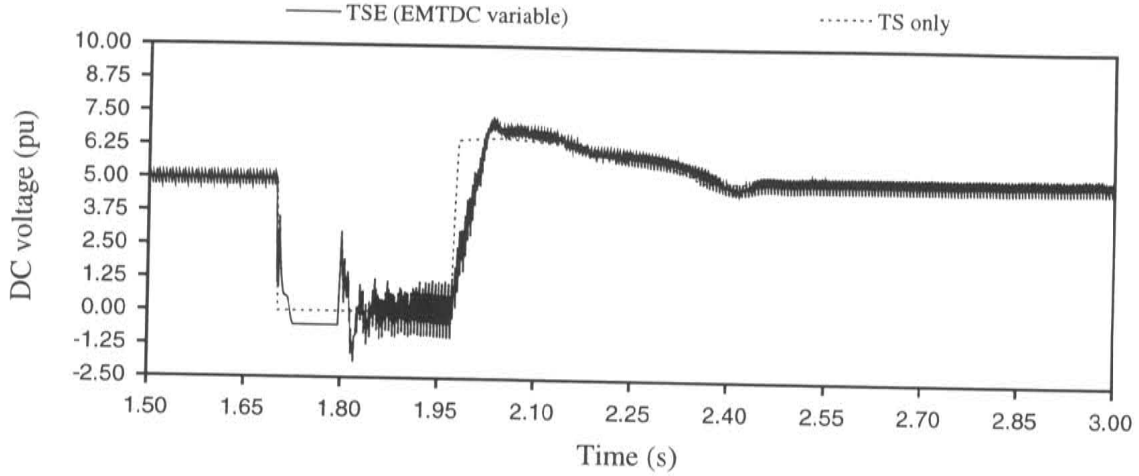

(b)

Figure 7.24 Rectifier terminal *dc* voltage comparisons

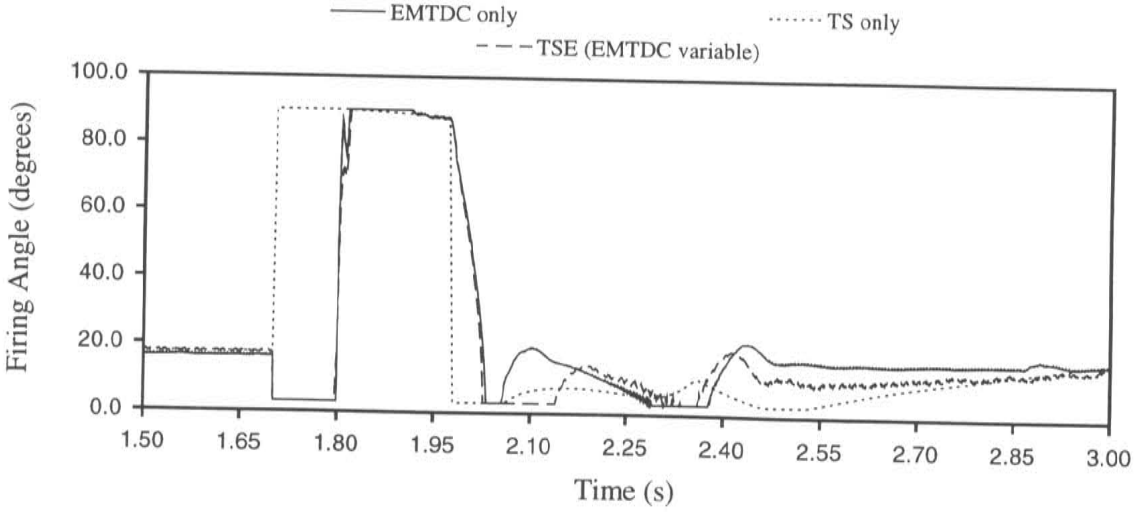

Figure 7.25 Rectifier terminal *dc* firing order comparison

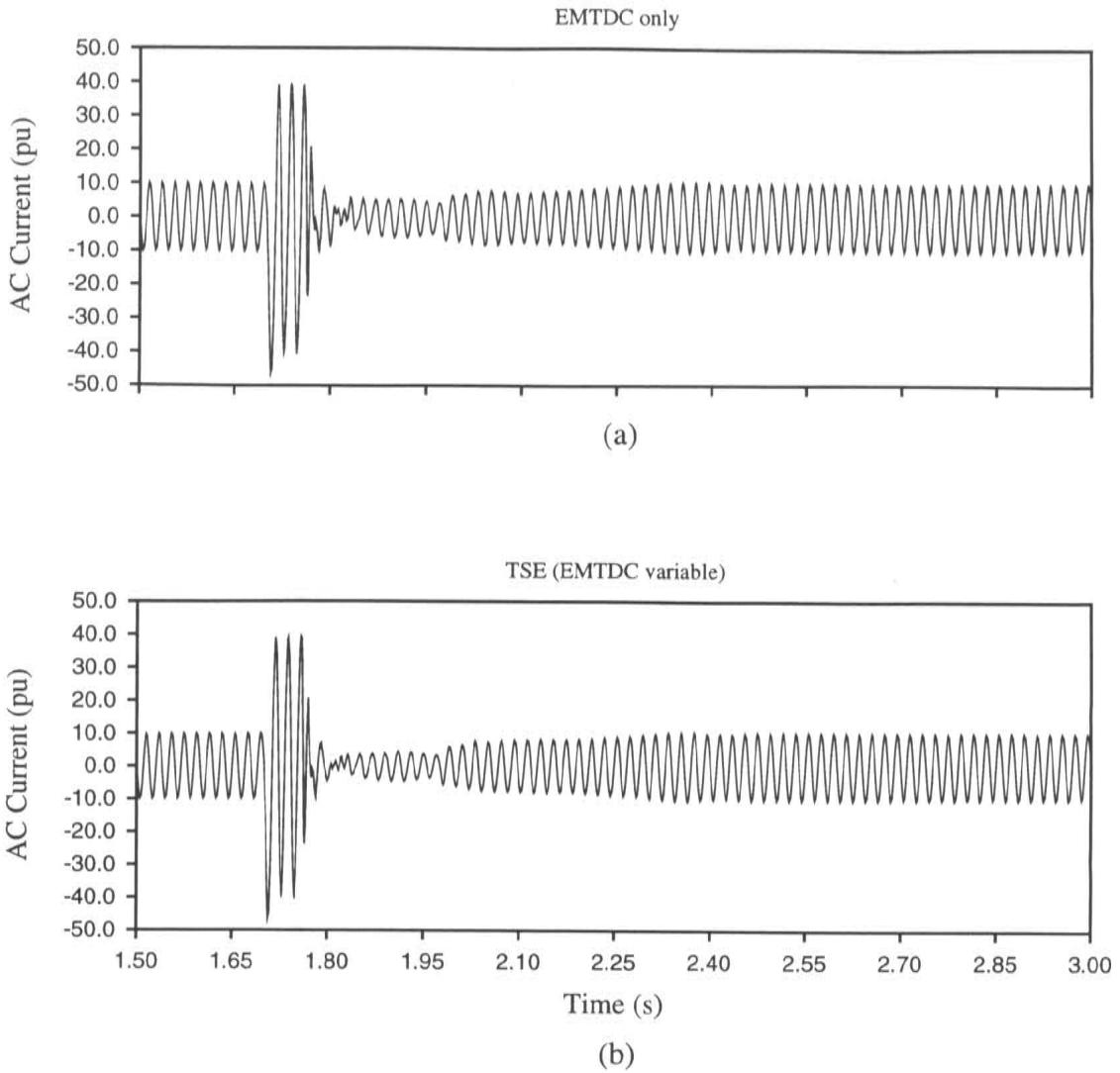

Figure 7.26 Rectifier *ac* current across interface

TSE from time $t = 1.8sec$ on are a direct result of the differences in the firing angle alpha from Figure 7.25. When the firing angle in TSE is low, compared to TS, the reactive requirements of the link are also low in comparison. This can be explained mathematically from equations 2.34 and 2.35 in Section 2.4.1 of Chapter 2.

7.4 Summary

Two different disturbances were applied to a simple test system to examine the results using the TSE hybrid and compare them to the conventional electro-mechanical stability and electromagnetic transient approaches.

The minor disturbance showed the validity of the hybrid in that the response was practically identical to that of the electro-mechanical stability program TS. This is to be expected since the QSS model used in TS is generally a very good estimate of the *dc* link response under a minor or remote disturbance [Meredith, 1983].

The second disturbance applied a three phase fault at the rectifier converter terminal and

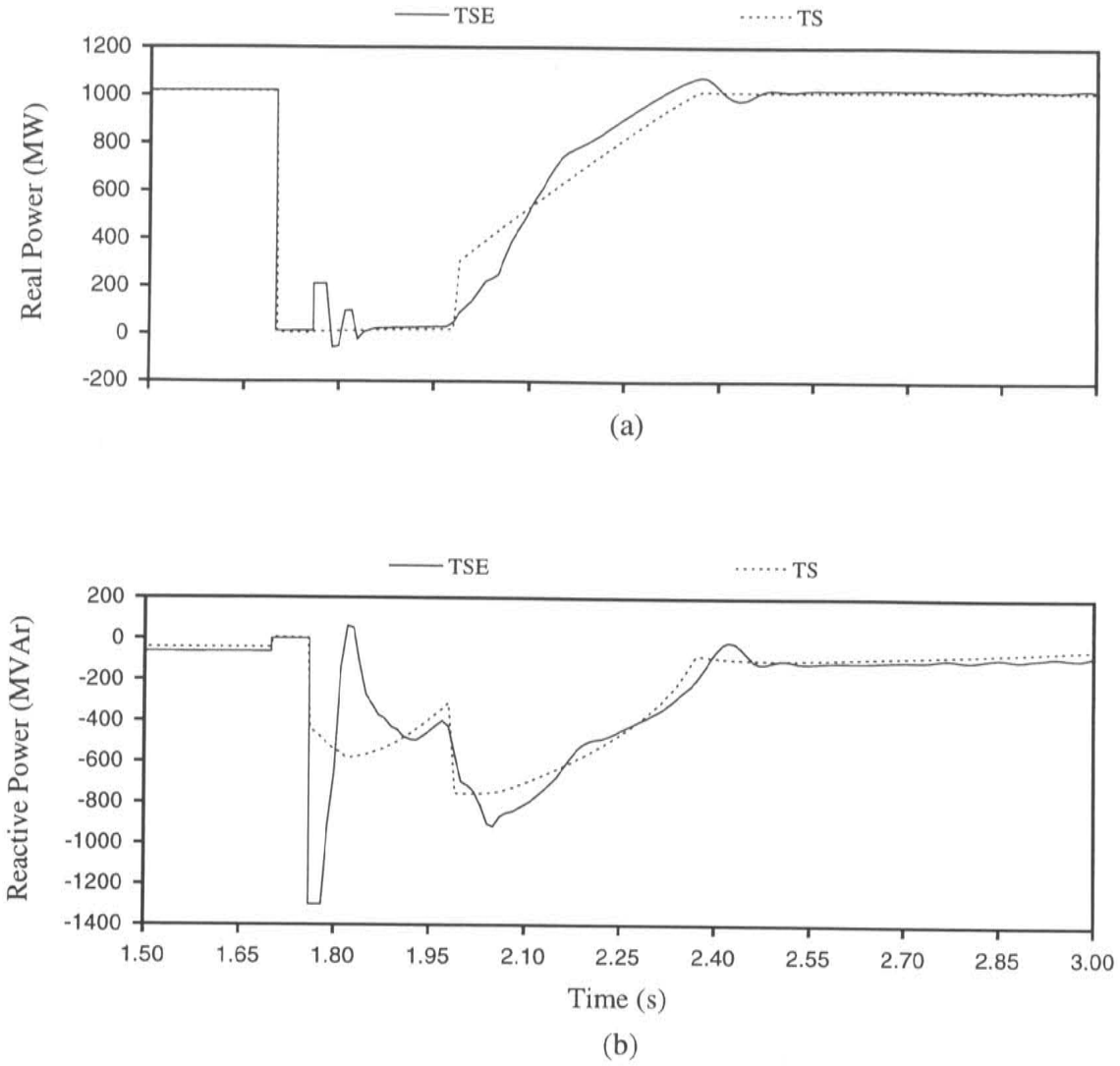

Figure 7.27 Real and reactive power across interface

exemplified the differences between the two types of solutions. The electro-mechanical solution showed the slower dynamic response of the *ac* system while the electromagnetic solution displayed the fast dynamics of the rapidly switched converter. In the hybrid, these responses were combined to give a more realistic overall picture of the entire system. The electro-mechanical modelling of the *ac* system was improved by the inclusion of the actual response of the fast acting HV*dc* link, while the link behaviour was also more realistic through the inclusion of the generator controller response varying the *ac* system voltage at the converter terminal. In a practical situation, neither one program on their own can provide a realistic response of both *ac* and *dc* systems.

Chapter 8

CONCLUSIONS AND FURTHER WORK

8.1 Conclusions

The modelling of power system networks has always been important, but it has become even more necessary with the advent of such fast switched devices as HV*dc* converters and FACTS. Power grid networks are more complex than ever before with power electronic technology. As these new technologies are applied to increasingly weaker *ac* systems, accurate modelling to ensure a stable power system is essential.

The stability analysis of faults at distant locations from the terminals of such components as HV*dc* links are successfully accomplished through the use of steady state or quasi-steady state equations. These equations are entirely adequate for determining the load changes due to remote disturbances or even minor disturbances at converter terminals themselves. What these equations cannot represent, is the complex response of a fast-acting component when subjected to a significant transient change in conditions at its terminals. A fundamental frequency single phase analysis is no longer sufficient. A detailed three phase, point on wave type approach is imperative to adequately describe the components operation during a major disturbance, and its subsequent recovery.

This thesis has described an effective hybrid approach to modelling a power system network which uses a conventional fundamental frequency transient stability program for the relatively slow dynamics of a machine based *ac* network, and a detailed three phase analysis for any dynamically fast changing components. The influence of the overall *ac* network can then be incorporated into a detailed study of say an HV*dc* link, which would normally be restricted to a simple *ac* equivalent. Conversely, accurate modelling of the rapid action of an HV*dc* link can then also be used to influence the stability recovery of an *ac* network after it has been subjected to some form of disturbance. Effects such as phase imbalance, high frequency transients, and transformer saturation, for example, can be modelled in detail on specific components, and the consequences transferred to the relatively simple *ac* system stability study.

The hybrid developed uses an efficient curve fitting routine, providing optimum extraction of the appropriate variables to transfer the necessary information between programs. Analysis work has been presented in Chapter 4 to determine the ideal method of deriving this interfacing data. The hybrid utilises two modern and accepted analysis programs but at the same time has been created so that only minimal change to these programs was necessary. Adaptation of the hybrid techniques are then possible to a host of other similar

type stability and EMT type programs.

A major difference in this hybrid compared with previous work in this area, is its approach to interface location and variables. The effectiveness of a hybrid must be determined by its ability to use the inherent advantages that a hybrid solution offers. These include computational efficiency, detailed modelling of dynamically fast devices, and overall accuracy by utilising the influences of both *ac* and *dc* systems on each other. The interface location then, is an important consideration. Any attempt to move the interface location away from the terminals of a dynamically fast switched device diminishes both the computational efficiency and the simplicity of a hybrid. Conversely, the terminals of such a device during a disturbance, make it a difficult place to both extract data and provide a realistic picture of the *ac* system interfaced to it.

This thesis has described a solution that allows the full advantages of a hybrid by allowing interfacing of programs at the terminals of a fast switched device, and yet also overcomes the difficulties that this presents. A frequency dependent equivalent of the *ac* network modelled in the stability analysis, is used to represent the impedance of all frequencies to the detailed solution. This was proven to be extremely effective as an alternative to relocating the interface out into the *ac* system.

The variables for information interchange have also been carefully examined to allow the most realistic transfer of data between programs. The inherent differences between the programs, and the inherent constraints of a positive sequence fundamental frequency stability analysis reduce the selection of available variables. Power variables in their various forms were shown to be somewhat subjective and consequently voltage and current were deemed the obvious choice.

The hybrid solution was finally applied to a selection of disturbances in Chapter 7. The hybrid analysis of a minor disturbance was shown to be very similar to that of a stability analysis using quasi-steady state equations, as expected. The necessity of a hybrid for a major disturbance was however also shown, with considerable differences apparent between both a stability analysis only and a detailed three phase analysis only of the same fault.

In the analysis of an HV*dc* converter, the inherent differences between the two programs were very apparent and included aspects of both their control response and frequency response. The differences between an elemental R-L-C type model in the detailed solution versus an equation based model in the stability solution was also significant. The requirement of a detailed three phase model of the HV*dc* converter was plainly evident.

Only the hybrid solution however, allowed the dynamically slower influence of the *ac* system to permeate the reaction and recovery of the detailed model to provide the most accurate overall response.

8.2 Further Work

The possibilities in the application of hybrid solutions are almost endless and there is still much work to be done in this area. Initialisation of the EMTDC snapshot, for example, still requires considerable time. There is not yet any fast initialisation of devices such as

HV*dc* converters or even *ac* generators, although the possibility of achieving this in EMT type programs exists [Usaola and Mayordomo, 1990].

Automation of the hybrid could be enhanced further, particularly through the use of advanced graphical front-ends such as that of PSCAD with EMTDC. The possibility also exists in the future of only needing to have one data file to run loadflow, stability, fault, EMT type analysis, or a hybrid program. This would offer considerable time savings in data preparation. Such a host of applications could well be incorporated into a user friendly front-end such as PSCAD.

In the interfacing of a detailed three phase program with a conventional stability analysis, the concept of frequency dependent equivalents has been introduced in this thesis. Further work could examine the possibility of modifying the frequency dependent equivalent to allow network changes to occur in the stability modelled *ac* network. One of the difficulties with this is that the modified frequency dependent equivalent circuit may need to be pre-initialised, although a 'prepared' EMTDC snapshot to cater for this is entirely possible.

Finally, with the advent of the real time digital simulation of HV*dc* converters, and the prospect of real time stability analysis of very large *ac* networks, hybrid programs could find a very useful place in linking these high technology tools to enable very large *ac-dc* systems to be accurately modelled in real time.

REFERENCES

[Adamson and Hingorani 1960]

Adamson, C. and Hingorani, N.G. *High Voltage Direct Current Power Transmission*, Garraway Ltd., London, 1st ed.

[Arnold 1976]

Arnold, C.P. *Solution of the Multimachine Power System Stability Problem*, PhD thesis, University of Manchester Institute of Science and Technology.

[Arrillaga 1983]

Arrillaga, J. *High Voltage Direct Current Transmission*, Peter Peregrinous Ltd.

[Arrillaga and Arnold 1990]

Arrillaga, J. and Arnold, C.P. *Computer Analysis of Power Systems*, John Wiley and Sons.

[Arrillaga *et al.* 1985]

Arrillaga, J., Bradley, D.A. and Bodger, P.S. *Power System Harmonics*, John Wiley and Sons Inc.

[Arrillaga *et al.* 1991]

Arrillaga, J., Sankar, S., Watson, N.R. and Arnold, C.P. "A Comparison of HVDC Transient Simulation Algorithms," *IEE Conference Publication*, No. 345, September, pp. 368–373.

[Berg 1973]

Berg, G.L. "Power System Load Representation," *Proceedings of the IEE*, Vol. 120, No. 3, March, pp. 344–348.

[Bergeron 1949]

Bergeron, L. *Du Coup de Belier en Hydraulique au Coup de Foudre en Electricite*, Wiley, New York (translated version) - 1961.

[Bloomfield 1976]

Bloomfield, P. *Fourier Analysis of Time Series: An Introduction*, John Wiley and Sons Inc., U.S.A.

[Bowles 1970]

Bowles, J.P. "AC system and Transformer Representation for HV-DC Transmission

Studies," *IEEE Transactions on Power Apparatus and Systems*, Vol. PAS-89, No. 7, September, pp. 1603–1609.

[Brigham 1988]
Brigham, E.O. *The Fast Fourier Transform and its Applications*, Prentice-Hall Inc., U.S.A.

[Chapman *et al.* 1988a]
Chapman, D.G., Davies, J.B., Alvarado, F.L., Lasseter, R.H., Lefebvre, S., Krishnayya, P.C.S., Reeve, J. and Balu, N.J. "Programs for the Study of HVdc Systems," *IEEE Transactions on Power Delivery*, Vol. 3, No. 3, July, pp. 1182–1188.

[Chapman *et al.* 1988b]
Chapman, D.G., Davies, J.B., McNichol, J.R., Gulachenski, E.M., Doe, S. and Balu, N.J. "Test Experience with Multiterminal HVdc Load Flow and Stability Programs," *IEEE Transactions on Power Delivery*, Vol. 3, No. 3, July, pp. 1173–1181.

[Clarke 1950]
Clarke, E. *Circuit Analysis of A-C Power Systems*, Vol. II, John Wiley and Sons Inc., New York.

[Dandeno and Kundur 1973]
Dandeno, P.L. and Kundur, P. "A Noniterative Transient Stability Program including the effects of Variable Load-Voltage Characteristics," *IEEE Transactions on Power Apparatus and Systems*, Vol. PAS-92, No. 5, pp. 1478–1484.

[Dommel 1969]
Dommel, H.W. "Digital computer simulation of electromagnetic transients in single and multiphase networks," *IEEE Transactions on Power Apparatus and Systems*, Vol. PAS-88, No. 4, April, pp. 388–399.

[Dommel and Meyer 1974]
Dommel, H.W. and Meyer, W.S. "Computation of Electromagnetic Transients," *Proceedings of the IEEE*, Vol. 62, No. 7, pp. 983–993.

[Dommel and Sato 1972]
Dommel, H.W. and Sato, N. "Fast Transient Stability Solutions," *IEEE Transactions on Power Apparatus and Systems*, Vol. PAS-91, No. 4, pp. 1643–1650.

[Elahi *et al.* 1993]
Elahi, H., Bennett, M., Thio, C., Burtnyk, V. and Christofersen, J. "WG 14-04 report. HVdc reliability, maintenance, and diagnostics survey," *CIGRE International Colloquium on HVdc and FACTS, New Zealand*, September, pp. 4.4–1 to 4.4–11.

[Emanuel 1990]
Emanuel, A.E. "Powers in Nonsinusoidal Situations - A Review of Definitions and Physical Meaning," *IEEE Transactions on Power Delivery*, Vol. 5, No. 3, July, pp. 1377–1383.

[Emanuel 1993]
Emanuel, A.E. "On the Definition of Power Factor and Apparent Power in Unbalanced Polyphase Circuits with Sinusoidal Voltage and Currents," *IEEE Transactions on Power Delivery*, Vol. 8, No. 3, July, pp. 841–847.

[Giesner and Arrillaga 1970]
Giesner, D.B. and Arrillaga, J. "Operating Modes of the Three-Phase Bridge Converter," *Int. J. Elect. Eng. Educ.*, Vol. 8, pp. 373–388.

[Giray and Sachdev 1989]
Giray, M.M. and Sachdev, M.S. "Off-Nominal Frequency Measurements in Electric Power Systems," *IEEE Transactions on Power Delivery*, Vol. PD-4, No. 3, July, pp. 1573–1578.

[Gole and Sood 1990]
Gole, A.M. and Sood, V.K. "A Static Compensator Model for use with Electromagnetic Transients Simulation Programs," *IEEE Transactions on Power Delivery*, Vol. PD-5, No. 3, July, pp. 1398–1405.

[Harris 1978]
Harris, F.J. "On the Use of Windows for Harmonic Analysis with the Discrete Fourier Transform," *Proceedings of the IEEE*, Vol. 66, No. 1, January.

[Hauth *et al.* 1982]
Hauth, R.L., Miske(Jr), S.A. and Nozari, F. "The Role and Benefits of Static VAr Systems in High Voltage Power System Applications," *IEEE Transactions on Power Apparatus and Systems*, Vol. PAS-101, No. 10, October, pp. 3761–3769.

[Heffernan *et al.* 1981]
Heffernan, M.D., Turner, K.S., Arrillaga, J. and Arnold, C.P. "Computation of AC-DC System Disturbances, Parts I, II and III," *IEEE Trans. on Power Apparatus and Systems*, Vol. PAS-100, No. 11, November, pp. 4341–4363.

[Hingorani and Burbery 1970]
Hingorani, N.G. and Burbery, M.F. "Simulation of AC System Impedance in HVDC System Studies," *IEEE Transactions on Power Apparatus and Systems*, Vol. PAS-89, No. 5/6, pp. 820–826.

[Humpage *et al.* 1980]
Humpage, W.D., Wong, K.P. and Nguyen, T.T. "Development of Z-Transform Electromagnetic Transient Analysis Methods for Multinode Power Networks," *Proceedings of the IEE*, Vol. 127, No. 6, pp. 379–385.

[IEC 1979]
IEC *Reactive Power in Nonsinusoidal Situations*, Technical Committee No. 25 TC 25/WG7, International Electrotechnical Commission, December.

[IEEE 1968]
IEEE "Computer Representation of Exciter Systems," *IEEE Transactions on Power Apparatus and Systems*, Vol. PAS-87, No. 6, June, pp. 1460–1464. IEEE Committee Report.

[IEEE 1973]
IEEE "Dynamic Models for Steam and Hydro Turbines in Power-System Studies," *IEEE Transactions on Power Apparatus and Systems*, Vol. PAS-92, No. 6, pp. 1904–1915. IEEE Committee Report.

[Kay and Marple 1981]
Kay, S.M. and Marple, S.L. "Spectral Analysis - A Modern Perspective," *Proceedings of the IEEE*, Vol. 69, No. 11, November, pp. 4341–4363.

[Kimbark 1956]
Kimbark, E.W. *Power System Stability*, Vol. III - Synchronous Machines, Dover Publications Inc., 1968 ed.

[Kimbark 1971]
Kimbark, E.W. *Direct Current Transmission*, Vol. I, Wiley and Sons Inc., New York.

[Kuh and Rohrer 1965]
Kuh, E.S. and Rohrer, R.A. "The State Variable Approach to Network Analysis by Digital Computer - A State Space Approach," *Proceedings of the third Allerton Conference on Circuit and System Theory*, October.

[Kulicke 1981]
Kulicke, B. "Netomac Digital Program for Simulating Electromechanical and Electromagnetic Transient Phenomena in ac Systems," *Siemens Aktienngesellschaft*. Order No. E 15/1722-101.

[Meredith 1983]
Meredith, R.J. *Methodology for Integration of HVDC Links in Large AC Systems - Phase I: Reference Manual*, Research Project, Ebasco Services Incorporated, March.

[Ong and Hamzeinejad 1985]
Ong, C.M. and Hamzeinejad, A. "Digital Simulation of Multiterminal HVdc Systems for Transient Stability Studies using a Simplified dc System Representation," *IEEE Transactions on Power Apparatus and Systems*, Vol. PAS-104, No. 6, June, pp. 1411–1417.

[Park 1929]
Park, R.H. "Two Reaction Theory of Synchronous Machines - Part I : Generalized Method of Analysis," *Transactions of the American Institute of Electrical Engineers*, Vol. 48, July, pp. 716–730.

[Park 1933]
Park, R.H. "Two Reaction Theory of Synchronous Machines - Part II :," *Transactions of the American Institute of Electrical Engineers*, Vol. 52, June, pp. 352–355.

[Reeve and Adapa 1988]
Reeve, J. and Adapa, R. "A New Approach to Dynamic Analysis of AC Networks Incorporating Detailed Modelling of DC Systems, Parts I and II," *IEEE Trans on Power Delivery*, Vol. PD-3, No. 4, October.

[Reeve *et al.* 1991]
Reeve, J., Lane-Smith, S.P. and Wikston, J.M. "Incorporation of FACTS into Transients Programs for System Simulation," *IEE 5th International Conference on AC and DC Power Transmission*, September.

[Sachdev and Giray 1985]
Sachdev, M.S. and Giray, M.M. "A Least Error Squares Technique for Determining Power System Frequency," *IEEE Transactions on Power Apparatus and Systems*, Vol. PAS-104, No. 2, February, pp. 435–444.

[Szechtman *et al.* 1991]
Szechtman, M., Weiss, T. and Thio, C.V. "First benchmark model for HVdc control studies.," *Electra*, No. 135, April, pp. 55–75.

[Tinney and Walker 1967]
Tinney, W.F. and Walker, J.W. "Direct Solutions of Sparse Network Equations by Optimally Ordered Triangular Factorization," *Proceedings of the IEEE*, No. 11, November, pp. 1801–1809.

[Usaola and Mayordomo 1990]
Usaola, J. and Mayordomo, J.G. "Fast Steady-State Technique for Harmonic Analysis," *Paper presented at ICHPS IV, 4th International Conference on Harmonics in Power Systems, Budapest, Hungary*, October.

[Watson *et al.* 1985]
Watson, N.R., Arrillaga, J. and Joosten, A.P.B. "AC System Equivalents for the Dynamic Simulation of HVdc Convertors," *IEE Conference Publication*, No. 255, September, pp. 366–371.

[Woodford 1985]
Woodford, D.A. "Validation of digital simulation of dc links," *IEEE Transactions on Power Apparatus and System*, Vol. PAS-104, No. 9, September, pp. 2588–2595.

[Woodford *et al.* 1983]
Woodford, D.A., Gole, A.M. and Menzies, R.W. "Digital Simulation of DC Links and AC machines," *IEEE Transactions on Power Apparatus and System*, Vol. PAS-102, No. 6, June, pp. 1616–1623.

[Zollenkopf 1972]
Zollenkopf, K. *Bi-Factorisation, Basic Computational Algorithm and Programming Techniques*, Academic Press.

Appendix A

TEST SYSTEMS

There are three test systems used in this thesis, all of them utilising the CIGRE HV*dc* benchmark model as their *dc* link component [Szechtman *et al.*, 1991]. Chapter 4 uses this benchmark model for a rectifier fault simulation. Test system A is used in Chapter 6 and has an inverter *ac* system design based on a test system described by Reeves [Reeve and Adapa, 1988]. Test system B is used in Chapter 7 and has a simplified rectifier *ac* system representation based on the central South Island power system of New Zealand. The rectifier *ac* system in test system A, the inverter *ac* system in test system B, and the *dc* system, are as per the original CIGRE benchmark model described in A.1.

A.1 CIGRE HV*dc* Benchmark Model

The arrangement of the CIGRE model is shown in Figure A.1. Component values for resistance, inductance, and capacitance are in Ohms, Henrys, and micro-Farads respectively. Voltage sources are in per unit.

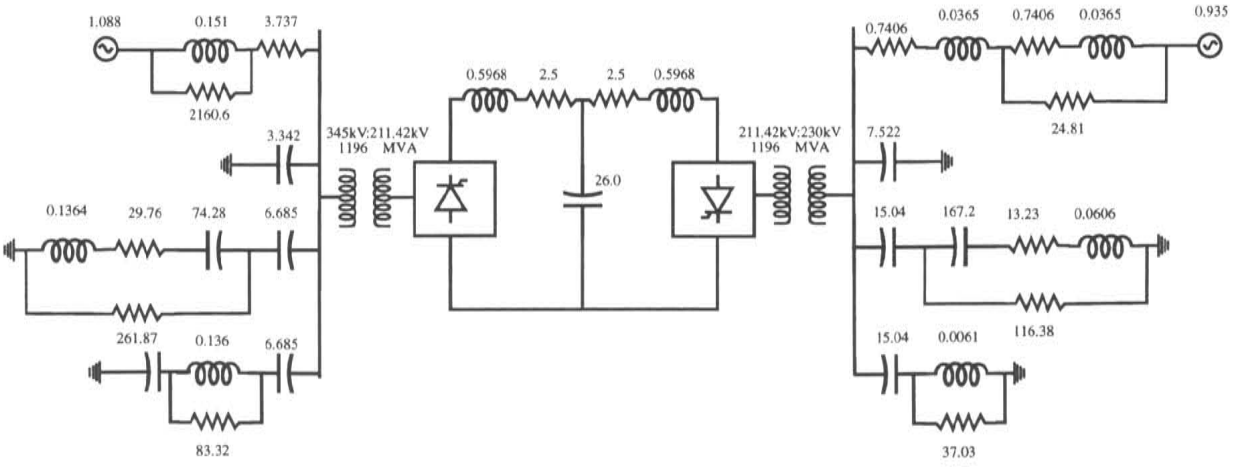

Figure A.1 CIGRE HV*dc* benchmark model

In addition to Figure A.1, the model has the following parameters :-

Parameter	Rectifier	Inverter
ac system voltage	345 kV *l-l*	230 kV *l-l*
ac system impedance magnitude	119.03 Ω	52.9 Ω
converter transformer tap (prim. side)	1.01	0.989
equivalent commutation reactance	27 Ω	27 Ω
dc voltage	505 kV	495 kV
dc current	2 kA	2 kA
firing angle	15°	15°
dc power	1010 MW	990 MW

Table A.1 CIGRE HV*dc* benchmark model parameters

A.2 Test System A

This system is shown in Figure A.2 and uses the HV*dc* benchmark model described in A.1 for both the rectifier *ac* system and the *dc* link. The inverter *ac* system is modified and described below. Inverter per unit values are based on 100 MVA and 230 kV *l-l*.

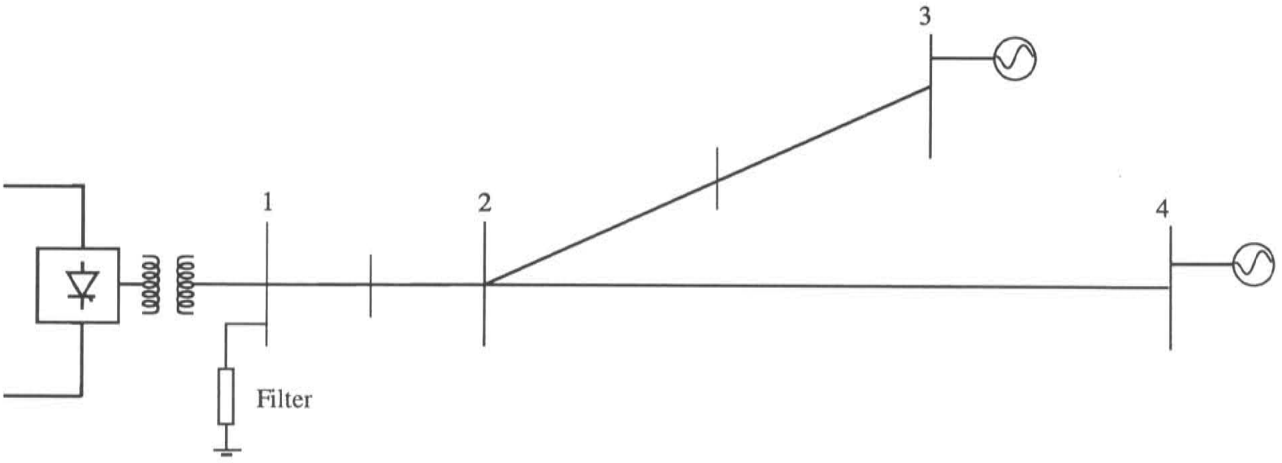

Figure A.2 Test system A

Bus	$\|V\|_{pu}$	$\theta°$
1	1.001	19.377
2	0.983	3.635
3	0.992	0.0
4	1.005	-7.049

Table A.2 Test system A *ac* bus parameters

Line	R *pu*	X *pu*
1-2	0.00452	0.02832
2-3	0.00334	0.01154
2-4	0.00010	0.04256

Table A.3 Test system A *ac* line parameters

A.3 Test System B

Similar to test system A, test system B uses the CIGRE HV*dc* benchmark model for its *dc* link component although with slightly modified *dc* conditions. The inverter *ac* system in this case however, is as per the benchmark model, while the rectifier *ac* system is modified. The rectifier *ac* system is shown in Figure A.3 and is representative of the central South Island power system of New Zealand. The parameters for this test system are described below. Rectifier *ac* system per unit values are based on 100 MVA and 345 kV *l-l*.

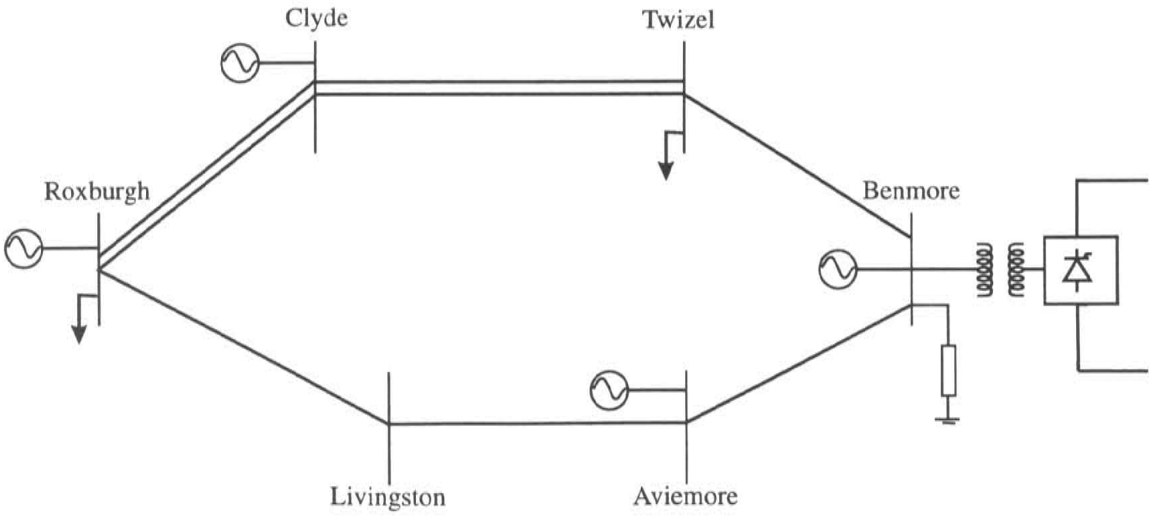

Figure A.3 Test system B

	Rectifier	Inverter
V_{dc}	500 kV	490 kV
I_{dc}	2 kA	2 kA
α	17.65°	15°
P_{dc}	1000 MW	980 MW
Q_{dc}	583 MVAr	545 MVAr

Table A.4 Test system B steady state *dc* conditions

Bus	$\|V\|_{pu}$	$\theta°$
Aviemore	1.015	1.338
Benmore	1.000	0.000
Clyde	1.043	6.479
Roxburgh	1.042	6.338
Livingston	1.024	2.415
Twizel	1.015	1.564

Table A.5 Test system B rectifier *ac* system bus parameters

Bus (from)	Bus (to)	Circuit	R *pu*	X *pu*	B *pu*
Aviemore	Benmore		0.00151	0.01034	0.17038
Aviemore	Livingston		0.00304	0.01459	0.12685
Benmore	Twizel		0.00151	0.01034	0.17038
Clyde	Roxburgh	A	0.00216	0.01297	0.11566
Clyde	Roxburgh	B	0.00216	0.01297	0.11566
Clyde	Twizel	A	0.00405	0.04792	0.47925
Clyde	Twizel	B	0.00405	0.04792	0.47925
Livingston	Roxburgh		0.01088	0.05209	0.45406

Table A.6 Test system B rectifier *ac* system line parameters

Bus	P (MW)	Q (MVAr)
Roxburgh	150.0	75.0
Twizel	100.0	15.0

Table A.7 Test system B rectifier *ac* system load parameters

Bus	H (MWs/MVA)	X'_d *pu*	X_d *pu*	R_a *pu*	T'_{do} (s)	T'_{qo} (s)	X''_d *pu*	T''_{do} (s)
Aviemore	6.273	0.108	0.299	0.0024	1.47	0.43	0.066	0.053
Benmore	12.337	0.069	0.259	0.0011	8.7	0.43	0.044	0.080
Clyde	14.68	0.117	0.181	0.000	6.1	99.99	0.117	0.0
Roxburgh	6.42	0.103	0.54	0.002	7.16	0.36	0.062	0.055

Table A.8 Test system B rectifier *ac* system generator parameters

Bus	Regulator gain *pu*	Regulator TC (s)	Feedback gain *pu*	Feedback TC (s)
Aviemore	400.0	0.02	0.03	1.0
Benmore	50.0	0.2	0.04	0.4
Clyde	50.0	0.2	0.04	0.4
Roxburgh	50.0	0.2	0.04	0.4

Bus	Exciter gain *pu*	Exciter TC (s)	Regulator max. limit *pu*	Reg. min. limit *pu*
Aviemore	1.0	0.01	1.6	-1.0
Benmore	-0.05	0.5	2.0	-1.0
Clyde	-0.05	0.5	2.0	-1.0
Roxburgh	-0.05	0.5	2.0	-1.0

Bus	Exciter max. limit *pu*	Exciter min. limit *pu*
Aviemore	1.6	-1.3
Benmore	3.0	-1.0
Clyde	3.0	-1.0
Roxburgh	3.0	-1.0

Table A.9 Test system B rectifier *ac* system AVR parameters

All AVR's are IEEE type 1 [IEEE, 1968]. A block diagram of this AVR is shown on page 164 of [Arrillaga and Arnold, 1990].

Bus	Regulation *pu*	Governor TC (s)	Governor lead TC (s)	Governor TC (s)
Aviemore	5.0	16.0	2.4	0.92
Benmore	5.0	25.0	2.8	0.50
Clyde	5.0	20.0	4.0	0.50
Roxburgh	5.0	12.0	3.0	0.50

Bus	Water TC (s)	Turbine TC (s)
Aviemore	0.3	0.15
Benmore	0.43	0.215
Clyde	0.3	0.15
Roxburgh	0.35	0.175

Table A.10 Test system B rectifier *ac* system speed governor parameters

A block diagram of this governor is shown on page 166 of [Arrillaga and Arnold, 1990].

Appendix B

LIST OF PUBLICATIONS

- 'A New hybrid AC-DC Transient Stability Program', presented at the International Conference on Power System Transients, Lisbon, Portugal, Sept. 3-7 1995.

- 'A New Hybrid Algorithm for Analysis of HV*dc* and FACTs Systems', presented at the International Conference on Energy Management and Power Delivery, Singapore, Nov. 21-23 1995.